State of Oregon
Oregon Department of Geology and Mineral Industries
Ruarri J. Day-Stirrat, State Geologist

SPECIAL PAPER 54

GEOLOGIC ASSESSMENT OF POTENTIAL CABLE LANDING SITES ALONG THE OREGON COAST

by Reed J. Burgette[1], Eduardo F. Guerrero[1], Jonathan C. Allan[2], Fletcher E. O'Brien[1], Jason D. McClaughry[1,3], Lowell H. Anthony[1], Robert W. Hairston-Porter[1], and Jon Franczyk[1]

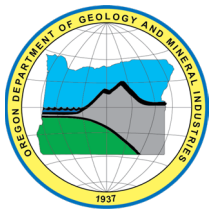

2023

[1]Oregon Department of Geology and Mineral Industries, 800 NE Oregon Street, Suite 965, Portland, OR 97232
[2]Oregon Department of Geology and Mineral Industries, Coastal Field Office, P.O. Box 1033, Newport, OR
[3]Oregon Department of Geology and Mineral Industries, Baker City Field Office, Baker County Courthouse, 1995 3rd Street, Ste. 130, Baker City, OR 97814

DISCLAIMER

This product is for informational purposes and may not have been prepared for or be suitable for legal, engineering, or surveying purposes. Users of this information should review or consult the primary data and information sources to ascertain the usability of the information. This publication cannot substitute for site-specific investigations by qualified practitioners. Site-specific data may give results that differ from the results shown in the publication.

Oregon Department of Geology and Mineral Industries Special Paper 54
Published in conformance with ORS 516.030

For additional information:
Administrative Offices
800 NE Oregon Street, Suite 965
Portland, OR 97232
Telephone (971) 673-1555
https://www.oregongeology.org
https://oregon.gov/DOGAMI/

TABLE OF CONTENTS

LIST OF FIGURES

LIST OF TABLES

LIST OF MAP PLATES

See the digital publication folder for files.

GEOGRAPHIC INFORMATION SYSTEM (GIS) DATA

See the digital publication folder for files.
Geodatabase is Esri® version 10.7 format. Metadata is embedded in the geodatabase and is also provided as separate .xml format files.

SP54_Coastal_Cable_Data_Inventory.gdb:

Feature dataset: Land_sampling

feature classes:

Beaches_and_Dunes (polygon)
Coastal_Roads (polyline)
Contacts_and_Faults (polyline)
Geologic_Units (polygon)
Groundwater_Sources (polygon)
Historic_Landslides (point)
Quaternary_Faults (polyline)
Surface_Water_Sources (polygon)
Tsunami_Inundation (polygon)
Wetlands (polygon)

Feature dataset: Shoreline_Sampling

feature classes:

Bluff_Heights (point)
Coastal_Erosion (polyline)
Coastal_Geomorphology (polyline)
Headlands_Spits_Landslides (polyline)

Feature dataset: Marine_Sampling

feature classes:

Bathy_10m_Contour (polyline)
Marine_Reserves_and_MPAs (polygon)
Offshore_Faults (polyline)
Reefs (polygon)
Seafloor_Substrate (polygon)

Feature dataset: Other_Not_Sampled

feature classes:

Faults_and_Folds (polyline)
Well_Sediment_Thickness (point)

Raster data:

Landslide_Susceptibility
Lidar_Slope
Liquefaction_Susceptibility_Map

Suitability analysis data:

feature classes:

Shoreline (polyline)
Suitability_Scores (point)

EXECUTIVE SUMMARY

This report analyzes the geology of the Oregon coastal zone including the Oregon Territorial Sea to assess the siting potential of landing sites for cables that carry information and/or power from offshore. We focus on subsea cables given current uses, but much of the information we have compiled will be relevant for other uses of the seafloor that may be covered by the Oregon Territorial Sea Plan, Part 4. We review the construction of cable landing infrastructure, particularly the cable landing sites where cables cross the shoreline through subsurface conduits commonly installed with the horizontal directional drilling (HDD) method. We review best practices and challenges in HDD construction, illustrated with examples of issues that occurred during construction of recent Oregon cable landing sites. Geologic hazards and processes that should be considered during siting and construction of cable landings are summarized. We present a summary of the geologic framework of the Oregon coastal zone that extends interpretive geologic mapping offshore across the Oregon Territorial Sea and synthesizes geologic units present within an equivalent distance onshore. The geology of the coastal zone defines the material that cable infrastructure must cross in the transition from offshore locations to terrestrial fiber optic networks or the power grid. Analysis of existing and new data provides a better understanding of coastal dynamics along the Oregon Coast that should inform siting future cable landings in positions that are resilient over infrastructure life cycles. Other new data improve understanding of geologic hazards and coastal geomorphology. The major analysis is a coastwide systematic survey that leverages many geospatial data layers produced in this project and obtained from other sources to assess the suitability of potential cable landing sites along the Oregon Coast in a comprehensive way. This effort provides a consistent, regional-scale view of where future cable landings can be built with fewer construction complications and impacts on the environment and communities. A major conclusion is that detailed, site-specific investigations of the many geologic, environmental, and cultural factors are needed to bridge between this coastwide reconnaissance effort and successfully completed projects.

1.0 INTRODUCTION

1.1 Background on Submarine Cables and the Oregon Coast

Cables that traverse the seafloor are an important component of modern infrastructure. Fiber optic communication cables transmit large volumes of data with low latency around the planet. Other cables transmit power generated at offshore wind or wave energy generating equipment to the onshore power grid. The locations where cables come onshore are critical parts of these systems, as the cables cross shallow water of the coastal zone where human interaction is more likely, and dynamic geologic processes are active. The nearshore terrestrial areas where submarine cables land also host many human communities and sensitive environments where there is potential for negative effects during construction activities. We recognize other potential future uses of the seafloor such as pipelines transporting fluids for energy. Much of the information in this report is relevant for other forms of seafloor infrastructure, but we specifically focus on considerations for routing and landing cables.

Coastal Oregon hosts landings for numerous cables, and future development of power and communications infrastructure is likely to drive additional landing sites. The first submarine telecommunication cable landing in Oregon was developed in 1995 (bandoncable.org, 2023), and a total of 17 telecommunication and research cables have been constructed as of early 2023, although some have been decommissioned (**Figure 1-1**). Current cables are distributed along the coast at nine landing sites in

six areas of the Oregon Coast, from the two at Bandon in the south to Warrenton in the north (**Figure 1-1**). Demand for increased data transmission capability and system redundancy is expected to grow into the future (e.g., Wopschall, 2023). Cables transmitting power from offshore marine renewable energy facilities are likely to drive demand for additional cable landings in Oregon. A cable landing site for offshore generated power was constructed on the central Oregon Coast in 2022 (Freeman and others, 2022; PacWave, 2022). Additionally, two areas have been designated for possible offshore wind development along the southern Oregon Coast (see yellow outlined areas, **Figure 1-1**)(BOEM, 2022).

Routing of cables and construction of cable landings are dependent on the geology of the continental shelf and coastal margin when best practices are followed (Wopschall, 2023). Ideally, cables are buried in sediment across the continental shelf to protect them from being damaged by fishing activities and other human or natural processes. Following U.S. standard practice, where a cable traverses nearshore water depths less than approximately 10 m (33 ft), the cable is routed through a borehole constructed through sediment and/or rock to protect it from wave action and human interference (Wopschall, 2023). The landward termination of a submarine fiber optic cable is located in a beach manhole where it transitions to a fronthaul route cable. The fronthaul portion of the cable system is often a few kilometers long and connects to a cable landing station where telecommunication infrastructure is housed (**Figure 1-2**). Fiber optic cables connect from the cable landing station along a backhaul route to a data center or internet exchange. Power cables have analogous on-land connections from the beach manhole to local substations or other power facilities that further connect into a regional electric grid (Wopschall, 2023).

Figure 1-1. Map of existing cable landings and cables along the Oregon Coast. The seafloor geology (Goldfinger and others, 2014) is unmapped outside of the colored area in the dataset. The Oregon Territorial Sea is the 3 nautical mile-wide strip of the Pacific Ocean adjacent to the shoreline.

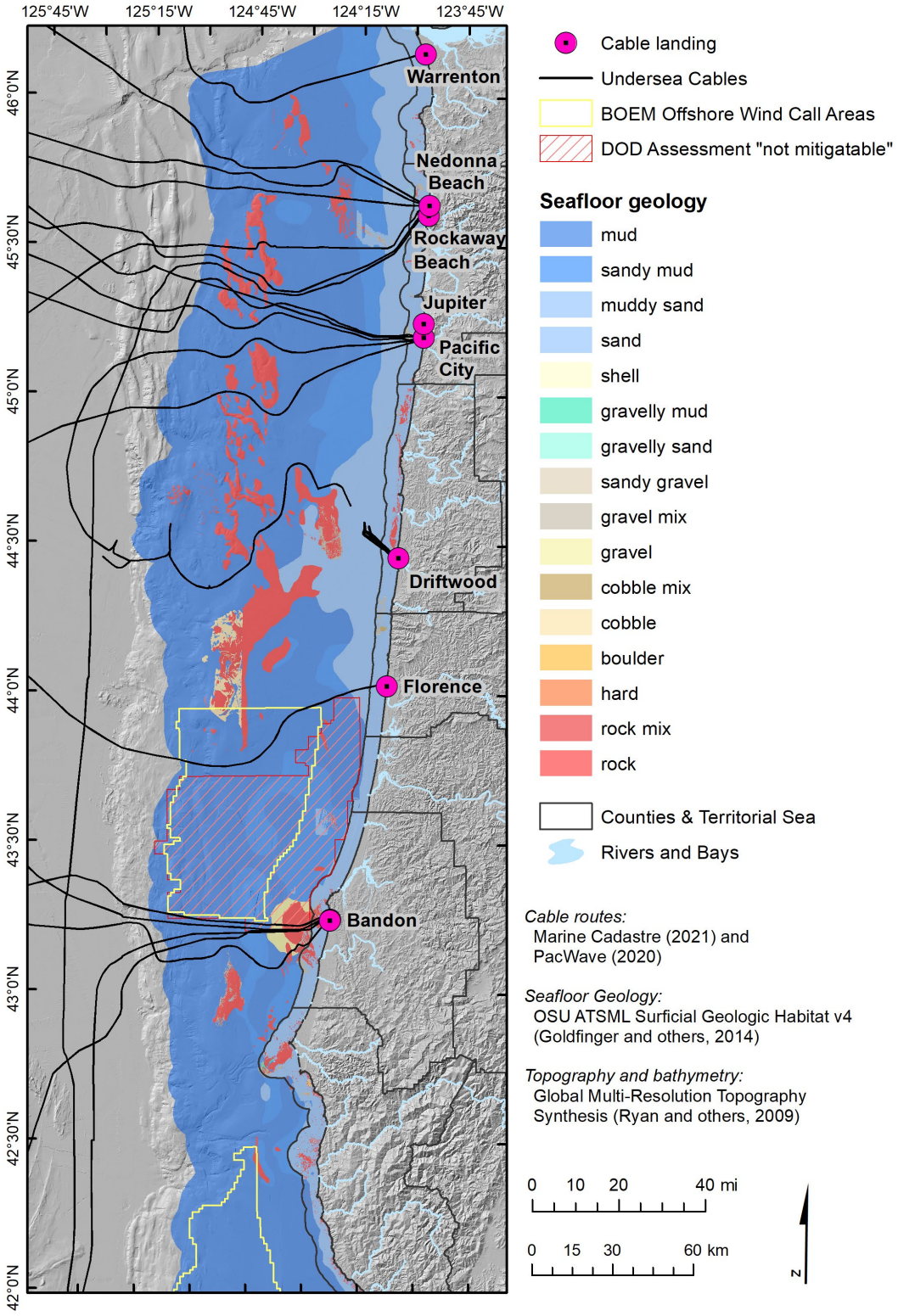

Figure 1-2. Schematic view of a cable landing showing components of a cable system in the coastal zone. Cables land at beach manholes via conduits emplaced in boreholes with horizontal directional drilling (HDD) methods. These holes are commonly drilled through the bedrock (e.g., Neogene sedimentary rock, Ng) to an offshore point where the cable is more shallowly buried in unconsolidated modern sediment, e.g., sand (Qs). From the beach manhole cables connect to other infrastructure on land (e.g. cable landing stations) that are commonly built on higher landforms such as the marine terrace depicted here (Qt).

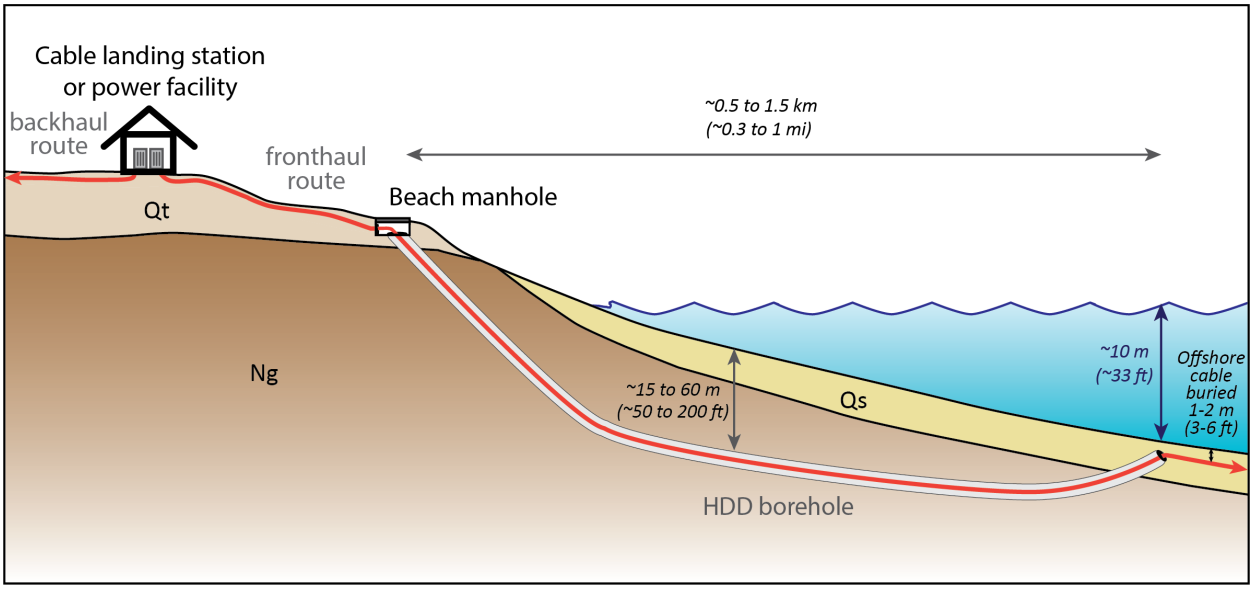

1.2 Scope of the Report

This report synthesizes geologic information along the Oregon Coast relevant to the siting, construction, and longevity of cable infrastructure. Details of the geology and coastal processes are particularly important for construction of cable landing sites where the cable is routed through the subsurface between a beach manhole and where it emerges at the seafloor below wave base (**Figure 1-2**). Consequently, we focus on an area of interest (AOI) that encompasses the Oregon Territorial Sea and a roughly equivalent distance inland. The Territorial Sea is defined as the strip of the Pacific Ocean under state jurisdiction that extends 5.5 km (3 nautical miles; 3.4 mi) westward from the coastline (**Figure 1-1**; OPAC, 1994). For the purposes of this report, AOI extends approximately 11.11 km (6 nautical miles; 6.9 mi) eastward from the western boundary of Oregon's Territorial Sea and follows the irregular shape of the Oregon Coast. The AOI extends 588 km (365 mi) from the Washington border (46°15'41" N) to the California border (41°59'54" N). This AOI represents most of the area that controls where cables may be routed across the inner part of the continental shelf and terrestrial geology along a coastal strip that is relevant to cable landing construction and resilience.

This report summarizes how boreholes are constructed to route cables through subsurface rock and sediment and potential complications that have been experienced in coastal Oregon as well as many other locations. The subsequent section summarizes the geology of the Oregon Coast and its influence on potential cable landing sites. We provide estimates of recent coastal change along the entire Oregon Coast from repeated observations to understand potential magnitudes of future erosion and deposition. We

review seismic and landslide hazards posed to coastal infrastructure. The geologic information is combined in a comprehensive suitability analysis to identify areas along the coast that are relatively more or less amenable to construction of resilient cable landing sites with minimal complications from the physical environment.

This study has a large geographic scope, and while we have endeavored to use the best available datasets, the results are necessarily relatively coarse. Many of the issues that arise during borehole drilling involve geologic heterogeneities at a spatial scale shorter than the most detailed geologic maps, and at depths inaccessible to comprehensive mapping and analysis. Additionally, the suitability analysis applies a strategy that is effective at integrating many factors over the length of the entire coast, but it cannot assess detailed suitability for a potential individual cable that could be planned in great detail. Many of the factors addressed here can and should be considered in site-specific studies in support of locating future cables that traverse the Oregon Territorial Sea. Our study provides a regional-scale starting point for understanding promise and challenges for landing cables in different locations along the Oregon Coast.

2.0 INTERSECTION OF GEOLOGY AND COASTAL PROCESSES WITH CABLE LANDING CONSTRUCTION AND CABLE LONGEVITY

The geologic history of the Oregon Coast and active Earth system processes produce spatially varying characteristics that are relevant to both the construction phase of a cable landing project as well as its resilience over the design life of a project. The initial portion of this section provides a review of the influences of geologic materials on the construction of cable landing sites. Secondly, we review geologic processes that pose a hazard to coastal infrastructure including offshore cables and on-land portions of utility systems. Subsequent sections summarize specific characteristics along the Oregon Coast that are relevant to the issues highlighted here.

2.1 Overview of Cable Landing Construction and Potential Challenges

New cable landing sites are commonly chosen based on the availability of a suitable beach manhole site where a cable can come onshore within some proximity (<10 km; <6.2 mi) to a new or existing cable landing station that is connected to an existing or new backhaul route (**Figure 1-2**; Wopschall, 2023). A key component of a cable landing is the construction of a subsurface conduit that connects the beach manhole to a point offshore where the cable emerges onto the seafloor. An early Oregon cable landing at Nedonna Beach was constructed using direct trenching of the beach (**Figure 1-1**; McMullen, 1999). More recently, the most common practice in the United States involves the emplacement of conduits through boreholes constructed with the horizontal directional drilling (HDD) method (Wopschall, 2023). Recent Oregon cable landing construction has employed HDD methods to minimize impacts to the shore and to provide deeper burial and protection of cables.

HDD is a common construction practice that allows emplacement of pipes and/or cables into the subsurface over distances up to approximately 1500 m (5000 ft) from a surface endpoint. In HDD construction, a borehole is excavated as a drill head is steered through sediment and/or rock along a precise trajectory from a surface entry point to surface exit point. Conduit pipes can be pulled through a completed borehole or, as is common practice for Oregon cable landings, the conduit pipe can be used as the drill string and left in place upon intersection of the seafloor at the punchout location (Bennett and

Ariaratnam, 2017; ERM, 2020). Construction strategies are similar for both fiber optic and power cable landings, although conduits are thinner diameter (~10 to 13 cm; ~4 to 5 in) for fiber optic cables, and thicker (20 cm; 8 in or greater) for power cables (Wopschall, 2023). On land, HDD methods are commonly used where the disturbance of trenching and direct burial of cables or pipes would harm sensitive habitat or the built environment. While the HDD method generally produces minimal surface impacts, three classes of potential issues have been identified: pipe stress, inadvertent return (IR), and settlement (Bennett and Ariaratnam, 2017). Most of the existing Oregon cable landings have been constructed without publicized problems, but public records show that all three of these complications have arisen during the construction of two recent cable landings on the Oregon Coast.

2.1.1 Drilling conditions and pipe stress

Adequate geotechnical investigation and engineering design preceding an HDD project are key for successful project completion (Bennett and Ariaratnam, 2017). Understanding the properties of materials that will be encountered along the subsurface drill path is a critical component for planning the equipment and methods that are appropriate for a particular project. Methods for assessing the subsurface material include interpretation of local geology, geophysical imaging, and testing and sampling subsurface sediment or rock using vertical borings along the proposed HDD route. Subsurface information from complementary geophysical methods like seismic velocity and electrical resistivity are less invasive than drilling methods and can be applied over challenging nearshore wave environments (e.g., Alcorn and others, 2017).

HDD projects have been executed successfully through many geologic materials; however, some subsurface materials are more problematic than others. The HDD Good Practices Guidelines identifies the following materials as involving high levels of risk that may preclude HDD construction: boulders, cobbles, gravel, wood, hard or variable rock, and anthropogenic fill debris or structures (Bennett and Ariaratnam, 2017). Risks posed by these materials grow with greater size, frequency, and hardness along a proposed bore path. Subsurface voids or high artesian groundwater pressure are other problematic conditions for HDD construction.

Once the likely subsurface material has been characterized, planning the details of the borehole design and construction equipment and materials is important for successful drilling. Matching drill bits, drilling equipment, and drilling mud characteristics to the local material ensures that a project can be completed in a safe and efficient manner. The planned borehole geometry must be designed to transit from the entry point to the subsea exit point through appropriate rock and sediment, with curved segments that will not exert stress on the drill string (pipe) in excess of its strength during the dynamic drilling process. In the event of breakage of the drill string, continuity of the drilling equipment is lost, and collapse of the well bore is possible if specialized tools are not available on site to retrieve the drill head and pipe stranded in the subsurface.

Breakage of a drill string occurred during construction of the Jupiter cable landing in Tierra del Mar, Oregon in April, 2020 (**Figure 1-1**; ERM, 2020). Based on initial geologic and geophysical reconnaissance for the project, consistent soft sedimentary rock was expected along the bore path. However, the drill head encountered unexpected harder rock approximately 515 m (1690 ft) from the drill site. Drilling speed, thrust, and drill bits appropriate for soft rock were applied, the drill string experienced stress that exceeded the design specifications of the steel drill pipe, and a pipe segment broke, disconnecting ~357 m (1170 ft) of pipe and drill head assembly from the surface drilling operation (ERM 2020, Edge Cable Holdings USA LLC, 2020). Attempts to retrieve the broken drill pipe were unsuccessful, and the remaining

intact drill string and casing were removed. This resulted in the collapse of the borehole and stranding of the drill head and broken pipe along with bentonite-water drilling mud roughly 15.2 to 21.3 m (50 to 70 ft) below the seafloor (ERM, 2020). Subsequent seismic and electrical resistivity studies showed a body of rock with higher density in the offshore subsurface (SubCom, 2020). Based on the geophysical properties and geologic setting, this harder body was interpreted to be an invasive basaltic dike or a more indurated portion of sandstone trending north-south across the planned borehole route (SubCom, 2020). A revised drilling plan was formulated to deal with the harder rock portion of the borehole (Edge Cable Holdings USA LLC, 2020), and the HDD conduit portion of the cable landing was completed by March 2021 (OPRD, 2022).

2.1.2 Inadvertent return (IR)

One of the risks associated with HDD construction projects is inadvertent return (IR) that results in the loss of drilling fluid out of the borehole during construction. The pressurized drilling mud can escape into the surrounding material and can flow through a fracture or other permeable pathway onto the surface. The drilling mud is commonly a mixture of bentonite clay and water with minor additives that control gel strength, and is generally perceived as relatively environmentally benign (e.g., ERM, 2020). The most serious impacts are those associated with IRs that discharge mud into areas of sensitive habitats where ponding and burial of the land surface or seafloor will adversely affect the local organisms (Bennett and Ariaratnam, 2017). IRs are also more consequential where the drilling path underlies areas of cultural importance or the built environment. Impacts on groundwater from IR events that do not reach the surface are thought to be less impactful, with local changes in aquifer permeability as the primary effects (Nachman and others, 2021). We have not found documentation of the frequency of IRs during HDD projects in the U.S., but such issues appear to be relatively common. One study based on interviews with HDD contractors found that IR is one of the most probable complications in HDD projects (Onsarigo and others, 2014). The two most recent Oregon cable landing HDD projects both experienced IR events (HGI, 2021; PacWave Energy, 2022).

An IR occurs when the pressure of the mud that circulates during drilling and keeps the borehole from collapsing exceeds the strength of the sediment or rock being drilled. This condition can be reached in cases where the annular pressure exerted around the borehole is greater than the strength and confining stress of the intact soil or rock, producing a hydraulic fracture that propagates toward the surface (Bennett and Ariaratnam, 2017). The drilling fluid (slurry of water and clay) will follow the fracture out of the borehole and potentially reach the surface above the bore path. This fracture process has led to IRs being referred to colloquially as “frac-outs”. IRs also commonly occur in situations where heterogeneities in the permeability structure of the materials being drilled result in a lower local capacity of near-surface sediment to retain mud in the borehole. Examples of these situations include natural fractures in the soil, seepage paths along anthropogenic structures, and gravel layers with large, connected pore spaces (Bennett and Ariaratnam, 2017).

The risks of IR can be minimized by designing HDD projects so that downhole pressures will not exceed the strength of the material being drilled (Bennett and Ariaratnam, 2017). The risks of IR are greatest near the entry and exit points of boreholes, where confining pressures are low and less consolidated soil and sediment is common (e.g., Macauley Trenchless and Jacobs, 2020). Boreholes constructed with shorter lengths, wider diameters, and greater depths exert less pressure on the wall material relative to the confining pressure (Bennett and Ariaratnam, 2017). Other mitigation measures include use of conductor casing over the initial portion of the borehole, careful design of drilling fluid composition and

circulation rates, and detailed monitoring of downhole fluid pressures (Bennett and Ariaratnam, 2017). Conductor casings are larger diameter pipes emplaced into the upper part of the borehole to confine the drilling fluid in the part of the borehole most susceptible to IR. The IR issues experienced at the PacWave cable landing project (**Figure 1-1**) occurred near the downhole end of a conductor casing, and were thought to result from an imperfect seal of the casing with the stronger rock at greater depth (PacWave Energy, 2022).

The second key for mitigating IR is developing an understanding of the distribution of the types and strengths of soil and rocks that will be encountered along the boring route. This information can be found through pre-HDD vertical borings, geophysical surveys, rock property testing and knowledge of the local geology to match the technical approach of the drilling program to the specific locality (Bennett and Ariaratnam, 2017; Terracon, 2020). Broad engineering properties of Oregon coastal rocks have been described in early reconnaissance reports (e.g., Schlicker and others, 1972; 1973). However, specific behavior of rock units is generally not available in peer-reviewed literature. Informal public information regarding the PacWave energy cable landing south of Newport, Oregon, describes swelling of the Nye Mudstone when pressurized by drilling fluid, resulting in even greater annular pressures than would be predicted for most rocks (Kramer, 2022; Kezdi, 2022). Building and using knowledge of the relevant local geology will improve the success of future installations. Some irregularities in subsurface soil and rock properties, such as preexisting fractures, are unlikely to be recognized in every case prior to drilling, making IRs a risk associated even for well-planned projects. Careful monitoring for IR events and advance preparation for containing and remediating surface spills are important steps in addition to other project design considerations (Bennett and Ariaratnam, 2017). Identifying and avoiding areas where an IR spill would have unacceptable impacts on environmental or cultural features that could not be reasonably remediated may be necessary in the most sensitive areas.

2.1.3 Settlement

A third type of issue is settlement or subsidence of the land surface above the HDD borehole. Settlement issues above HDD projects have been classified as either large or systematic (Bennett and Ariaratnam, 2017). Larger amounts of settlement are generally associated with drilling larger diameter void spaces or drilling through adverse material where collapse of the overlying material during drilling produces larger cavities than the planned borehole. Systematic subsidence above HDD bores occurs due to collapse of annular space between the borehole wall and installed conduit as well as compaction of the soil due to drilling disturbance (Bennett and Ariaratnam, 2017). Geologic conditions that favor greater subsidence involve the presence of weak soils, soft clay and/or silt, or well sorted (poorly graded) loose sand, and loose gravelly sand (Bennett and Ariaratnam, 2017).

Similar to avoidance of the preceding HDD complications, one of the principal ways to minimize the risk of settlement is through a detailed understanding of the subsurface geologic material and how material properties may vary along and above the planned bore path (Bennett and Ariaratnam, 2017). Deeper bore path geometries are less likely to produce significant surface settlement. The construction of smaller diameter boreholes and smaller annular volumes around the emplaced conduits during drilling also limits effects of subsidence once the borehole collapses around the pipe. Practices that keep the borehole filled with drilling fluid during construction minimize opportunities for borehole collapse and widening during drilling. Grouting the annular space of completed HDD boreholes is another way to avoid surface subsidence (Bennett and Ariaratnam, 2017). However, standard practice for construction of cable landing boreholes that have an exit point on the seafloor is to flush the drilling fluid out of the borehole

with water during the drilling of the last ~45 m (~150 ft) prior to punchout (e.g., Edge Cable Holdings USA LLC, 2021a), which may be incompatible with filling completed boreholes with grout.

The recent Oregon case of observed settlement occurred above the HDD bore at the Jupiter cable landing site. Up to four sinkholes formed along the cable conduit route near the base of the vegetated small coastal bluff seaward of the beach manhole (OPRD, 2022; Edge Cable Holdings USA LLC, 2021b). The sinkholes were observed in April and November, 2021, following the completion of HDD construction in March 2021 (OPRD, 2022). The largest sinkhole was reported as ~0.9-1.2 m (3-4 ft) wide and ~1.5-1.8 m (~5-6 ft) deep, and the holes were filled with sand in response (OPRD, 2022). The portion of the borehole where the surface voids formed was above part of the HDD bore that had a 40.6 or 45.7 cm (16 or 18 in) conductor casing installed during construction. Upon complete installation of the ~16.5 cm (~6.5 in) fiber optic conduit, the larger pipe was removed (OPRD, 2022; Edge Cable Holdings USA LLC, 2021a; 2021b). Contractors involved with the installation interpreted these settlement features to be related to collapse of the annular space surrounding the conduit accompanied by local pit formation at the surface (Edge Cable Holdings USA LLC, 2021b). The timing of the sinkhole formation was interpreted to be related to changes in the water content of the subsurface sand due to high tides or other hydrologic changes that promoted mobility of the sediment around the HDD bore (Edge Cable Holdings USA LLC, 2021b). Electrical resistivity and seismic surface wave surveys did not show subsurface voids of resolvable size, supporting the interpretation that the sinkholes were related to settlement accompanying the removal of the guide casing (HGI, 2021). The sinkhole areas were remediated through filling with sand and compaction during high tide intervals. We are unaware of subsequent settlement associated with this project.

As with IRs the impact of settlement related to HDD construction is also coupled with the susceptibility of the overlying built and natural environment to be damaged by the process. Where HDD bores are constructed below roads, buildings, and other pipes, for example, relatively modest amounts of settlement may produce significant negative effects (Bennett and Ariaratnam, 2017). Equivalent amounts of spatially distributed subsidence in a vegetated area or area of high sediment mobility (e.g., dunes or beach) may be difficult to recognize and have minimal effects. With better understanding of the engineering properties of the soil, sediment, or rock overlying a planned borehole, the potential for localized settlement and sinkhole formation can more likely be predicted and mitigated in the design and construction phases of a project. Competing goals for cable landing boreholes need to be balanced against each other, e.g., the need to flush out drilling mud during borehole completion, the use of large diameter casing to prevent IRs, and avoiding settlement may be in conflict with one another and require careful planning and management of risk.

Overall, the reported incidents and potential for other complications during construction motivate developing a detailed understanding of the local geology along the proposed path of cables. These risks during construction may be mitigated by investigation and engineering planning, but the potential for unknown complications may motivate siting facilities where an unforeseen disruption above the cable trajectory will not damage sensitive natural areas, cultural features, or the built environment.

2.2 Resilience of Cable Infrastructure

In addition to the construction considerations for siting and emplacing a cable across the shoreline, there are other factors that control the favorability of different sites along the coast. Geologic and surficial coastal processes can damage cables on the seafloor as well as the related infrastructure onshore such as

cable landing stations. This section summarizes conditions and processes that are relevant to building cable landings that cause minimal impact to the environment and are resilient to natural hazards.

2.2.1 Rocky seafloor

The Oregon shoreline and seafloor have spatially variable rock and sediment types exposed at the surface due to the geologic history and ongoing geologic processes. Most existing cable routes that land on the Oregon Coast avoid exposed rock on the seafloor (**Figure 1-1**), for multiple reasons. First, rocky seafloor is an important habitat for sensitive species and fisheries, so avoiding rock outcrops minimizes negative impacts on the fishing industry and marine life (e.g., TSP, Part 3). Second, routing cables through sandy portions of the seafloor over the depth range where commercial fishing occurs allows subsurface burial that protects cables from accidental damage (Wopschall, 2023). Third, burial of cables in loose sediment also protects cables from being abraded on rocks when agitated by currents (Wopschall, 2023).

Rocky versus sediment-mantled seafloor reflects the geologic history of the Oregon continental shelf. Rock outcrops occur where more erosion-resistant rock types are near the surface, such as the basaltic rocks that form many of the headlands along the central and northern Oregon Coast. Other areas of rock correspond to areas of local uplift that are produced by the many faults and related folds that have grown in the recent geologic past in the forearc prism of the Cascadia subduction zone (CSZ) (e.g., McNeill and others, 2000). The distribution and types of sediment present on the seafloor are also related to inputs of clastic sediment from river systems that transport eroded geologic material from terrestrial western North America. Marine current systems redistribute sediment on the continental shelf, and farther offshore; submarine channels transport sediment to the deep seafloor and CSZ trench system via turbidity currents and other processes. Additionally, fluctuations in global sea level of ~100 m (~330 ft) over the last few million years have caused cyclic migration of the shoreline and associated progradation of terrestrial river systems and other environments across parts of the continental shelf.

Surficial geologic material types, or substrate types, have been mapped through many different surveys, and we use the most recent compilation produced by the Pacific Marine and Estuarine Fish Habitat Partnership (PMEP, 2022) that enhances mapping by Oregon State University Active Tectonics and Seafloor Mapping Laboratory (Goldfinger and others, 2014) with nearshore mapping by the Oregon Department of Land Conservation and Development. This dataset provides comprehensive coverage of the Oregon Territorial Sea and the continental shelf, with varying spatial resolution. This compilation of substrate material provides critical regional-scale information for broadly planning future cable placement in a way that will minimize conflict with other uses of the Oregon Territorial Sea and protect submarine cables from damage. A key contribution of this report is an effort to apply the lithologic mapping of rock and sediment units offshore across the Oregon Territorial Sea, integrating the substrate type with interpretations based on the more exposed and accessible geology mapped onshore.

2.2.2 Coastal dynamics

Another important consideration for how and where to site cable landing infrastructure is the action of coastal processes that erode or accrete sediment and rock to and from the seafloor and coastline. Wave energy and currents vary spatially and are changing some portions of the coast more rapidly than others. Ongoing sea-level rise will amplify these processes in predictable ways. Understanding these processes is important for ensuring that seafloor cables remain protected within boreholes below shallower water depths where wave action in storms causes erosion and deposition on interannual timescales. Resolution of the pattern of coastline change is helpful for avoiding erosion that can damage beach manhole locations (e.g., **Figure 2-1**; Wopschall, 2023). Observations of spatial patterns and magnitudes of erosion and deposition across the shallow seafloor and coastline are key to developing landing sites with suitable

setbacks. We summarize existing observations of coastal change and present new analysis for the entire Oregon Coast in Section 4.

Figure 2-1. Cable landing infrastructure exposed by coastal erosion in the Rockaway Beach, Oregon area in late 2001. Image source: J. Allan.

2.2.3 Landslides

Landslides are a common geologic hazard along the Oregon Coast. Combinations of steep slopes, large areas of weak rock, and high precipitation drive both shallow and deep-seated landslides in the mountains of coastal Oregon. Along the shoreline, unconsolidated sediment and active coastal erosion at the foot of bluffs makes many slopes unstable. This hazard is spatially variable, and therefore, we use SLIDO, the statewide compilation of landslide hazard (Franczyk and others, 2021) to assess exposure to this process. Beach manholes are commonly sited in nearshore, upland areas like marine terraces and bluff tops. Best practices that emplace the cable in the subsurface via HDD construction should largely avoid cable damage associated with landsliding, but larger, deep-seated coastal landslides could potentially damage cables where they come onshore if landings are not designed appropriately. Cable landing stations are more likely to be sited away from local steep slopes along the coast but may also be exposed to landslide hazard related to steep mountain slopes that flank the developed coastal plains.

Farther offshore, submarine landslides that produce turbidity currents pose a hazard to cables that cross the continental shelf. This hazard is faced by nearly all transoceanic cables, and damage to fiber optic cables in turbidity currents is common (Carter and others, 2014), although much less frequent than damage due to fishing vessels (Wopschall, 2023). Most major turbidity currents in the Holocene (last ~10 ka) along the continental margin offshore of Oregon have been interpreted as being triggered by CSZ earthquakes, which suggests this hazard may be linked to earthquake occurrence (e.g., Goldfinger and others, 2012), although earthquake triggering appears to vary globally (Pope and others, 2017). We do not specifically address offshore mass movement hazards given our focus on the Oregon Territorial Sea.

2.2.4 Earthquakes and associated hazards

Western Oregon is exposed to seismic hazards from two classes of faults. The most impactful source is the CSZ, which is a major plate boundary fault that accommodates relative convergence between the continental North America tectonic plate and the smaller oceanic Juan de Fuca plate to the west. The subduction zone produces large earthquakes (M8 to M9.1) that rupture part or all of the plate boundary zone from northern California to southern British Columbia (e.g., Walton and others, 2021). There are also many smaller faults within the crust of western Oregon that host smaller earthquakes (<M ~7.5) at longer repeat intervals (Madin and others, 2021; Goldfinger and Beeson, 2023). These crustal faults pose significant hazard to local areas due to proximity of the earthquake source to people and infrastructure. There are several aspects of earthquakes that produce damage that can affect cable infrastructure.

2.2.4.1 Shaking

One of the most direct components of earthquake hazards is shaking caused by the elastic seismic waves produced when a fault experiences rapid slip. Expected levels of shaking for a CSZ earthquake, like the most recent one that occurred January 26, 1700, are predicted to be intense for the coastal fringe of Oregon (Wirth and others, 2021; Madin and others, 2021). The probability of a Cascadia earthquake in the 25-to-40-year lifecycle of an undersea cable is uncertain depending upon the details of recurrence models and interpretation of the paleoseismic and historical records (e.g., Walton and others, 2021; Melgar, 2021). However, published estimates of the probability of a large earthquake range from ~16% to 22% in the next 50 years (Goldfinger and others, 2017) to as high as 37–43% for a partial rupture of the subduction zone in southern Cascadia (Goldfinger and others, 2012), necessitating engineering and construction of the most and critical infrastructure, like cable landing stations, to survive likely levels of shaking. Lower levels of shaking are expected at the same probability threshold for crustal faults given their smaller magnitudes and slower slip rates/longer repeat times (Madin and others, 2021).

2.2.4.2 Ground rupture and vertical displacement

Another direct hazard from earthquakes is the sudden, localized displacement of the ground surface or seafloor that occurs when a fault experiences an earthquake. Cables or buildings that are anchored on two sides of a fault may experience damage as they experience high levels of strain when a fault slips. The relatively low probability of crustal faults experiencing displacement over the design life of a cable may not justify costs to mitigate this hazard, but where cable landing infrastructure and cable routes both offshore and onshore can avoid known active faults, communication or power cables will be more resilient. In the case of cables crossing the Cascadia megathrust, building in flexibility for cables to accommodate possible large (10 m/33 ft or more) displacement of the seafloor may be justified. A classic example of a well-engineered fault crossing comes from the Alaskan Pipeline that survived displacement across the Denali fault during the 2002 earthquake (Fuis and Wald, 2003).

A distributed mode of crustal displacement occurs during large earthquakes due to changes in elastic strain in the crust. Between Cascadia earthquake events, most of the Oregon Coast is rising at rates up to ~3.5 mm/yr (~0.13 in/yr) (Burgette and others, 2009). This uplift is roughly reversed during earthquake slip with most parts of the Oregon Coast experiencing coseismic subsidence of decimeters (1 dm = 3.9 in) based on marsh studies (e.g., Walton and others 2021). The details of seismic cycle deformation are more complex than this simple model; however, the likelihood of subsidence in an earthquake warrants considering the effects that would accompany the large, instantaneous rise of sea level relative to the land.

2.2.4.3 Tsunamis

Tsunamis are unusually large waves produced when the ocean water column is suddenly displaced by fault movement or a landslide. There are records of large tsunamis generated during CSZ earthquakes that have repeatedly inundated the Oregon Coast (e.g., Nelson and others, 2021; Goldfinger and others, 2017). Tsunami waves generate strong currents as seawater flows over the land that can cause large magnitudes of erosion, destruction of buildings, and exposure of buried infrastructure. In addition to the large-magnitude tsunamis triggered by local Cascadia earthquakes, the Oregon Coast is also impacted by smaller tsunami waves generated by distant sources like other subduction zones in the northern Pacific basin (Allan and others, 2018). The most hazardous distant tsunami sources are from the Aleutian area of southwestern Alaska that may produce inundation of several meters (feet) along the Oregon Coast (González and others, 2009). Modeling of potential tsunami effects has been completed for the Oregon Coast (Priest and others, 2010; Witter and others, 2013), and the best practice is to site critical facilities like cable landing stations outside of the local tsunami hazard zone (Wopschall, 2023). Beach manhole locations are necessarily closer to the coastline and many locations will be within local tsunami hazard zones, but siting these facilities at the highest elevations that permit reasonable HDD drilling distance to the desired offshore depth will make landings more resilient to tsunami damage.

2.2.4.4 Liquefaction

Liquefaction is a process that affects water-saturated, unconsolidated sediment during cyclic agitation of such as that which occurs during earthquake shaking. Some types of sediment are more susceptible to experiencing this effect during earthquakes. High levels of instability of the ground surface produce much greater levels of earthquake-related damage than that experienced by structures built on more stable geologic material. Regional-scale data are available for liquefaction susceptibility across Oregon based on geologic mapping (Madin and others, 2021). Siting infrastructure on material less prone to liquefaction improves the resilience of communication and power systems in the event of crustal or subduction zone earthquakes.

2.2.4.5 Coseismic landslides

Earthquake shaking dynamically changes the near-surface stress field, and slopes that are stable under static gravitational loads may experience landslide instability (e.g., Schulz and others, 2012). The triggering potential is further elevated if an earthquake occurs in a season when the groundwater table is high; pore-water effects seem to be the dominant trigger for landslides in the Oregon Coast Range (OCR) (LaHusen and others, 2020). Overall, the spatial patterns of earthquake-generated landslide susceptibility are similar to the relative patterns of normal landslide potential. The enhanced landslide sensitivity during earthquakes motivates greater caution when constructing infrastructure in coastal Oregon.

3.0 GEOLOGY OF OREGON'S COAST AND TERRITORIAL SEA

3.1 Geographic and Physiographic Setting of the Oregon Coast and Territorial Sea

3.1.1 Northern province

The northern province begins at the Washington/Oregon border at the mouth of the Columbia River, north of Fort Stevens State Park and extends southward to Newport and is subdivided into segments N1 and N2 (**Figure 3-2**). This section of the Oregon Coast is characterized by prominent headlands with steep

slopes including Tillamook Head, Cape Falcon, Cape Meares, Cape Lookout, Cascade Head, Cape Foulweather, and Yaquina Head (**Figure 3-1**). Relief from sea level through rocky sea cliffs to high points in the headlands ranges from ~60 m (~197 ft) at Yaquina Head to ~400 m (~1,312 ft) at Cascade Head. The coast between the prominent headlands is characterized by outlets of rivers, many with wide floodplains, which drain the western slope of the OCR. These include the Columbia, Nehalem, Wilson, Nestucca, Siletz, and Yaquina Rivers. The river mouths typically co-occur with sandbars and barrier spits that separate the estuaries from the open ocean. Mixing between fresh and seawater occurs in the estuaries that have formed as drowned river valleys mainly due to post-Pleistocene sea-level rise and the cycle of interseismic uplift and coseismic subsidence associated with subduction of Cascadia earthquake occurrence (e.g., Kelsey and Bockheim, 1994; Burgette and others, 2009; Walton and others, 2021). Beaches in the northern province range are variably backed by prominent foredunes and/or uplifted coastal marine terraces that connect to the higher topography of the OCR.

Population centers within the northern province include Warrenton, Gearhart, Seaside, Cannon Beach, Manzanita, Garibaldi, Rockaway Beach, Oceanside, Netarts, Pacific City, Tierra del Mar, Neskowin, Lincoln City, Depoe Bay, Beverly Beach, and Newport (**Figure 3-1**). Larger population centers such as Astoria and Tillamook are located within 12 km (~7.5 mi) of the shoreline but are outside of the Oregon Coast and Territorial Sea study area. US Highway 101 traverses the northern province from north to south starting in Warrenton in the north and stays within ~1.5 km (~1 mi) of the shoreline except where it veers inland around headlands and estuaries. The main transportation corridors that connect to the Willamette Valley include US Highway 30, which follows the south bank of the Columbia River to Portland, US Highway 26, which extends from US Highway 101 between Seaside and Cannon Beach east toward Portland, and State Highway 6, which connects Tillamook to State Highway 26 in Banks in the Tualatin Basin. State Highway 18 connects to US 101 near Lincoln City and extends east through Grand Ronde to the western Willamette Valley near Willamina. US Highway 20 connects to US Highway 101 at Newport and extends east to Philomath and Corvallis. Several small state routes and highways interconnect communities within this region of the Coast Range.

3.1.2 Central province

The central province extends from Newport in the north to Coos Bay in the south and is subdivided into segments C3 and C4 (**Figure 3-2**). This province of the Oregon Coast is characterized by generally lower topographic relief than the northern province. A few prominent basalt headlands exist in along the central Oregon Coast, in segment C3, between Newport and Florence. These include Cape Perpetua (elevation ~200 m /~650 ft) and Heceta Head (elevation ~75 m /~250 ft) (**Figure 3-1**). Besides these headlands, sea cliffs that occur in this province are mostly the result of wave erosion into uplifted Quaternary coastal marine terraces (Hapke and others, 2014). Between Heceta Head and Coos Bay, the distance between the shoreline and the higher topography of the OCR increases and the landscape becomes dominated by large tracts of active and inactive, vegetated sand dunes and contains intra-dune lakes such as Siltcoos Lake (Peterson and others, 2007; Hunter and others, 1983). The rivers in the Central province are the Yaquina, Alsea, Yachats, Siuslaw, Umpqua, and Coos.

The main population centers in the Central province are Newport, South Beach, Waldport, Yachats, Florence, Reedsport, and Coos Bay (**Figure 3-1**). U.S. 101 remains the main north-south transportation corridor within ~1.5 km (~0.9 mi) of the shoreline except where it veers to ~3 km (~1.9 mi) inland near Florence and Reedsport. US Highway 20 and Route 34 link Newport and Waldport to the Corvallis area, Oregon Route 126 joins Florence to the southern Willamette Valley in Eugene, and State Route 38 provides access from Reedsport to the I-5 corridor south of Cottage Grove.

Figure 3-1. Map of the Oregon Coast showing major headlands, estuaries, towns, and highways. The left panel shows northern Oregon; the right panel depicts the southern coast.

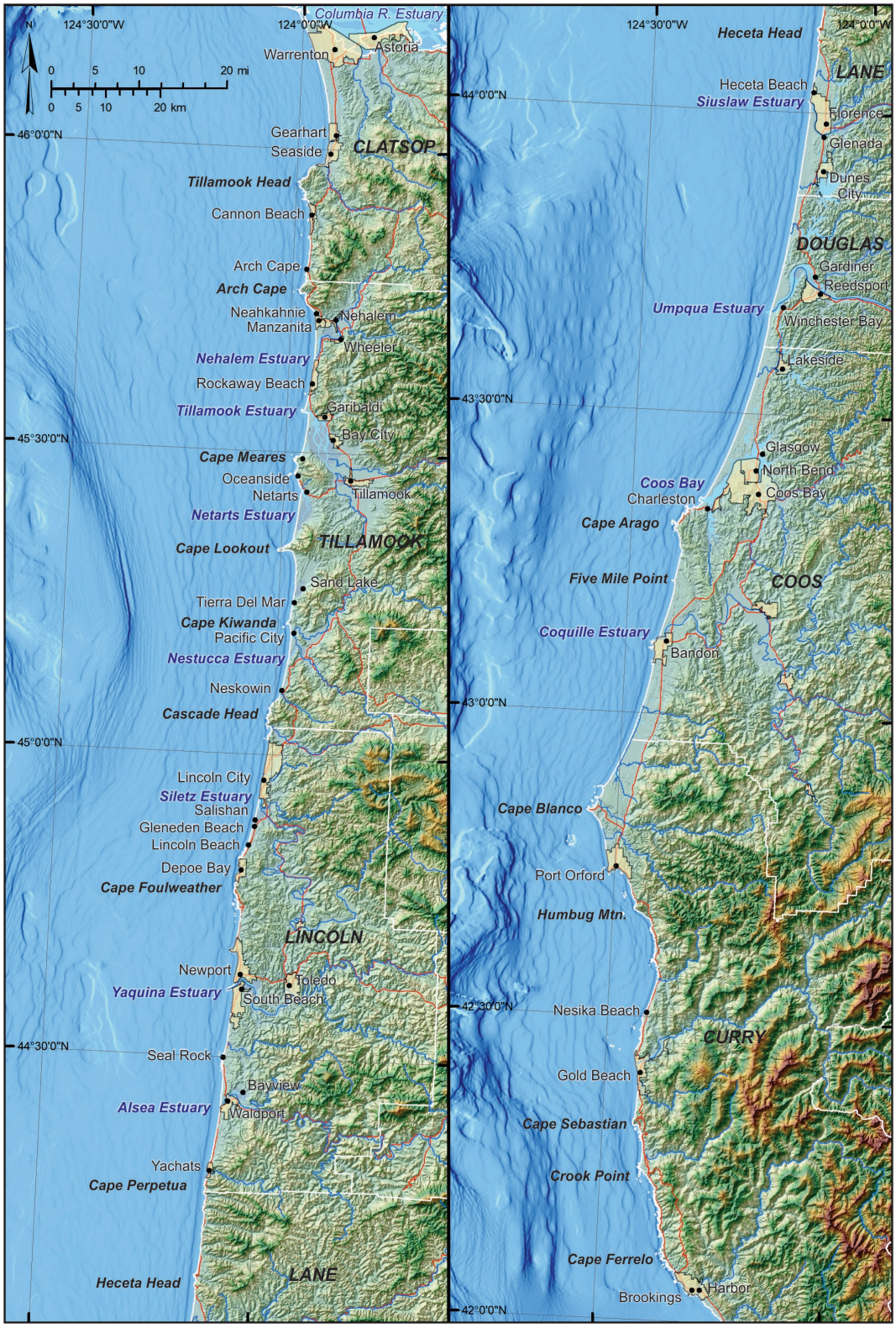

3.1.3 Southern province

The Southern province of the Oregon Coast extends south from Coos Bay to the California border and is subdivided into segments S5 and S6 (**Figure 3-2**). The topography of this province is typified by a commonly narrow (0 to 7 km/0.0 to 4.3 mi wide) flight of marine terraces that transitions abruptly into the southern part of the Oregon Coast Range (OCR) and Klamath Mountains. The Klamath Mountains are the most rugged portion of the Oregon coastal mountains, with greater elevation, topographic relief and catchment-averaged erosion rates than the OCR to the north (Balco and others, 2013). The mountains are flanked by marine terraces which record ongoing rock and surface uplift associated with CSZ and Mendocino triple junction deformation. This province of the study area is drained by several watersheds whose rivers flow into the Pacific Ocean, including the Coos, Coquille, Sixes, Elk, Rogue, Pistol, Chetco, and Winchuk Rivers.

The main population centers south of Coos Bay include Charleston, Bandon, Port Orford, Ophir, Nesika Beach, Gold Beach, Pistol River, and Brookings (**Figure 3-1**). South of Coos Bay, US 101 reaches its farthest from the shoreline in the state of Oregon, approximately 14 km (8.7 mi), and it remains inland until it reaches Port Orford, where it continues to follow the coast. State Route 42 connects Coos Bay to the Roseburg area to the east. State Route 542 travels south from Coos Bay and connects to Gold Beach via an inland route through the OCR.

3.2 Geologic Setting of the Oregon Coast and Territorial Sea

The geologic features of the Oregon Coast and adjacent Territorial Sea (**Figure 3-2**) are the result of an active and ongoing process known as subduction, which is occurring at the westernmost edge of the North American continent at the latitude of the state. This boundary is known as the Cascadia subduction zone (CSZ), and it is where two different types of fragments of Earth's lithosphere (also known as tectonic plates) meet at a convergent margin. Subduction is the process by which the thinner and denser fragment of oceanic lithosphere that is known as the Juan de Fuca plate slides beneath the thicker and more buoyant continental lithosphere of the North America plate at the CSZ (e.g., Walton and others, 2021). The CSZ extends for more than 1,300 km (807 mi) from the northern end of Vancouver Island, British Columbia to Cape Mendocino, California (Walton and others, 2021). The Juan de Fuca plate is moving in a generally eastward direction relative to the Oregon forearc, at a rate of 30-32 mm/yr (1.2-1.3 in/yr) (McCaffrey and others, 2007; Burgette and others, 2009). The surface expression of the CSZ plate boundary between Juan de Fuca and North America off the Oregon Coast is identified by where the lower continental slope meets the abyssal plain, ~120 km (~74 mi) west of Astoria in the north and to ~77 km (~48 mi) west of Brookings in the south (**Figure 1-1**; **Figure 3-2**; Komar, 1997). The Juan de Fuca plate is overridden by the North America plate, and it dips to the east as it dives deeper into the Earth's mantle. The geological complexity of the OCR and Territorial Sea is owed to the 400-million-year geologic history of subduction-related processes. These include folding and faulting, rock and surface uplift that causes erosion and extensional faulting, subsidence that localizes sedimentation, large-scale landsliding, intrusion of molten rock into the overriding plate (notably forming volcanoes of the Cascade Range), and underplating of rock scraped from the lower plate (e.g., Darin et al., 2022). The oceanic plate transports crustal scraps to the subduction zone in a manner like a conveyor belt.

Figure 3-2. Tectonic setting of the United States, Pacific Northwest region displaying the CSZ, regional plate boundaries, and particular Quaternary faults on the North American plate (modified after Nelson and others, 2004). Barbed line is assumed to be the surface projection of the Cascadia thrust fault, where the abyssal plain meets the continental slope. Major Cascade Range volcanoes are shown as triangles. The provinces of the Oregon Coast included in this study are identified by north (N), central (C), and south (S), each one of which is subdivided into two informal segments (N1, N2, C3, C4, S5, S6).

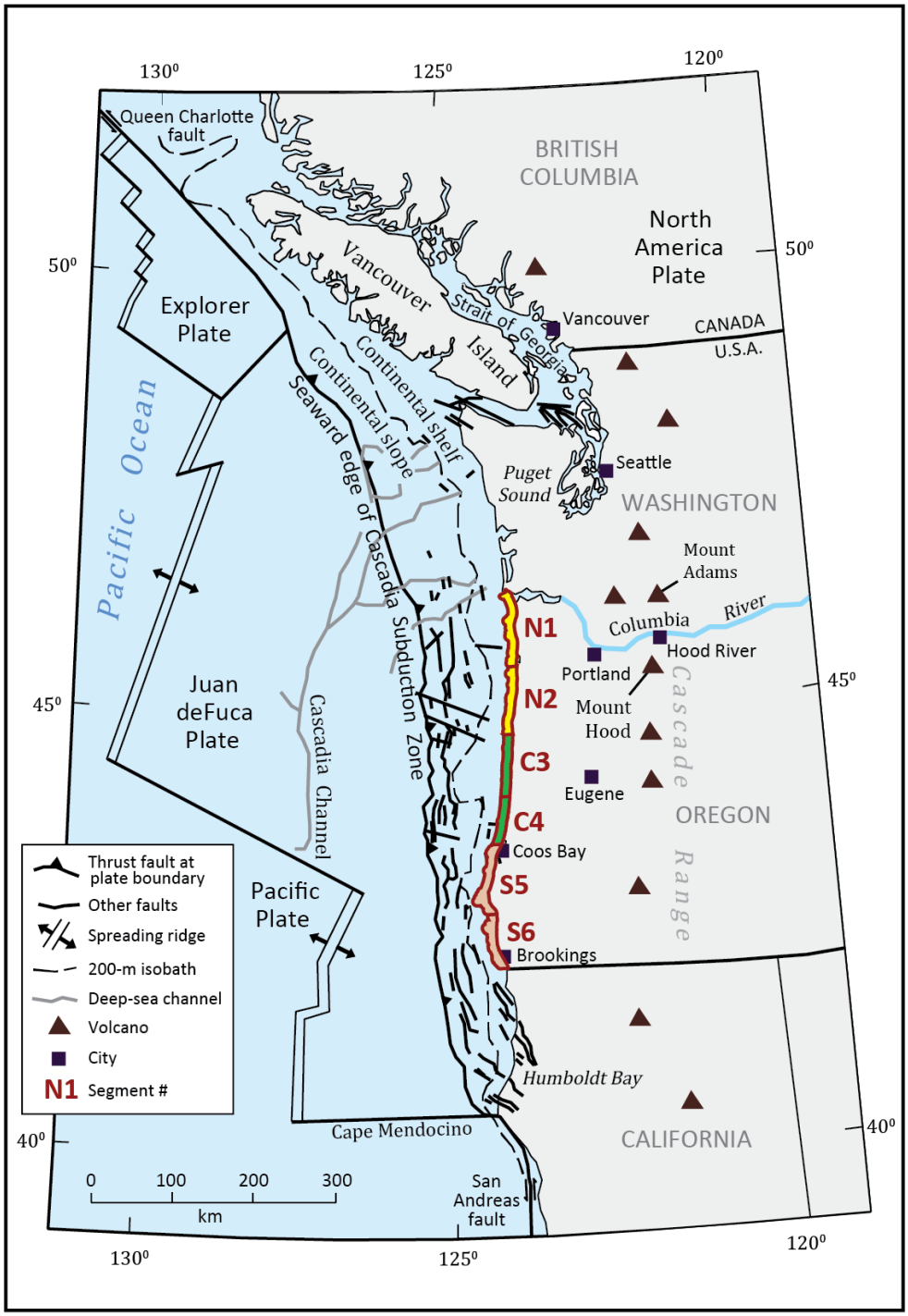

The geology of the Oregon Coast region is best understood by dividing the region into three informal provinces that share common geologic history. We further split the maps for each province into halves that allow for a better display of units and structures along the length and narrow width of the Oregon Territorial Sea study area (**Figure 3-2**):

- Northern province (segments N1, N2) from Washington border south to Newport,
- Central province (segments C3, C4) from Newport south to Florence, and,
- Southern province (segments S5, S6) from Coos Bay south to the California border.

The emplacement, and subsequent structural modification of discrete units deposited after the accretion of Siletzia after ca. 50 million years in the northern and central provinces together with Mesozoic tectonostratigraphic terranes in the central and southern provinces largely control the morphology of the Oregon Coast. Sea cliffs make up 58% of the landforms along the Oregon Coast, with the remaining 42% of the landforms along the coast composed of wave-cut shore platforms, and wide to narrow sandy, gravel, or cobble beaches which may be backed by either sand dunes or sea cliffs (Hapke and others, 2014). The discontinuous sea cliffs may be separated by landforms such as barrier spits, estuaries, lagoons, or river deltas.

The geologic units within these provinces have been grouped throughout the study area, each having its distinct, yet interconnected geologic history. The Klamath Mountains area of the southern province is mostly Mesozoic age rocks, the geologic units are subdivided into tectonostratigraphic terranes. Tectonostratigraphic terranes are fault-bounded areas of rock that each have depositional and tectonic history, distinct from adjacent bodies of rock (Jones and others, 1983). Examples of tectonostratigraphic terranes include forearc or backarc successions of sedimentary, volcanic, and intrusive rock as well as intensely deformed complexes of geologic units (e.g., volcanic and associated intrusive rocks) that are bounded by faults (Nokleberg and others, 1994). The Siletz tectonostratigraphic terrane underlies the Central and Northern provinces of the OCR north of Coos Bay, and the geology of these areas is best understood through analysis of formal or informal stratigraphic groups that may share tectonic, sedimentary, volcanic, or intrusive environments of formation or origin (NACSN, 2005). Within each province, tectonostratigraphic terranes and groups are described in chronological order from oldest to youngest.

There are six accreted tectonostratigraphic terranes along the Oregon coast that underlie the Klamath Mountains and OCR onshore and continental shelf offshore (Blake and others, 1985): Yolla Bolly, Gold Beach, Western Klamath, Pickett Peak, Snow Camp, and Siletzia. Siletzia is the largest terrane within the study area and is overlain by post-accretion late Paleogene and early Neogene sedimentary groups that occur across the south, central, and northern provinces. A few Paleogene and Neogene sedimentary rocks can be found in the southern province, and these were deposited in a marine environment and then accreted on the smaller and more numerous tectonostratigraphic terranes in the southern province. All seem to have developed along continental and oceanic tectonic margins and each has a unique early geologic history prior to the process of accretion which added them to the North American continent. At least one of the Mesozoic terranes (Whitsett subterrane) likely developed partially or entirely in the southern hemisphere, according to fossil evidence in large blocks and studies of the remnant paleomagnetic fields of the rocks (Sliter, 1984; Blake and others, 1985; Tarduno, 1987). Recent provenance data suggest many terranes including the Western Klamath terrane may have originated near the North America continental margin (e.g., LaMaskin and others, 2022). Bedrock that is older than 58 million years (Paleocene) is intricately and intensely folded and faulted within each Mesozoic

tectonostratigraphic terrane of the Southern province unlike the Siletz terrane of the Central and northern provinces.

Faults and other structures within and between terranes affect engineering properties and can juxtapose geologic units of different strength. For example, the volcanic rocks, sandstone, and conglomerate of the Mesozoic Klamath Mountains and five tectonostratigraphic terranes are very well-cemented and form many wave-resistant sea stacks offshore for several miles between the California border north to Brookings and Bandon (McClaughry and others, 2013). Intervening highly sheared low-grade metamorphosed mudstone is landslide prone. In contrast, the post-accretion overlap sequence of Tyee Formation and younger rocks (e.g., Oligocene sandstone) in the central and northern provinces are not as well cemented, and contain smectite expandable clay (e.g., Schlicker and others, 1973), which can present challenges for HDD construction (Bennett and Ariaratnam, 2017).

3.3 Regional Geology Overview by Terranes and Groups

The geologic units and structure at the surface and subsurface coastal Oregon, and their relevant properties, reflect the unique geologic histories of different coastal provinces. Here, we summarize broad groupings of rock units from generally oldest to youngest, noting the geographic and physiographic provinces of the coast where they are exposed. We use major divisions established in the regional geologic literature, including tectonic terranes, which are coherent packages of rock that were accreted to build the crustal basement, and groups, which describe sets of rocks with related characteristics and origins. The terrane and group summary is presented in sequence from roughly oldest to youngest, and figures are also presented in a similar sequence, beginning with the oldest rocks exposed in the study area, which are in the southernmost part of the Oregon Coast and Territorial Sea (**Table 3.1**).

The geologic data in this report were compiled to present the best available information regarding types of rock and sediment present across the landscape of the Oregon Coast and the seascape of the Territorial Sea. South of Coos Bay, consistent, updated, and detailed geologic mapping was completed using modern lidar and geochronologic data (McClaughry and others, 2013; Wiley and others, 2014; 2015). Geologic mapping has been extended across the Territorial Sea, using seafloor substrate data (Goldfinger and others, 2014) combined with interpretations of terrestrial observations (McClaughry and others, in preparation). A major contribution of this project was continuing the strategy of McClaughry and others (in preparation) across the Territorial Sea from Coos Bay north to the mouth of the Columbia River to develop an integrated view of both onshore and offshore geology. We joined the terrestrial Oregon Geologic Data Compilation, release 7 (OGDC-7; Franczyk and others, 2020), with seafloor geology (substrate) data (Goldfinger and others, 2014; PMEP, 2022) to interpret specific geologic units where rock is exposed on the seafloor. The geologic map data in the figures of this section and the associated GIS data consist of data from McClaughry and others (in preparation) south of Coos Bay, and the extended data modified from OGDC-7 (Franczyk and others, 2020) in areas to the north. Geologic structures (faults and folds) are derived from OGDC-7 (Franczyk and others, 2020) on land, and Goldfinger and Beeson (2023) offshore.

Table 3.1. Tectonostratigraphic terranes and sedimentary groups of the Oregon Coast.

Terrane/Group	Description	Age (Period)	Abbrev.
Quaternary Surficial Deposits	Deposits of unconsolidated sediments	Quaternary	Qs
Neogene Sedimentary Rocks	Sedimentary	Neogene	Ns
Neogene Volcanic Rocks	Igneous	Neogene	Nv
Columbia River Basalt Group	Basalt and basaltic andesite lava flows	Neogene	Nc
Whalecove-Gnat Creek Group	Marine sandstone and mudstone	Paleogene/ Neogene	PNw
Astoria Group	Marine Sandstone and siltstone, including slope channel, deltaic and turbidite sandstone, and slope mudstone	Neogene	Na
Keasey-Alsea Group	Tuffaceous marine sedimentary rocks	Paleogene	Pk
Elkton-Yamhill Group	Marine slope mudstones within the Cascadia Forearc Basin.	Paleogene	Pe
Yaquina-Pittsburg Bluff Group	Tuffaceous sedimentary rocks	Paleogene/ Neogene	PNy
Coaledo-Cowlitz Group	Marine deltaic sandstone and slope mudstone, locally coal-bearing.	Paleogene	Pc
Nestucca-Hamlet	Slope mudstone and shelf sandstone.	Paleogene	Pn
Yachats-Tillamook Group	Marine sandstone and terrestrial sedimentary rocks.	Paleogene	Py
Tyee Group	Marine turbidite sandstone.	Paleogene	Pt
Umpqua Group	Marine sandstone, conglomerate, shale, and siltstone.	Paleogene	Pu
Siletzia Terrane	Submarine basalt, pillow basalt and deep marine sediments that formed as an oceanic island chain and then accreted to North America.	Paleogene	Ps
Snow Camp Terrane	Metamorphic, volcanic, intrusive and ultramafic rocks and mélange.	Jurassic/ Cretaceous	JKsc
Pickett Peak Terrane	Metamorphic and ultramafic rocks and serpentinite.	Jurassic/ Cretaceous	JKp
Western Klamath Terrane	Marine sedimentary, mafic volcanic and volcaniclastic, ultramafic, metamorphic, and mélange rocks and serpentine.	Cretaceous	Kw
Gold Beach Terrane	Severely folded and deformed marine sedimentary rocks and mafic volcanic rocks.	Jurassic/ Cretaceous	JKg
Yolla Bolly Terrane	Basaltic volcanic rocks, marine sandstone, mudstone and chert, and mélange.	Jurassic/ Cretaceous	JKy

The maps in this section of the report display simplified rock and sediment types grouped by terranes or formal and informal sedimentary and volcanic stratigraphic groups. Much greater detail of the geology of the Oregon Coast at the formation level is available in the GIS data of this report. Plates 1 and 2 show the geology in two example areas on the southern and northern Oregon Coast, respectively. In contrast to the higher resolution, consistent data of the southern coast (e.g., Plate 1) the OGDC-7 compilation (Franczyk and others, 2020) includes spatial heterogeneity in geologic unit interpretations and original map scale (e.g., Plate 2). The simplified structural features presented in the sequence of terrane and group maps presented in this section, for example **Figure 3-3b**, represent the total accumulation of faults and folds that have been identified on shore along the Oregon Coast (Franczyk and others, 2020). Offshore faults and folds emphasize structures with more recent activity (Goldfinger and Beeson, 2023).

3.3.1 Yolla Bolly terrane: southern province

The Yolla Bolly terrane (Blake and others, 1985) (**Figure 3-3**; **Figure 3-4**) contains rocks of the upper Cretaceous Dothan Formation (Dott, 1971; Wiley and others, 2017). The Dothan Formation has experienced low grade metamorphism and is characterized by sandstone that encloses large blocks of volcanic arc rocks and smaller exotic fault blocks of other lithologies. It is interpreted as structurally thickened turbidite and debris flow submarine fan sequences (Aalto, 1989). Rocks of the Dothan Formation are hard and form numerous sea stacks in the nearshore.

The Dothan Formation consists predominantly of hard, dense beds of graywacke sandstone interbedded with thick, well indurated gritty to pebbly debris flow sandstone and volcaniclastic turbidites. (Baldwin, 1974). These sedimentary units contain large (dozens of meters thick) blocks of tectonically incorporated meta-pillow lavas (greenstones) and breccias, volcaniclastic rocks, radiolarian chert, and serpentinite. Some of the blocks may have been deposited as olistostromes, which are blocks deposited by submarine landslides (Baldwin, 1974; Aalto, 1989). The environment of formation for these various units is interpreted as being deep water volcaniclastic turbidites, submarine slope, fan, and fan-channel settings adjacent to a volcanic island arc (Dott, 1971; McClaughry and others, 2013). The terrane equivalent of the Yolla Bolly/Dothan Formation across the California border is the Franciscan Group, which is also mapped as amalgamated exotic terranes (Blake and others, 1985; Seiders and Blome, 1987), mélange (Walker and McLeod, 1991), and a more-intact accretionary complex with exotic components (Roure and others, 1986).

3.3.2 Gold Beach terrane: southern province

The Gold Beach terrane extends in a strip from Whaleshead Island near Brookings to Ophir in the north (**Figure 3-3**, **Figure 3-4**). It is the westernmost terrane that underlies the coastal area of southwestern Oregon (Blake and others, 1985; Bourgeois and Dott, 1985; McClaughry and others, 2013). This terrane is composed of the Jurassic Otter Point Formation (Koch, 1966; Aalto and Dott, 1970), the less widespread Houstenaden Creek Formation, the Hunters Cove Formation, and the Cape Sebastian Sandstone (Dott, 1971; McClaughry and others, 2013).

Figure 3-3. Terrane/Group geologic map (A) and simplified structural features map (B) of the south-6 (S6) segment of the Oregon Coast study area. Geologic data modified from McClaughry and others (2013), McClaughry and others (in preparation), Franczyk and others (2020), Goldfinger and others (2014), and Goldfinger and Beeson (2023).

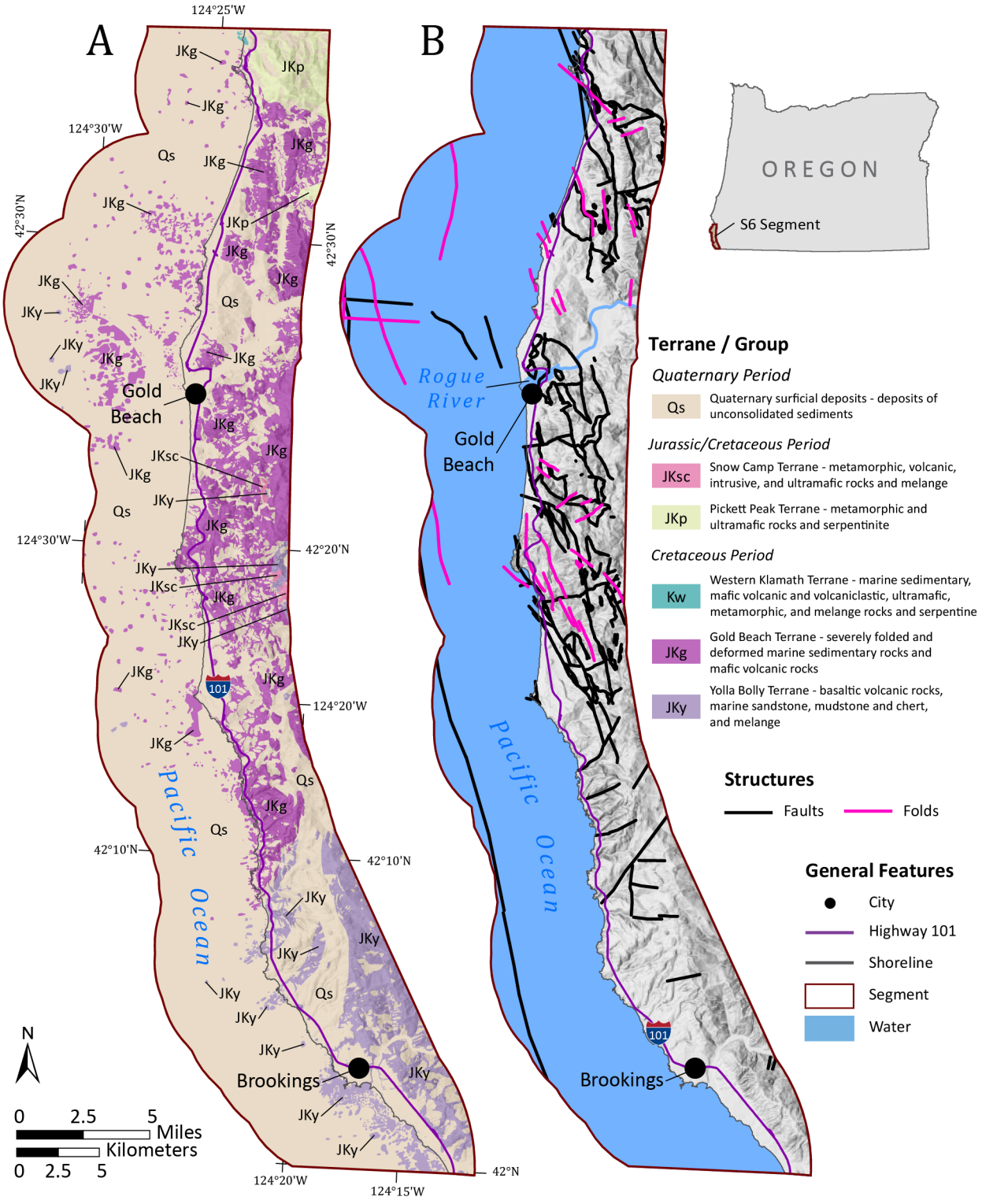

Figure 3-4. Terrane/Group geologic map (A) and simplified structural features map (B) of the south-5 (S5) segment of the Oregon Coast study area. Geologic data modified from McClaughry and others (2013), Wiley and others (2014; 2015), McClaughry and others (in preparation), Franczyk and others (2020), Goldfinger and others (2014), and Goldfinger and Beeson (2023).

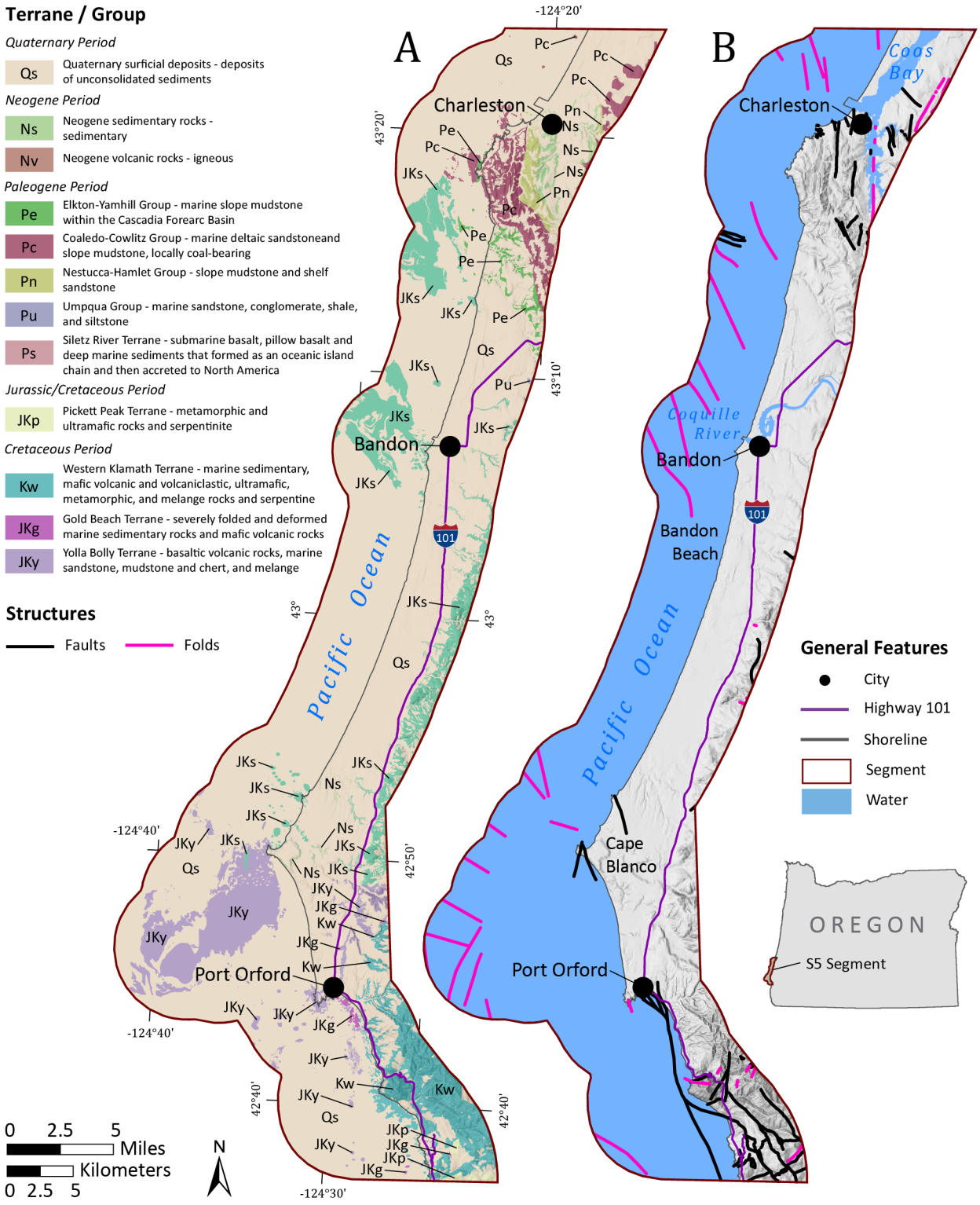

The Otter Point Formation forms numerous hard, erosion-resistant sea stacks along the coastline which extend seaward a few miles and is made up of a structurally complex succession of volcaniclastic sandstone, mudstone, and conglomerate (Koch, 1966; Aalto, 1968; Aalto and Dott Jr, 1970; Dott, 1971; Walker and McLeod, 1991). Between Sundown Mountain and Sisters Rock State Park, north of Ophir, approximately 6.4 km (4 miles), inland southeast of Cape Sebastian, the formation contains north-northwest trending bands of pillow lava and volcanic breccia. There are also lines of scattered indurated blocks of volcanic rock, diorite, chert, and serpentinized ultramafic rock, which mark the surface traces of intraformational shear zones and faults (Blake and others, 1985). The sedimentary rocks of the Otter Point Formation formed during the early Cretaceous, 145 to 100 million years ago and range from cherty mudstone to chert-pebble conglomerate near the Rogue River and chert-rich sandstone and pebbly sandstone near the Pistol River.

The youngest portion of the Houstenaden Creek conglomerate and the oldest part of the Cape Sebastian Sandstone are composed of a variety of pebble- to cobble-sized clasts of fine-grained, silicic to intermediate volcanic rocks, welded tuffs, quartzite, and felsic plutonic rocks. The sedimentary units of the Hunters Cove and Cape Sebastian formations are largely composed of clasts that were eroded from the Otter Point Formation and deposited nearby as part of their respective formations. These sedimentary units are pervasively faulted; however, they are not intensely sheared, which indicates that these units did not experience metamorphism to the same degree as the underlying Otter Point Formation (McClaughry and others, 2013).

3.3.3 Western Klamath terrane: southern province

The Western Klamath terrane (**Figure 3-3**, **Figure 3-4**) is the youngest part of a stack of structures known as imbricate thrust sheets, which form in convergent margin settings and cause units to thicken and repeat in vertical sequences. Much of the Western Klamath terrane is composed of the Galice Formation, which is interpreted to have formed between 157 and 152 million years ago. It is a sequence of dark slate and slatey mudstone, metagraywacke, minor greenstone, thin-bedded sandstone, and chert (Dott, 1971; MacDonald and others, 2006; Giaramita and Harper, 2006; McClaughry and others, 2013; Wiley and others, 2015; LaMaskin and others, 2022).

Along the southwestern Oregon Coast, a fragment of the Western Klamath terrane, known as the Elk subterrane, is exposed between Humbug Mountain and Port Orford. The Galice Formation is intruded by the Pearce Peak diorite which was emplaced between 148 and 144 million years ago (Dott, 1971; Giaramita and Harper, 2006). It is characterized by fault blocks and slivers of dismembered oceanic crust which range from gabbro to low grade metamorphic pillow basalt (greenstone), which is overlain by unmetamorphosed conglomerates and sandstones.

3.3.4 Pickett Peak terrane: southern province

The Pickett Peak terrane includes distinctive phyllite, schist, and gneiss that are a part of the Colebrook Schist. These rocks are exposed over an area extending from Agness on the east to Lookout Rock on the coast and from as far north as Cape Blanco to south of the Pistol River (**Figure 3-3**, **Figure 3-4**). The Colebrooke Schist is a collection of thinly bedded shale, turbidite sandstone, pillow lavas, tuff, and chert that underwent metamorphism to grades halfway between blueschist and greenschist facies. It commonly has serpentinite-matrix mélange beneath it (Diller 1903; Dott, 1971; Coleman, 1972; Blake and others, 1985). The Pickett Peak terrane, which structurally overlies the lower-grade metamorphic rocks of the Gold Beach and Yolla Bolly terranes, tends to occupy high terrain to the south of the Canyonville fault as

part of a complexly faulted nappe structure (Wells and others, 2017). In the Pistol and Rogue River drainages, the Pickett Peak terrane is found near exposure of sedimentary rocks that are at least 70 million years old (Late Cretaceous) and include mudstone, chert-rich sandstone, pebbly sandstone, and conglomerate. These terranes are more coherent and do not contain evidence of the high levels of deformation associated with sheared mélange units in the area (e.g., broken formation) (Blake and others, 1985).

3.3.5 Siletzia terrane: northern and southern provinces

The Siletzia terrane is a thick accumulation of largely tholeiitic submarine and subaerial basalt flows, diabasic and gabbroic intrusive rocks, submarine breccias, minor, deep marine sedimentary rocks, and rare silicic flows which date between 59 and 47 million years old (**Figure 3-4**; **Figure 3-7**) (Howell and others, 1985; Silberling and others, 1987; Wells and others, 2014). Most outcrops of the Siletzia terrane occur as basement fault horst blocks and volcanic edifices (Snavely and others, 1968; Wells and others, 2000). The Siletzia terrane extends northward from the Roseburg area in the south, across western Washington, where it is known as the Crescent Formation (Snavely and others, 1968; Tabor and Cady, 1975), to the southernmost part of Vancouver Island, Canada (Wells and others, 2014). Siletzia terrane volcanic rocks are interpreted to be between 25 km and 35 km (15.5 and 21.7 mi) thick in the central part of the OCR (Trehu and others, 1994). These units are exposed at the surface in the north-central portion of the study area, where they are in depositional contact with the Elkton-Yamhill Group and the Yachats-Tillamook Group (**Figure 3-7**). The Siletzia terrane forms the basement rocks of the OCR and is only exposed at the surface in scattered locations (e.g., Roseburg area and along the Siletz River northeast of Newport) where rocks have experienced uplift because of the ongoing tectonic forcing associated with oblique Cascadia subduction zone (Wells and others, 2014). Volcanic units, formerly known as the Roseburg Volcanics (Baldwin; 1974), that form the Siletz terrane are thrust beneath the Mesozoic Sixes River terrane by the Wildlife Safari and associated faults in the Roseburg area. The timing of accretion of the Siletz terrane between 51 and 49 million years ago is bracketed by overlying lower-Eocene sedimentary rocks to the north of the Canyonville fault (Ryu and others, 1996; Wells and others, 2014).

Figure 3-5. Terrane/Group geologic map (A) and simplified structural features map (B) of the central-4 (C4) segment of the Oregon Coast study area. Geologic data modified from Franczyk and others (2020), Goldfinger and others (2014), and Goldfinger and Beeson (2023).

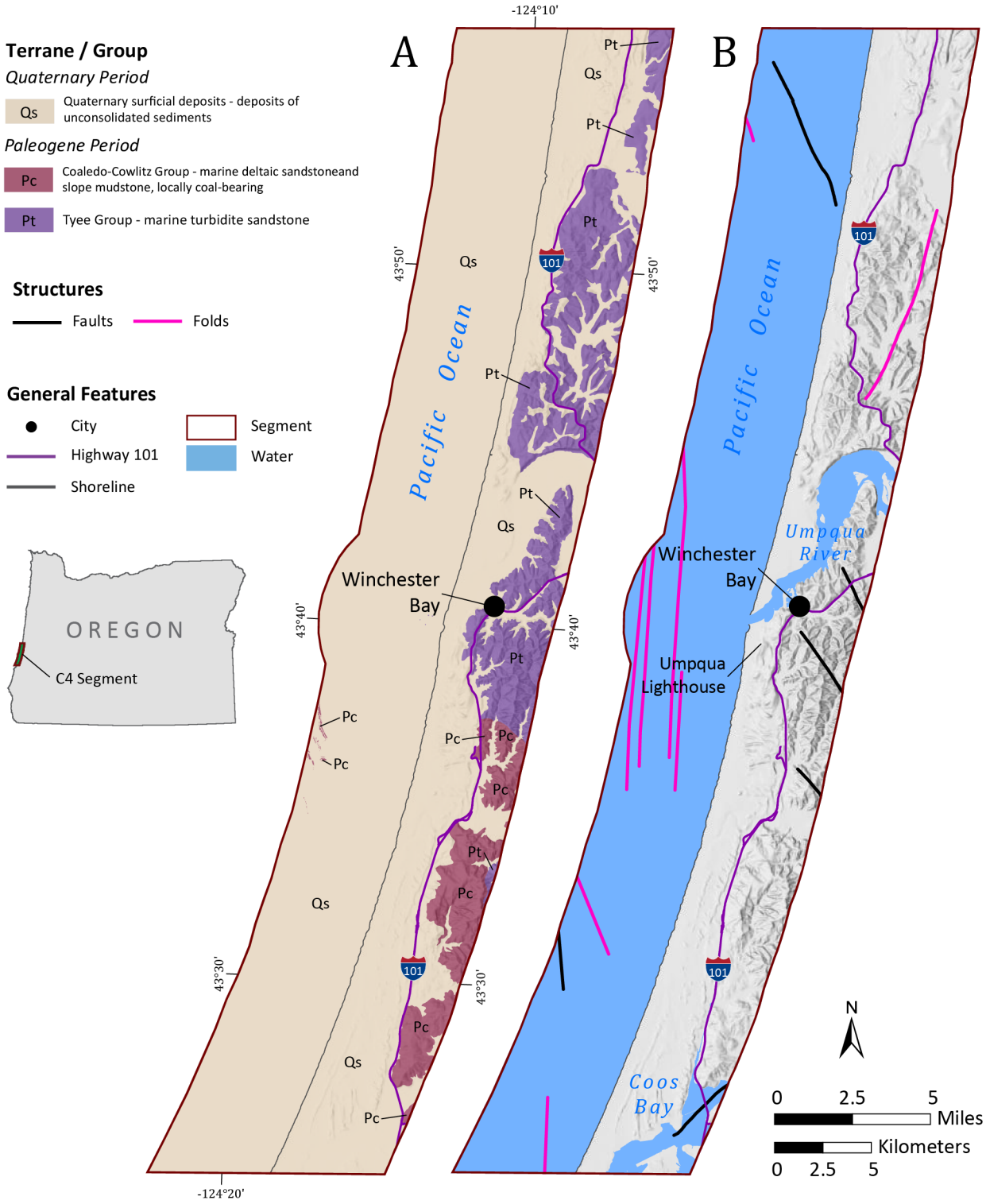

Figure 3-6. Terrane/Group geologic map (A) and simplified structural features map (B) of the central-3 (C3) segment of the Oregon Coast study area. Geologic data modified from Franczyk and others (2020), Goldfinger and others (2014), and Goldfinger and Beeson (2023).

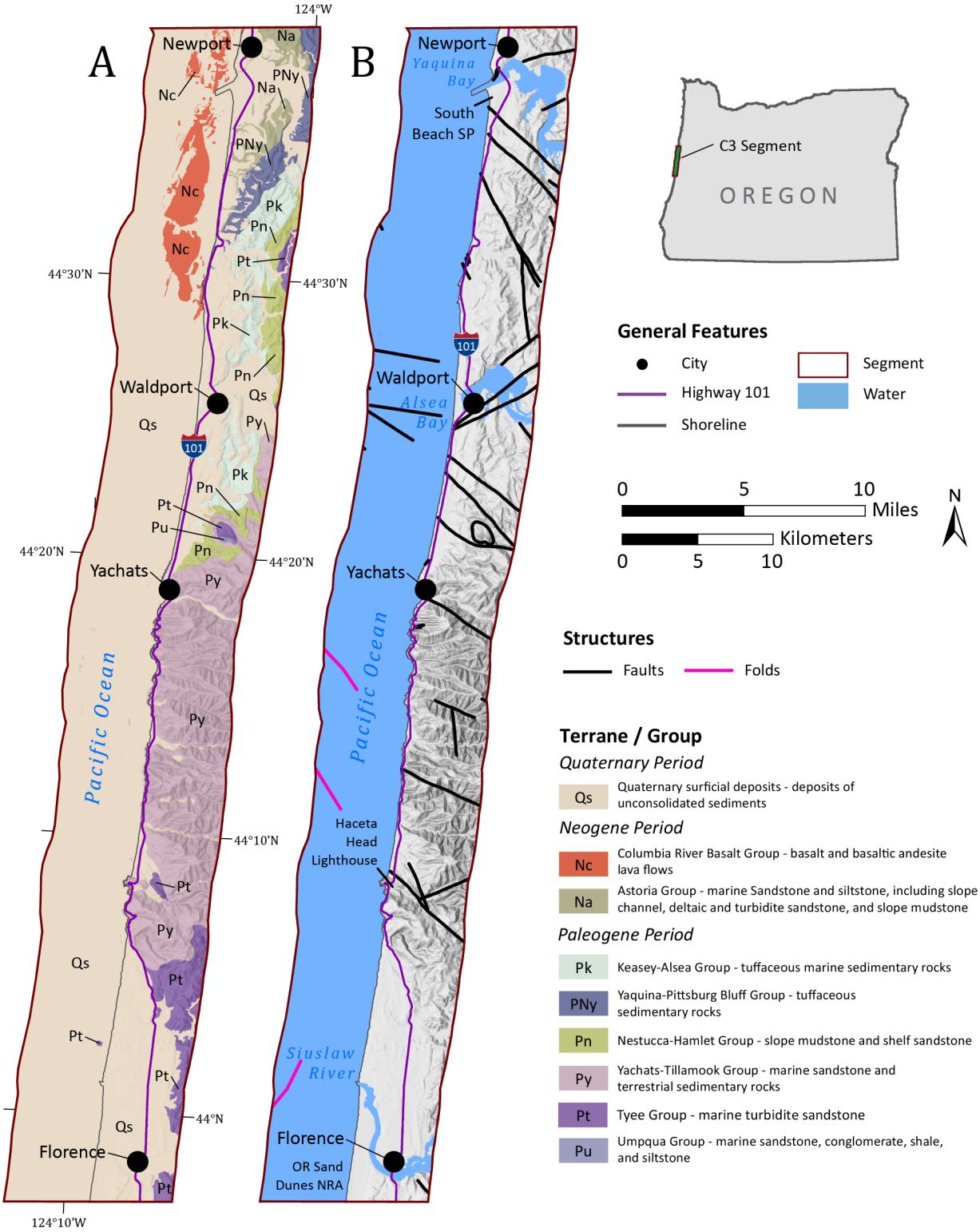

3.3.6 Umpqua Group: northern, central, and southern provinces

The Umpqua Group is composed of thick sequences of volcaniclastic sedimentary rocks that were deposited in a marine environment during the latest eruptive stages of volcanics forming the Siletz terrane ~52-49 million years ago (**Figure 3-4**, **Figure 3-6**, **Figure 3-7**, **Figure 3-8**; Ryu and Niem, 1999; Darin and others, 2022). The Umpqua Group sedimentary units overlie and interfinger with Siletzia terrane basalts at the oldest/lowest part of the group (Snavely and others, 1993; Wells et al., 2014). Strata that make up the Umpqua Group are well-indurated lithic turbidite sandstones largely derived from the Mesozoic Klamath Mountains and other sources. The sandstones are interbedded with deep-marine mudstone units and are interpreted to have been deposited post-accretion to the North America plate in a subduction zone setting as parts of submarine fans (Ryu and others, 1996). The oldest units of the Umpqua Group have experienced significant late middle Eocene deformation associated with the subduction zone and are tightly folded and indurated (McCrory and Wilson, 2013). Umpqua Group rocks can be found from the study area as far east and south as Roseburg (Wells and others, 2014). The units that make up the Umpqua Group record the development of a new subduction zone to the west, and closer to its present location in the early Paleogene (middle Eocene), when a very thick seamount clogged the active subduction zone during the accretion of the Siletzia terrane (Molenaar, 1985; Wells and others, 2014).

3.3.7 Tyee group: northern and central provinces

The Tyee group is made up of marine sedimentary rocks that were rapidly deposited within a 2-to-4-million-year period between 47 and 43 million years ago (Darin and others, 2022). The Tyee group comprises arkosic sandstone interbedded with mudstones and has been measured to a thickness of ~3 km (~1.8 mi) (**Figure 3-5**, **Figure 3-6**, **Figure 3-7**) (Snavely and others, 1964; Heller and others, 1985; Darin and others, 2022). The average thickness of individual beds that make up the Tyee group is less than 1.7m (5 ft), however there are examples near Tillamook that can reach up to 3m (10 ft). (Schlicker and others, 1972). The total thickness of the Tyee Formation is approximately 1,828 m (6,000 ft) and is continuously exposed to the west of the coastal area of interest for ~180 km^2 (600 mi^2) of the Coast Range (Schlicker and others, 1973).

3.3.8 Coaledo-Cowlitz group: central and southern provinces

The Coaledo-Cowlitz group includes rocks that were deposited during the middle to late Eocene between 45 and 33 million years ago in a broad coastal plain that developed adjacent to the subduction zone off the coast of North America at that time (**Figure 3-4**, **Figure 3-5**) (Dott Jr, 1966; Niem and others, 1989; Snavely and others, 1993; Darin and others, 2022). The Coaledo-Cowlitz group are feldspar and mica-rich sandstones (Heller and Ryberg, 1983). The late Eocene Coaledo group was deposited in the Coos basin, which was adjacent to the forearc basin in which Tyee group deltaic and turbidite sediments accumulated (Newton, 1980; Ryu and others, 1996). The Cowlitz members (i.e., Spencer and Cowlitz formations) are mapped in the northern Oregon Coast Range and share similar age and lithological characteristics with the Coaledo units and have been mapped inland in the northeastern part of the Oregon Coast Range where these strata form the main storage reservoir in the Mist Gas Field, ~64 km (40 mi) northwest of Portland.

3.3.9 Paleogene, Neogene, and Pleistocene units: southern province

The Siletzia and Yolla Bolly terranes are overlain by a more gently deformed post-accretion marine overlap sequence that contains sedimentary rocks and basalts that were deposited during the Paleogene (Paleocene to Oligocene time) between 65 and 23 million years ago (**Figure 3-3**, **Figure 3-4**). Many of these units can be found throughout the study area, such as the Tyee, Coaledo, and Bastendorff formations

(Baldwin, 1974; Molenaar, 1985; Wiley and others, 2014, 2015). These units alternate between sandstones and mudstones and are interpreted to be the result of repeated tectonically forced sea-level rises and falls, which changed the environments of deposition for the various sedimentary units that make up this sequence (McKeel, 1984; Ryu and Niem, 1999; McClaughry and others, 2010). The characteristics of middle to late Paleogene sedimentary rocks in southwest Oregon imply that the distribution of clastic rock types was significantly influenced by worldwide changes in sea level (e.g, eustatic changes).

Exposures of younger post-accretion sedimentary rocks that formed in marine environments during Neogene time (23 to 2.6 million years ago) can be found in a few minor areas throughout the study area, specifically in Coos Bay (Allen and Baldwin, 1944), Bandon (Orr and Zaitzeff, 1970; Orr and others, 1971), and at Cape Blanco (Bandy, 1941; Fowler and others, 1971; Addicott, 1983; Emerson, 2007; Raymond and others, 2008; Wiley and others, 2014).

For example, a gently dipping local coastal unit of semi-consolidated sand, mud, sandy mud, pebbly sand, and gravel which is known as the Port Orford Formation (Baldwin, 1945) formed during the early Pleistocene (~2.53 million years ago). It lies unconformably on early Miocene rocks and forms the sea cliffs north of the Elk River. The Coquille Formation, which is composed of weakly cemented sand and gravel beds and is dated to around the same time period can be found in the subsurface under the Quaternary terrace between Bandon and Whiskey Run. This post-Siletz terrane accretion formation was unconformably deposited on the Mesozoic Sixes River tectonostratigraphic terrane and underlies Quaternary marine terrace deposits north of Bandon which have experienced rock and minor surface uplift. This unit is also in contact with older Coast Range sedimentary rocks in the subsurface either through deposition over an angular unconformity or through juxtaposition by faulting. The Coquille formation of the late Miocene-Pliocene marine diatomaceous muds could be more extensive offshore, as younger Pleistocene terrace and Holocene beach, shelf, estuarine sand and mud and river mouth gravel formed during interglacial lower sea level due to worldwide deglaciation and/or local co-seismic tectonic subsidence or uplift events.

3.3.10 Yachats-Tillamook group: northern and central provinces

The Yachats-Tillamook group refers to basalt units that occur in the northern study area province (Tillamook; **Figure 3-7**; Plate 2) (Wells and others, 1994) and in the central province (Yachats; **Figure 3-6**) (Snavely and MacLeod, 1974), where they intrude into the older sedimentary rocks of the Tyee and Umpqua groups. An aggregate thickness of 600 m (~1970 ft) has been interpreted for this group based on an area between Cascade Head and the Salmon River (Snavely and MacLeod, 1974). In addition to lava flows, sills of diabase and gabbro have intruded the Tyee group units (Snavely and others, 1976). These two units are grouped because of their post-Tyee emplacement as oceanic basalt islands, with the Tillamook basalts interpreted as erupting over a Yellowstone hotspot (Wells and others, 2014). The Tillamook basalts are dated to 46 to 43 million years ago and the Yachats basalts span a time period from 36 to 30 million years ago (Parker and others, 2010).

Figure 3-7. Terrane/Group geologic map (A) and simplified structural features map (B) of the north-2 (N2) segment of the Oregon Coast study area. Geologic data modified from Franczyk and others (2020), Goldfinger and others (2014), and Goldfinger and Beeson (2023).

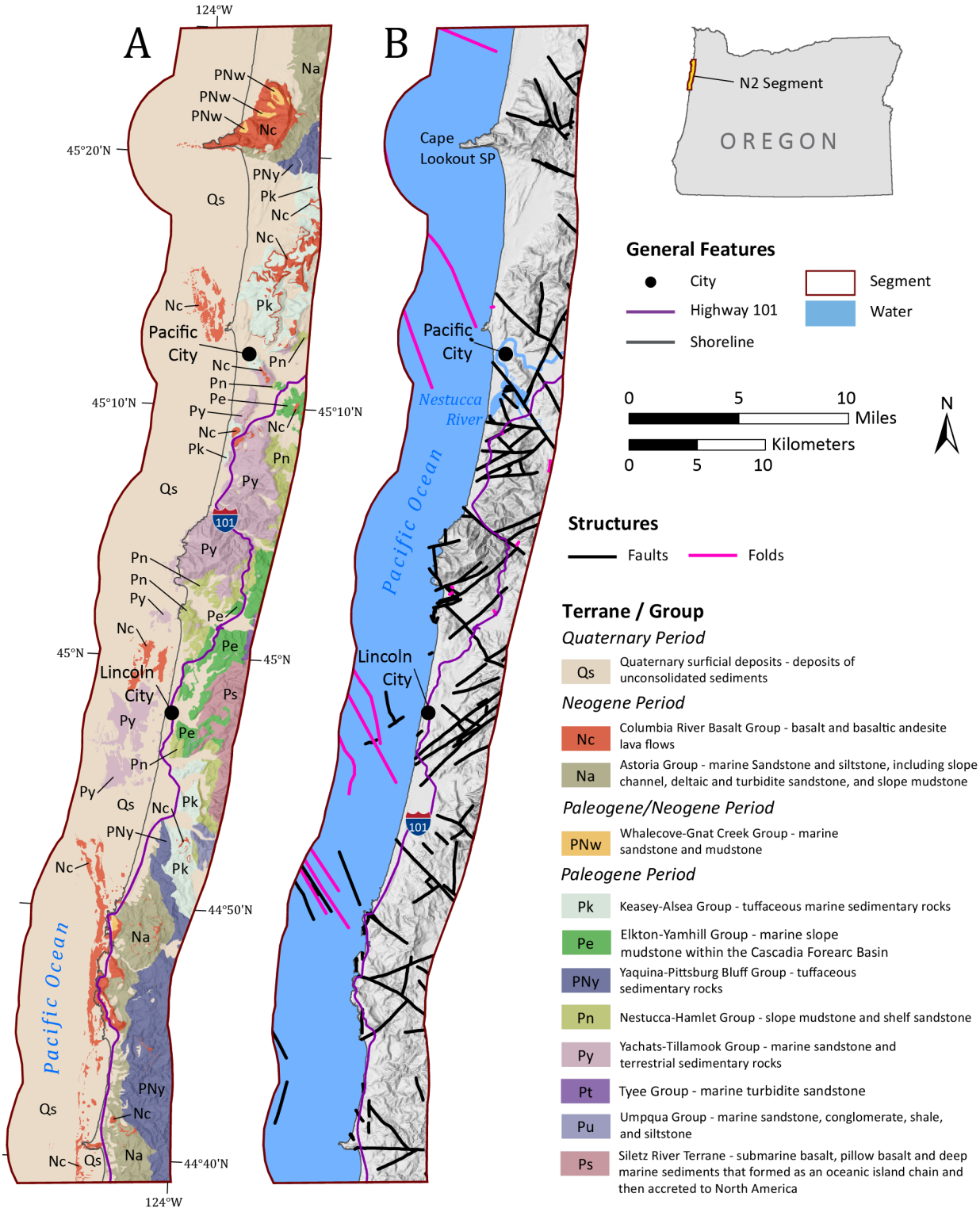

Figure 3-8. Terrane/Group geologic map (A) and simplified structural features map (B) of the north-1 (N1) segment of the Oregon Coast study area. Geologic data modified from Franczyk and others (2020), Goldfinger and others (2014), and Goldfinger and Beeson (2023).

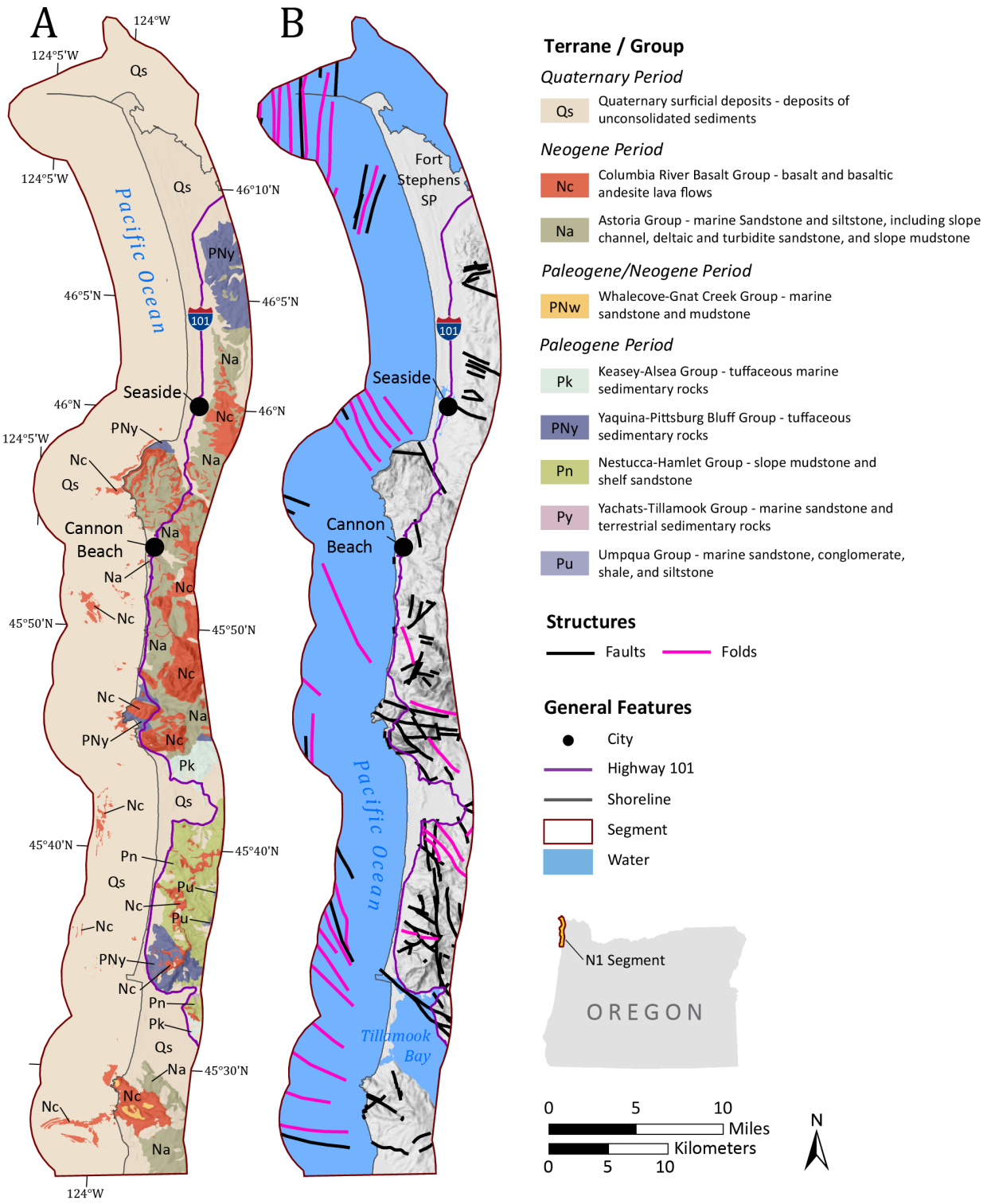

3.3.11 Nestucca-Hamlet group: northern, central, and southern provinces

The Nestucca-Hamlet group refers to two geographically distinct groups of rocks that are equivalent in age and share similar environments of deposition but are distinct in lithology (**Figure 3-7**). The Hamlet units occur as a sequence of massive carbonaceous mudstone interbedded with basaltic conglomerates and sandstone that were deposited in a shallow marine shelf environment adjacent to a rocky coast (Niem and Niem, 1985). The late Eocene Nestucca Formation is a 450 m- (~1,500 ft-) thick sequence of deep marine sedimentary rocks. Compositionally, this formation is characterized by micaceous mudstone containing carbonaceous terrestrial matter, microfossils, thin tuff beds of reworked western Cascade-derived ash, and lenses of glauconitic and volcanic sandstone (Snavely and others, 1976c). These units have been K/Ar dated as being 37 to 33 million years old (Snavely and others, 1980; late Eocene-early Oligocene). The radiometric age of the Nestucca Formation is consistent with interfingering relationships with the oceanic basalts of the Yachats-Tillamook volcanics (Snavely and others, 1976a, 1976b, 1976c).

3.3.12 Keasy-Alsea group: northern and central provinces

The Keasey-Alsea group refers to light yellowish-gray tuffaceous siltstone between 27 and 13 million years old (Snavely and others, 1993) that contains thin tuff beds derived from the western Cascades arc (**Figure 3-6**, **Figure 3-7**, **Figure 3-8**). At the base of the Alsea Formation, basaltic sandstone beds were locally deposited around basalt headlands in a marine environment. Units of this group are referred to as the Keasey Formation in the north (Niem and Niem, 1985) and as the Alsea Formation in the Newport basin (Snavely and others, 1976a, 1976b). The Keasey Formation is interpreted to have been deposited in a deep marine environment and is composed of gray tuffaceous siltstones and massive mudstones. The unit is further subdivided into three informal members: the lowest member is ~150 m (~492 ft) of micaceous laminated siltstone and mudstone, the middle member is ~500 m (~1640 ft) of light gray tuffaceous mudstones and siltstones with occasional ash layers, and the upper member is 50 m (~164 ft) of alternating light and dark siltstones and more resistant calcareous beds (Prothero and others, 2000).

3.3.13 Yaquina-Pittsburg Bluff group: northern and central provinces

The Yaquina-Pittsburg Bluff group overlies the Keasey-Alsea group and shares the shallow marine environment of deposition in the youngest parts of the Keasy-Alsea group. Changes in lithology (presence of coal and abundance of mica) and sedimentary structures indicate that the environment of deposition transitioned from shallow marine to deltaic nonmarine micaceous arkosic sandstone in the middle of the deposit (Goodwin, 1972). The shallow-marine micaceous arkosic sandstone and western Cascade pumiceous debris flow deposits of the Pittsburg Bluff Formation are resistant to weathering and erosion and can form ridges within the northern OCR. The Pittsburgh Bluff Formation was deposited between 27 and 23 million years ago (Niem and Niem, 1985). The Yaquina member of the group occurs in the Central province (i.e., the Newport basin; Snavely and others, 1976b) and has a measured thickness of 600 m (1,968 ft) (Goodwin, 1972). Strata of the of the Yaquina-Pittsburg Bluff group include re-worked volcanic clasts that were deposited in high energy environments interpreted as nearshore beach and inner shelf that experienced storm waves. Siltstones of this group are interpreted as being deposited in fluvial and coastal swamp/estuarine environments (Goodwin, 1972). The Alsea Formation is exposed in Yachats (Snavely and others, 1976a), where a section of Paleogene basalt of the Yachats-Tillamook group is

overlain by a pebble to boulder conglomerate that transitions abruptly to a coarse, pebbly basaltic sandstone (Vokes, and others 1949; Lund, 1972).

3.3.14 Astoria group: northern and central provinces

The Astoria group includes sedimentary facies corresponding to two marine environments approximately 20 million years ago based on fossil assemblages (**Figure 3-6**; **Figure 3-7**) (Niem and Niem, 1985). The shallow water facies is a sequence of deltaic coal-bearing, cross-bedded, pumiceous and tuffaceous arkosic sandstones that are locally glauconitic. A deep marine sequence comprises mudstone that is rhythmically interbedded with fine-grained sandstone turbidites in nested channels (Niem and Niem, 1985). The Astoria group crops out along the coast in the Northern and Central province between Seaside and Newport and extends offshore in the Astoria, Tillamook, and Newport basins (**Figure 3-6**; **Figure 3-7**; **Figure 3-8**). It contains many intrusions of Columbia River Basalt Group, particularly in the northernmost outcrops of our study area (Plate 2) (Niem and Niem, 1985).

There are distinct units, or members of the Astoria Formation in the study area. First, the Angora Peak member is composed of ~335 m (1,100 ft) alternating layers of thick sandstone, dark-gray, carbon-rich siltstone, and pebble conglomerates (Smith, 1974). The Silver Point member is a ~198 m (650 ft) layer of dark, laminated mudstones that overlies the Angora Peak member and contains fossils that are interpreted as having a deep marine environment of formation based on evidence at Ecola State Park (Niem, 1975). The Netarts Bay member is made up of arkosic sandstones that can have variable grading in terms of grain size that contains large blocks of siltstone and have been interpreted as the product of deposition in a channel occurring in the transition zone between the shallow marine shelf and the slope (Parker, 1990). The Cannon Beach member of the Astoria Formation extends from the Columbia River in the north and has been identified as far south as Cape Lookout, in the Tillamook area., and overlies both Angora Peak and Netarts members, as shown in Plate 2. The Cannon Beach member is the uppermost member of the Astoria Formation and is characterized by rhythmically bedded and channelized turbidite sandstone and mudstone lithology (Parker, 1990).

Strata of the Astoria group rock have variable engineering properties, but generally tend to be weak. In the northern province, bluffs along the coast have a mean slope of ~45° in places where bare talus slopes of mostly mudstones, siltstones, and tuffs of the Astoria group are exposed to weathering and erosion. Where undercut by storm waves, landslides occur on steep cliff exposures (Niem, 1975). In some locations the Astoria units are exposed as near-vertical cliffs where wave action undercuts slopes, or where more resistant sandstone units are exposed as headlands, such as Devil's Punch Bowl (Priest and Allan, 2004).

3.3.15 Columbia River Basalt Group: northern and central provinces

The Columbia River Basalt Group (CRBG) is a succession of tholeiitic basalt and basaltic andesite lava flows erupted in eastern Oregon, eastern Washington, and western Idaho between ca. 17 and 5.5 million years ago (e.g., early to late Miocene). The flood basalts cover more than 210,000 km^2 (~81,000 mi^2) (Reidel and others, 2013) (**Figure 3-6**, **Figure 3-7**, **Figure 3-8**). Along the Oregon Coast, these basaltic lava flows crop out from south of Newport to Astoria both onshore and offshore. CRBG occurs as subaerial lava flows and pillow lava deltas where the lava flows entered the Pacific Ocean and invasive sills and dikes. Invasive basalts are hosted by older or equivalent aged sedimentary units such as the Astoria group and Yaquina Formation (Plate 2) (Niem and Niem, 1985; Wells and others, 2009). An example of the relationship of the CRBG and older units is exposed at Seal Rock State Park, where basalt forms numerous dikes and a thick sill in the Oligocene Yaquina Formation (Snavely, 1980). Very thick sills of CRBG in the

Astoria group form the headlands at Tillamook Head and Neahkahnie Mountain. This hard basalt is also present in the offshore as rock reefs and sea stacks (**Figure 3-8**).

3.3.16 Whale Cove-Gnat Creek group: northern segment

The Whale Cove-Gnat Creek group was deposited as thin, shallow-marine and coal-bearing fluvial to estuarine sediments during the middle to late Miocene, between 13 and 11 million years ago. These units are interbedded with CRBG lava flows. This micaceous arkosic to basaltic sandstone is poorly consolidated and consequently friable (Murphy 1981; Niem and Niem, 1985; Snavely and others, 1976c).

3.3.17 Quaternary surficial deposits

By 2.5 million years ago, the position of the present CSZ was established into its present configuration (Wells, 1994). Four basins began accumulating continentally derived and marine sediments during the late Neogene: Astoria, Tillamook, Newport, and Coos. Sediments continue to be deposited in these basins and both sediments and underlying rock units are presently experiencing active deformation (e.g., **Figure 3-8b**), These inner and middle shelf basins are filled with ~1 km (~0.6 mi) of soft, semi-consolidated deep-marine mud, glauconitic quartzo-feldspathic sand and hemipelagic mud. The sediment sequence is broken by two major angular unconformities (Kulm and Scheidegger, 1979; Clarke and others, 1985; Niem and Niem, 1992; McNeil and others, 2000).

3.3.17.1 Northern and central provinces

Pleistocene and Holocene surficial deposits in the central and northern provinces are unconsolidated shallow-marine, estuarine, and alluvial sediments that are either in active transport or have yet to be buried to an extent where they become lithified and are the product of the last 1.8 million years of tectonic uplift and landscape evolution of the OCR. Throughout the northern and central provinces, prominent landforms include uplifted wave-cut coastal marine terraces underlain by rounded gravels and sand (up to 10 m/ 33 ft thick) (e.g., Kelsey and others, 1996; McKenzie and others, 2022). Sandy beaches, spits, and dunes are significant along many sectors of the coast (e.g., Plate 2). Inland, fluvial terraces are preserved along many streams, and along with bedrock channels, record progressive uplift and incision of the OCR (e.g., Personius, 1995; Kobor and Roering, 2004). More minor deposits include buried Pleistocene paleosols, estuarine mud beds, and layers of partially carbonized vegetation (Niem and Niem, 1985; Snavely and others, 1976). There is widespread basalt colluvium which consists of thick and structureless deposits of angular to sub-rounded basalt breccias and massive basalt boulders (up to 16 m/52 ft in diameter) (Niem and Niem, 1985). Active and inactive landslides are widely distributed across the study area and are commonly recognized by hummocky topography and other morphologic signatures (e.g., Burns and Madin, 2009; Burns and Mickelson, 2016). Landslide debris consists of a chaotic mixture of soil, blocks of bedrock, and woody fragments. Active and inactive sand dunes can be found along the shoreline within the northern and central provinces. A 20 km (13 mi) stretch of foredune ridges parallels the coast from Warrenton to Seaside (**Figure 3-8)** and from Florence to Reedsport (**Figure 3-5**; **Figure 3-6**) (Peterson, 2007). Locally, dune deposits may contain peat and lake mud deposits in and around intradune lakes.

3.3.17.2 Southern province

Much of the southern province contains Middle Pleistocene (1.8 million years old) and younger deposits of marine, fluvial, landslide, beach, dune, river, and alluvial fan deposits, all of which are unconsolidated. These deposits are highly susceptible to wave erosion along coastal bluffs and by hillslope and fluvial

processes inland driven often driven by heavy rainfall. Wave- and river-cut benches, along with related nearshore, fan, and river deposits, are preserved as terraces and related erosional flats (strath terraces). Groups of marine terraces are widespread along the Oregon Coast and Territorial Sea (**Figure 3-3**; **Figure 3-4**). They range in age from 80,000 years old to >200,000 years old and are located on wave-cut benches that rise from the sea to elevations of up to 330 m (1080 ft), respectively (McInelly and Kelsey, 1990; Kelsey and others, 1994). Fluvial terraces and strath terraces are inset into bedrock and into the youngest marine terraces along rivers and streams. The study area includes landslide deposits of varied types including rockfall deposits, debris fans, slumps, and deep-seated landslides (Niem and Niem, 1985; Burns and others, 2010; McClaughry and others, 2013; Wiley and others, 2014; 2015; Priest and Allan, 2004, Priest and others, 2004).

3.4 Structural Geology of the Oregon Coast and Territorial Sea

The movement and interaction of tectonic plates along their boundaries causes deformation of Earth's crust. In the upper ~10 to 15 km (6 to 10 mi) deformation is largely localized on faults, which are fractures that accommodate differential movement in Earth's crust. Faults can displace crustal blocks in vertical, horizontal, or oblique senses related to the orientation and magnitudes of stresses and rock properties. Faults are present throughout the Oregon Coast study area (e.g., **Figure 3-3b**) and are presented as a total accumulation, without distinguishing age or identified activity level. Faulting in western Oregon is related to the history of terrane accretion, the CSZ, and other plate boundary processes in western North America (Wells and others, 2014). Folds are a second type of structure that occurs where the crust bends in a distributed way. Anticlines are folds that are convex-upward, and synclines are concave-upward, and they generally form in pairs. In the upper crust, most folds are related to nonplanar geometries and/or slip gradients on faults present deeper in the crust (e.g., Burbank and Anderson, 2012), examples of these folds occur in sedimentary units or in the offshore region (e.g., **Figure 3-7**; **Figure 3-8**). Other folds exposed at the surface of the Earth today formed deeper in the crust where high temperatures allow the rocks to flow through plastic deformation at the scale of individual crystals, examples of which are in the southern province, where metamorphic units are present (e.g., **Figure 3-3**; **Figure 3-4**).

The distribution of mapped geologic units, faults, folds, and bedding attitudes (i.e., strikes and dips) as well as topographic lineaments as seen in high-resolution lidar, are data that describe the geologic structure along the Oregon Coast. Information such as total fault displacement can often be interpreted from offset of distinct lithologic units on either side of a fault. However, these contacts or markers are often absent across fault zones in the dense forests with deep soils of the OCR and Klamath Mountains due to nearly identical lithologies that occur on either side of the fault zones (McClaughry and others, 2013). In some cases, relative amount of offset is only locally well defined by geologic units seen along shore cutbanks or within area coal mines.

The Coast Range and Territorial Sea landscapes evolved to their present configuration because of the long-lived Mesozoic to Cenozoic geologic history of subduction of oceanic lithosphere and accretion of the various tectonostratigraphic terranes described above in **section 193.3**. The tectonic forces which moved these crustal blocks also resulted in deformation, which is generally brittle near the surface and ductile at depth. Tectonostratigraphic terranes were emplaced along major boundary faults which accommodated the movement of pieces of dismembered lithosphere into the current configuration and may juxtapose geologic units of varying hardness (sedimentary rocks with exotic greenstone, for example). There are also many joints and faults which postdate the emplacement of the tectonostratigraphic terranes and

result from the ongoing deformation associated with the subduction zone and continuing tectonic clockwise rotation as evidenced by paleomagnetism (Wells and McCaffrey, 2013). The style of faulting and magnitude of displacement of on the faults varies throughout the study area. However, the result of faulting is the juxtaposition of geologic units that do not necessarily share lithological characteristics such as sandstone, volcanic, intrusion, or metamorphic rock type and/or rock strength (e.g., Plates 1 and 2). Active faults and folds also pose hazards both as sources of seismic shaking as well as causing deformation of the ground surface above.

4.0 COASTAL DYNAMICS

This section provides information on coastal dynamics along the coast of Oregon, including descriptions of the characteristics of waves and water levels, predicted rates of sea-level rise, general beach dynamics (including closure depths), and beach and bluff change rates.

4.1 Wave Climate

Wave action is the dominant process affecting the shape and composition of beaches. Waves transport sand onshore (toward the beach), offshore (seaward to form nearshore bars), and along the beach (longshore transport). Short-term (seasonal to interannual) beach and shoreline variability (i.e., storm-related changes) is directly dependent on the size of the waves that break along the coast, ocean water levels, and cell circulation patterns associated with rip currents. Conversely, long-term (interannual to multidecadal) shoreline changes are also forced by additional factors including the balance in the beach sediment budget (sediment inputs versus losses), changes in sea level, storm patterns, and regional tectonics.

The Oregon Coast is exposed to one of the most dynamic ocean wave climates, due to its long fetches and the strength of the extratropical storms that develop and track across the North Pacific (Allan and Komar, 2002). **Figure 4-1** presents a 35-year (1987 to 2022) summary of wave conditions measured at the Stonewall Bank (#46050) National Data Buoy Center wave buoy, located 35 km (21 mi) offshore from Newport on the central Oregon Coast. As can be seen in the figure, the offshore wave climate is characterized by a pronounced seasonal cycle (solid blue line) producing larger waves in the winter (mean significant wave height (H_s) = 3.45 m (11.3 ft)) compared with summer conditions (mean = 1.54 m (5.0 ft)). However, the most extreme winter storm waves can exceed heights greater than 10 m (33 ft), while the largest storms may produce significant wave heights in the range of 14 to 15 m (45 to 50 ft). Estimates of the 100-year or 1% extreme storm wave have been found to range from 14.4 m (47 ft) (Ruggiero and others, 2010) to 15.6 m (51 ft) (Allan and Komar, 2006). In contrast, the summer months are dominated by smaller wave heights (**Figure 4-1**), enabling beaches to rebuild and gain sand eroded in the preceding winter. Thus, there is a seasonal exchange in the volume of sand present between summer (accreted) and winter (eroded). When large waves are superimposed on high tides, they can produce total water levels that are able to reach much higher elevations at the back of the beach, contributing to significantly higher rates of coastal erosion and flood hazards (e.g., **Figure 2-1**). It is the combined effect of these latter processes that leads to the erosion of coastal dunes and bluffs, causing them to retreat landward.

4.2 Tides

Tides along the Oregon Coast are classified as mesoscale, with an average range of about 1.8 m (6 ft) and a maximum range of up to 4.3 m (14 ft) (Komar, 1997). There are two highs and two lows each day, with successive highs (or lows) usually having markedly different levels. Tidal elevations are given in reference to the mean of the lower low water levels (MLLW) and can be easily adjusted to other datums, including the North American Vertical Datum of 1988 (NAVD88). Most tidal elevations are positive numbers with only the most extreme lows having negative values. **Figure 4-2** shows various tidal elevation statistics derived from the South Beach (#9435380) tide gauge located in Yaquina Bay, Newport for the period from 1967 to 2022; the tidal patterns at South Beach are typical of gauges along the Oregon Coast. The South Beach gauge is characterized by a mean[1] range of 1.9 m (6.3 ft) and a diurnal[2] range of 2.5 m (8.3 ft). The highest tide measured from this record reached 3.7 m (12 ft), recorded in December 1969 during a major storm.

Figure 4-1. Seasonal variability of ocean waves measured at the Stonewall Bank (#46050) wave buoy, offshore from Newport for the period from 1987 to 2022. Gray lines define all measurements since 1987. The seasonal cycle is depicted by the solid blue line, while the range +/- 1σ is shown by the two magenta lines accounting for 68% of the variability, and the red line shows +2σ (accounting for 95% of the observations).

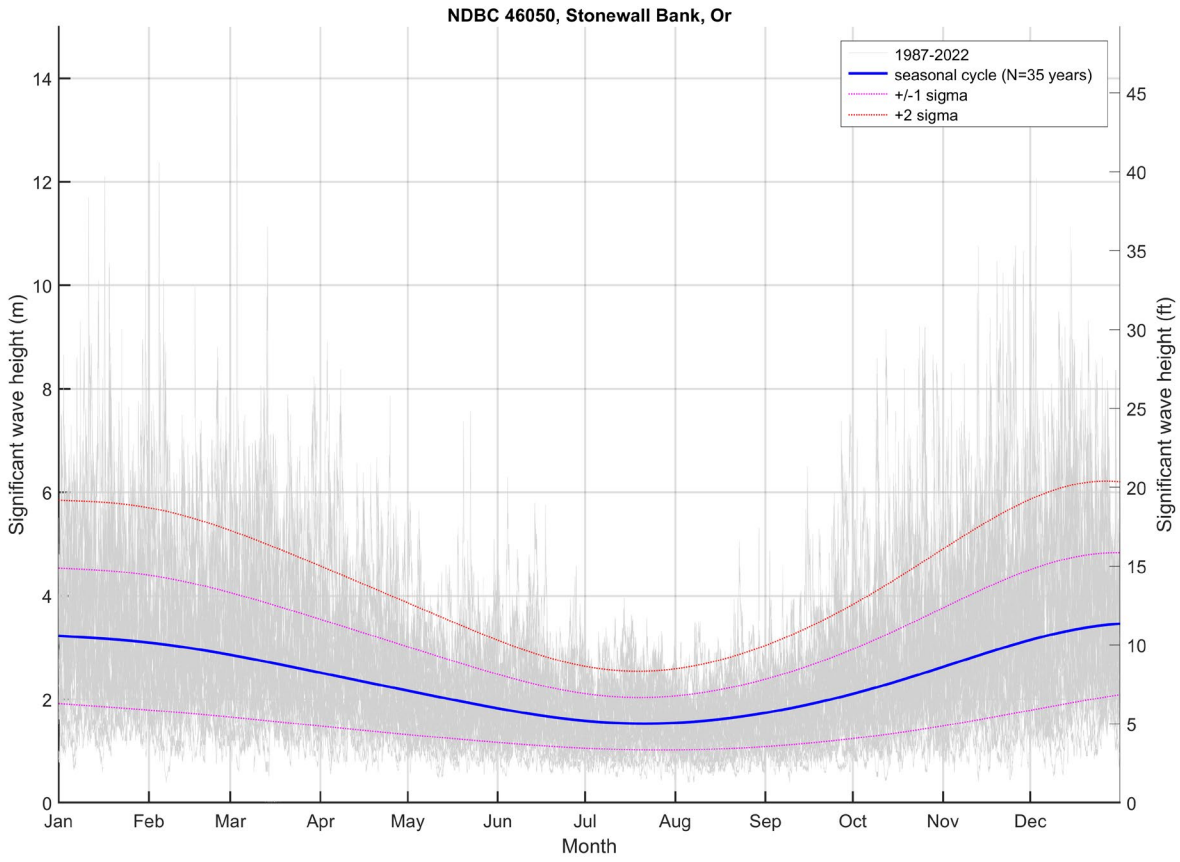

[1] The difference in height between mean high water and mean low water.

[2] The difference in height between mean higher high water and mean lower low water.

Tides on the Oregon Coast are enhanced during the winter months due to warmer water temperatures and the presence of northward-flowing ocean currents that raise water levels along the shore and persist throughout the winter rather than lasting for only a couple of days as is the case for a storm surge. This effect can be seen in the monthly averaged water levels derived from the combined time series (**Figure 4-3**). **Figure 4-3** indicates that, on average, monthly mean water levels during the winter are ~0.23 m (~0.75 ft) higher than in the summer. Water levels are most extreme during El Niño events, due to an intensification of these processes and enhanced sea surface temperatures offshore from the Oregon Coast. This effect was evident for the unusually strong 1982-83 and 1997-98 El Niños (Komar, 1997; Allan and Komar, 2002). As seen in **Figure 4-3**, monthly mean water levels during those climate events were approximately 0.25-0.3 m (0.8-1.0 ft) higher than the seasonal peak, and as much as 0.56 m (1.8 ft) higher than during the preceding summer, enabling wave swash processes to reach much higher elevations on the beach during the winter months, with storm surges potentially raising the water levels even further.

Figure 4-2. Daily tidal stages and elevations measured at South Beach (#9435380) tide gauge Yaquina Bay, Newport on the central Oregon Coast. Data from National Ocean Service (https://tidesandcurrents.noaa.gov/waterlevels.html?id=9435380).

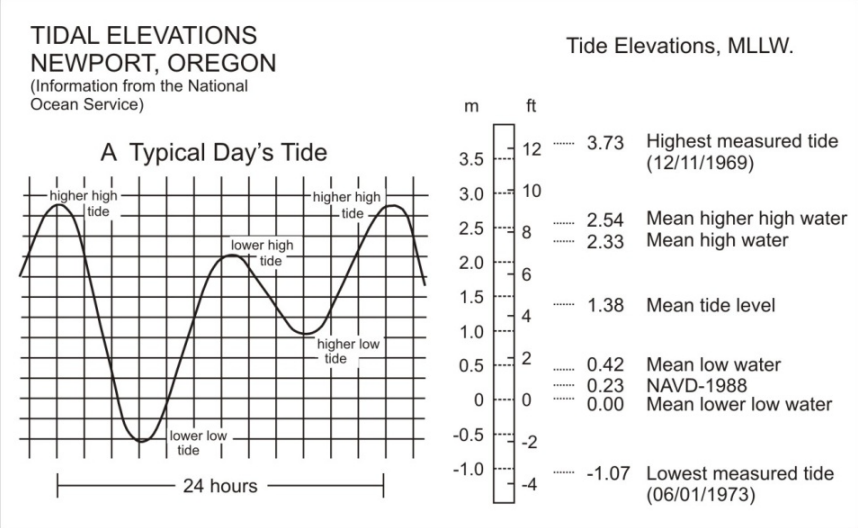

Figure 4-3. Seasonal cycles in monthly mean water levels based on data from the South Beach tide gauge (1967-2022). Data from National Ocean Service.

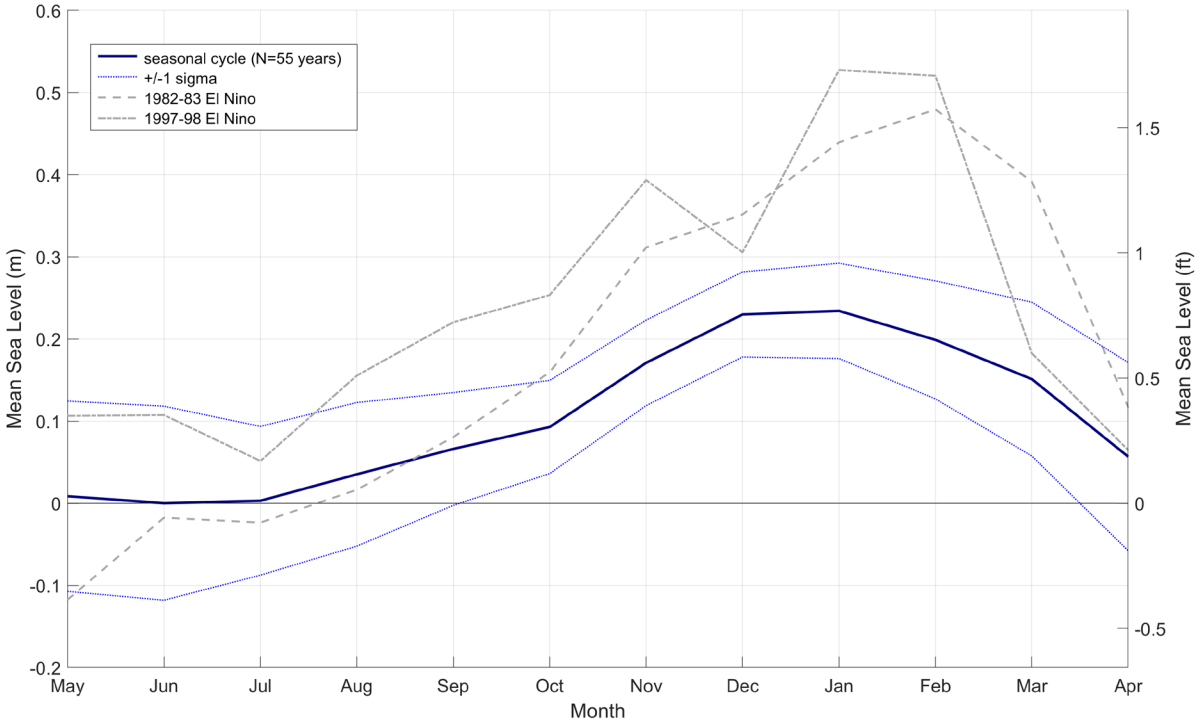

Aside from the seasonal and interannual effects of climate events on ocean water levels, also of interest are the long-term trends associated with relative sea-level changes on the Oregon Coast. Analyses by the NOS indicate that regional sea level at the South Beach tide gauge has risen relative to the land at a rate of ~1.75 ± 0.61 mm/yr (0.07 ± 0.02 in/yr) which equates to a sea-level increase of ~0.1 m (~0.3 ft) since 1967. However, the rate of sea-level change along the Oregon Coast is far from uniform due to regional variations in tectonic uplift and post-glacial isostatic adjustment (e.g., Burgette and others, 2009; Komar and others, 2011; Harvey and others 2021; He and others 2022). In general, analyses of GPS, leveling data from benchmarks, and sea-level gauge trends reveal that sea level is presently falling relative to the land on the southern Oregon Coast due to higher rates of tectonic uplift (a function of the coast being closer to the CSZ). Conversely, sea level is rising when compared with the land on the central to northern Oregon Coast south of Tillamook Head; at the mouth of the Columbia River the rate of sea level rise approximately matches the rate of tectonic uplift. These spatial variations are expected to continue in the absence a major earthquake, with forecasted rates of sea-level rise increasing across the region into the future (e.g., Sweet and others 2022).

4.2.1 Projected future sea levels for the Oregon Coast

Sea-level rise driven by climate change is considered to be a clear and present danger to many coastal communities located around the shorelines of the United States and its territories (Sweet and others, 2022). Global average sea level has increased by 0.2 m (0.66 ft) between 1901 and 2018 (IPCC, 2021), and relative sea level averaged along the contiguous United States has risen by 0.28 m (0.92 ft) in the same period (Sweet and others, 2022). Evaluation of global sea-level change derived from satellite altimetry indicates an increase of 3.56 mm/yr (0.14 in/yr) since 1993, while regional estimates for the North Pacific

are slightly lower at ~3.09 mm/yr (~0.12 in/yr) (AVISO, 2023). Combining knowledge of glacial isostatic rebound (the rate at which the Earth responds to the removal of ice from the last glaciations), regional tectonics, and future temperature patterns determined from global climate models, Sweet and others (2022) provided updated low, intermediate-low, intermediate, intermediate-high, and high-range forecasts for mean sea-level changes for the United States. For the purposes of this report, we focus on increases in sea level using the midrange (intermediate) scenario, given the large uncertainties associated with future climate predictions. Based on the estimates of Sweet and others (2022), the central Oregon Coast (Newport) is predicted to experience a regional sea-level increase of ~0.87 m (2.9 ft) by 2100 (**Table 4.1**), with alongshore variations in the magnitude of sea level rise due to local vertical land motion processes (**Figure 4-4**). It is important to stress that projections of future sea level assume that sea level is uniform year-round. However, as noted previously, sea level on the Oregon Coast exhibits a pronounced seasonal cycle of about 0.23 m (0.75 ft) between summer and winter, increasing to as much as 0.5 m (1.6 ft) in response to the development of a strong El Niño. Hence, when combined with projected future regional sea-level rise, it is apparent that the potential increase in sea level could be substantially greater depending on the time of year and role of the El Niño Southern Oscillation phenomena (**Table 4-1**). For example, by 2100, sea level during an El Niño winter could raise water levels by a total of 1.37 m (4.5 ft), raising the mean shoreline position by that amount, which will shift upward and landward as beaches respond to the change in mean water levels.

Table 4-1. Projected sea-level rise (SLR) for the central Oregon Coast. Data from Sweet and others, 2022.

	SLR (m)	SLR (ft)	El Niño + SLR (m)	El Niño + SLR (ft)
2050 midrange projection	0.20	0.66	0.7	2.3
Range	0.11 to 0.33	0.36 to 1.08	0.61 to 0.83	2 to 2.47
2100 midrange projection	0.87	2.85	1.37	4.5
Range	0.25 to 1.87	0.82 to 6.14	0.75 to 2.37	2.46 to 7.8

Figure 4-4. Observed and projected regional sea-level rise from 2000 through 2100 for the Newport tide gauge in Oregon (figure from Fleischman, 2023, with the data based on Sweet and others, 2022).

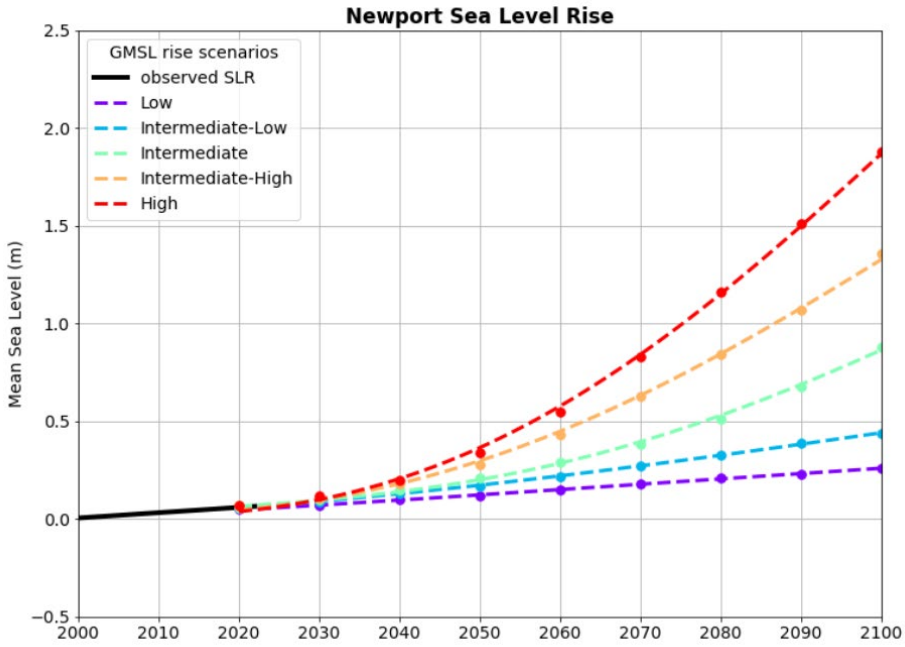

4.3 Sediment Transport

The turbulent process of wave breaking occurs across the nearshore surf zone and results in the entrainment of sediments, which are then moved about by nearshore currents. We can distinguish between those sediments that are moved in the cross-shore direction perpendicular to the beach (cross-shore sediment transport), and the movement of sediments parallel to the beach (longshore transport). Longshore transport is especially significant when waves approach the shore at oblique angles, producing strong currents confined to the breaker zone which can be responsible for the movement of substantial volumes of sediment along the shore.

On the Oregon Coast, the role of longshore currents is especially important due to seasonal variations in the directions of wave approach between summer and winter (**Figure 4-5**). During a "normal year," summer waves, driven by north to northwesterly winds, approach the coast from the northwest (**Figure 4-5**, left, top) and transport sand onshore and toward the southern ends of the littoral cells, causing the dry part of the beach to prograde while sand may accumulate in the dunes (Komar, 1998). In contrast, the arrival of large winter waves from the southwest (**Figure 4-5,** left, bottom) results in a reversal in the net sediment transport direction, which is now directed toward the north. The combination of oblique wave approach and the shift to larger winter waves contributes to erosion of the beach by moving the sand back offshore. Over several "normal" years, and in some Oregon littoral cells there can be an equilibrium balance such that the net sediment transport is close to zero (i.e., there is no net long-term buildup (accretion) of sediment at either end of the littoral cells). However, this pattern may be periodically disrupted by the occurrence of major El Niño events, which can contribute to a significantly larger net northward movement of the sediment (**Figure 4-5**, right). In particular, El Niño events have been shown

to cause "hot spot" erosion at the southern ends of littoral cells (north of headlands and jetties) and on the northern side of estuaries.

Figure 4-5. Patterns of sediment transport during "normal" (left) and El Niño (right) years (after Komar, 1986).

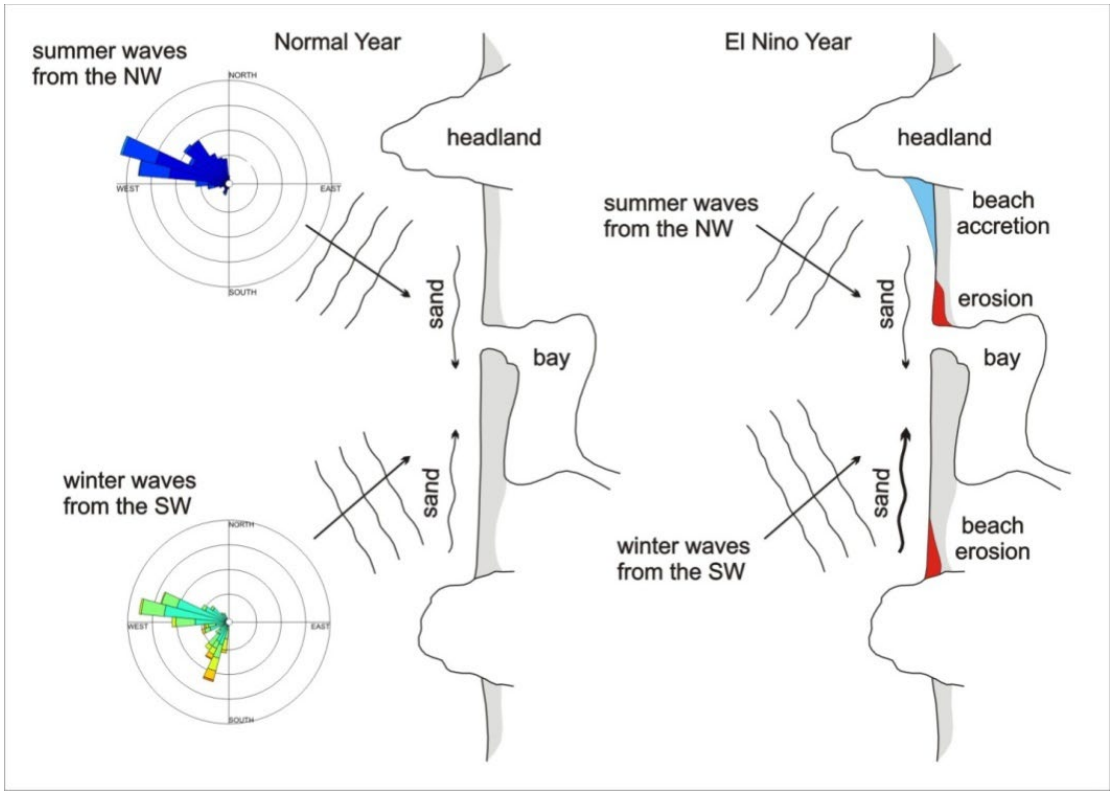

One of the earliest descriptions of the effect of El Niño events on the displacement of sand in littoral cells on the Oregon Coast is that of Komar (1986). While examining the effects of the 1982-83 El Niño in the Beverly Beach littoral cell north of Newport, Komar observed an unusually high northward drift of sand in the cell, with erosion immediately north of Yaquina Head and accretion to the north at Otter Rock. Komar (1986) attributed this response to a combination of factors, including the southward displacement of the storm systems, larger waves (and hence higher wave energy levels), and more acute wave approach angles from the southwest that contribute to the development of strong northward directed currents and sediment transport within the surf zone.

Peterson and others, (1990) were also interested in the effects of the 1982-83 El Niño, focusing their study on the quantification of the northward displacement of sand between Yachats and Seal Rock on the central Oregon Coast. They estimated some 4.8 x 10^6 m^3 (6.3 x 10^6 yd^3) of sand was displaced during the event along ~7.4 km (~4.6 mi) of shoreline. However, their analysis was based on only a few discrete transects, and their speculation of the thickness of the sand and beach slopes produced volume estimates that are large relative to more recent beach volume estimates (Allan and Hart, 2007; Allan and Hart, 2008) and changes observed elsewhere on the Oregon Coast. Regardless, they concluded that the sand shift was the result of a southward 10-15° latitude shift in the winter geostrophic wind, a proxy for the seasonal storm tracks. Essentially, this means that the predominant storm tracks are shifted to the south so that the storm waves arrive at relatively more acute angles relative to the shore, contributing to a stronger than normal north-directed wave energy flux.

In anticipation of potentially large erosional responses expected for the 1997-98 El Niño, airborne lidar was flown along the entire U.S. West Coast. The resultant data were subsequently analyzed in two studies in the Netarts littoral cell to assess the patterns and volume of sand transported as a result of the El Niño (Allan and others, 2003; Revell and others, 2002). In general, Revell and others found that the sand largely moved northward in the Netarts cell, with the greatest amount of erosion occurring at the south end of the cell at Cape Lookout State Park. They noted that the seasonal cycle of cross-shore sediment and beach change was about 320,000 m^3 (418,500 yd^3) of sand volume, while about 70,000 m^3 (91,557 yd^3) of sand was shifted to the north. Allan and others (2003) identified that the mean shoreline position along the southern 3 km (1.9 mi) of the Netarts cell (i.e., seaward of Cape Lookout State Park) eroded by ~20 m (~66 ft). More recently, Allan and others (2009) documented a rotational shift in the mean shoreline position in the Rockaway littoral cell located between Cape Meares and Neahkahnie Head in Tillamook County. Erosion was observed to occur at the south end of all three subcells, while accretion dominated the northern ends of the cells (Allan and others, 2009). In total, some 1.4×10^6 m^3 (1.9×10^6 yd^3) of sand was removed from the cell due to enhanced wave erosion, some of which was removed to the north where it accumulated on Nehalem Spit. These data reflect the accumulated change that took place over two winters, the 1997-98 El Niño and 1998-1999, when a series of particularly extreme storms occurred.

Anderson and others (2018) analyzed a 63-year record of hindcast waves (1950-2010) in order to calculate the monthly alongshore wave energy flux (a measure of the sediment transport potential). They found that the average monthly climatology of all 63 years results in zero net annual longshore directed wave energy flux, consistent with the hypothesis of Komar (1998). However, when individual years were examined, such as major El Niños, the northerly directed energy flux was found to be an order of magnitude greater than the climatological mean (i.e., more sand was transported to the north). Conversely, major La Niña events produced a comparable response, but in the opposite direction (Anderson and others, 2018). Incorporating a one-line shoreline change model and the long-term wave energy flux, Anderson and others (2018) identified decadal oscillations in the position of the shoreline between 1950 and 2010, which were strongly coupled to the occurrence of the El Niño/La Niña climate phenomena, as well as the longer-term Pacific Decadal Oscillation.

4.3.1 Closure depth

The seaward limit of measurable morphologic change is referred to as the depth of closure (DOC) and is a function of the nearshore wave climate and sediment characteristics (Birkemeier, 1985; Brutsché and others, 2016; Hallermeier, 1981). More specifically, the DOC reflects the depth at which there is little to no significant change in the bottom elevation. In this respect, the DOC provides a measure of the seaward extent of the littoral zone and is often thought of as the location at which repeat beach profile elevations converge through time. A second, deeper zone, was also defined that reflects the region where wave effects on the seafloor become negligible. Equations for calculating the offshore extreme surf-related effects of the littoral zone (d_l) and shoal zone (d_i) regions were originally developed by Hallermeier (1981) and modified by Birkemeier (1985). Using both sets of equations, Brutsché and others (2016) calculated DOCs for the entire US coastline, using Wave Information Study (WIS) hindcast stations. Their results are extremely useful for any coastal engineering analysis that requires an understanding of the seaward extent of significant net sediment transport in a region. Analyses of the DOCs calculated for the Oregon Coast using the Hallermeier equations indicated an average DOC of 15.9 m (52 ft), $\pm 1\sigma$ = 0.37 m (1 ft); empirical calculations using Birkemeier equations indicated a mean DOC of 12 m (40 ft). Allan and others

(2005) performed similar calculations and determined a DOC for the Oregon Coast that ranges from 10 to 14 m (33 to 46 ft), varying from year to year.

Figure 4-6 presents repeat surveys of bathymetric change measured at a long-term (1998 to 2021) coastal monitoring site on Long Beach Peninsula (075), Washington State (data from Ruggiero and others, 2016). The repeat surveys show the degree of variability across the nearshore and subaerial beach, with the largest vertical envelope of change occurring at depths less than ~10 m (~33 ft). Below the 10 m (33 ft) isobath, the degree of change is much lower (1σ = ~0.16 m (0.5 ft)). Hence, in the Long Beach example of repeat bathymetric measurements, the DOC is close to ~10 m (~33 ft). Analyses of serial bathymetric surveys at multiple transects in the Rockaway littoral cell (2008 to 2016) (**Figure 4-7**; Allan and others, 2015d; Cohn and others, 2019) suggest a deeper DOC that is ~14 to 15 m (~46 to 49 ft). In both cases, the results from repeat bathymetric surveys are generally consistent with the simple empirical estimates of the DOC calculated by Brutsché and others (2016).

Figure 4-6. Repeat topo-bathymetric surveys performed at line 075, Long Beach peninsula, Washington State. Top plots depict the serial beach and nearshore profile surveys and the bottom plot shows the envelope of variability determined from all surveys. Data from Ruggiero and others (2016).

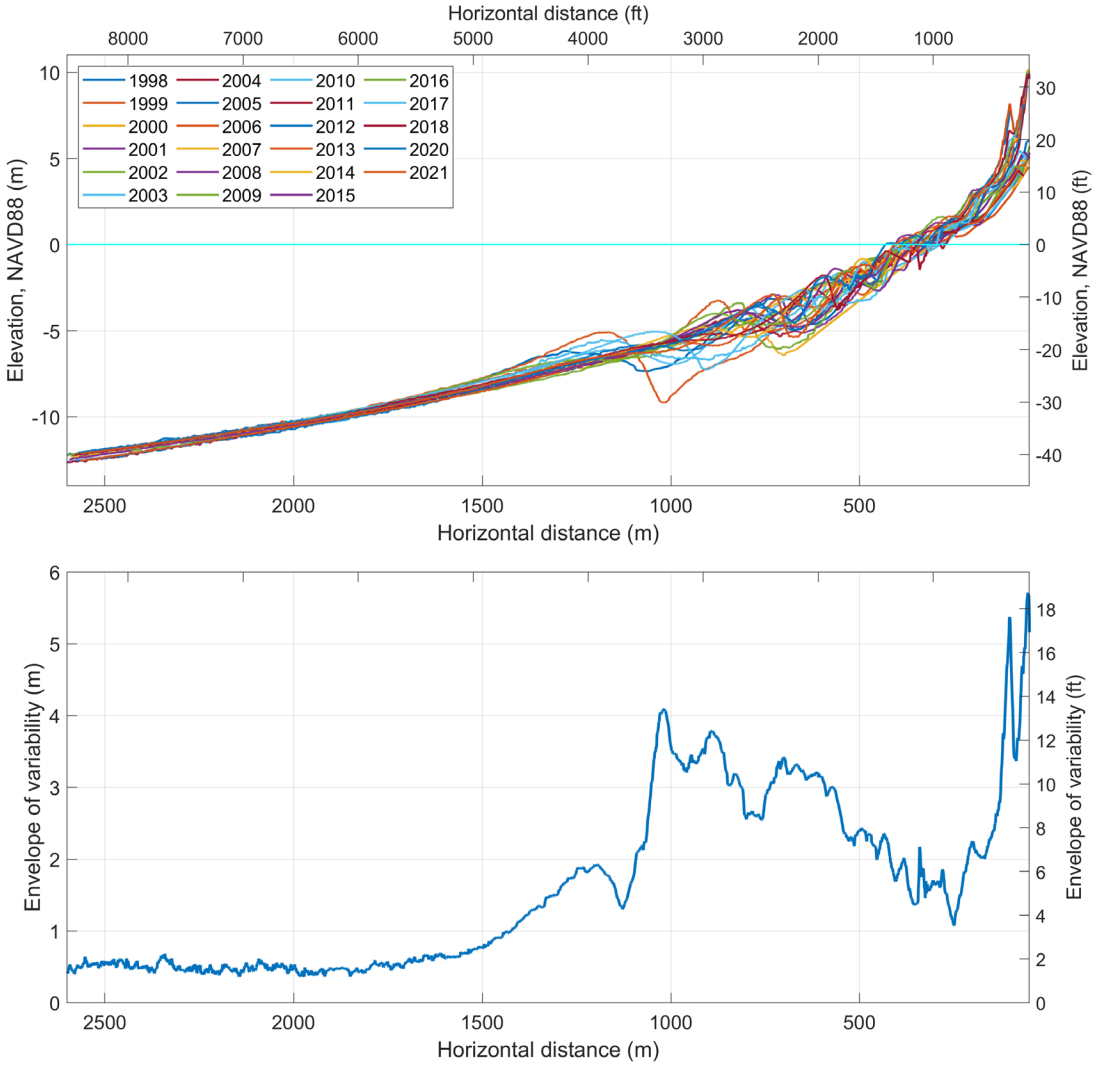

Figure 4-7. Repeat topo-bathymetric surveys performed at line 053, Rockaway Beach, Oregon. Top plots depict the serial beach and nearshore profile surveys and the bottom plot shows the envelope of variability determined from all surveys. Data from Allan and others (2015d) and Cohn and others (2019).

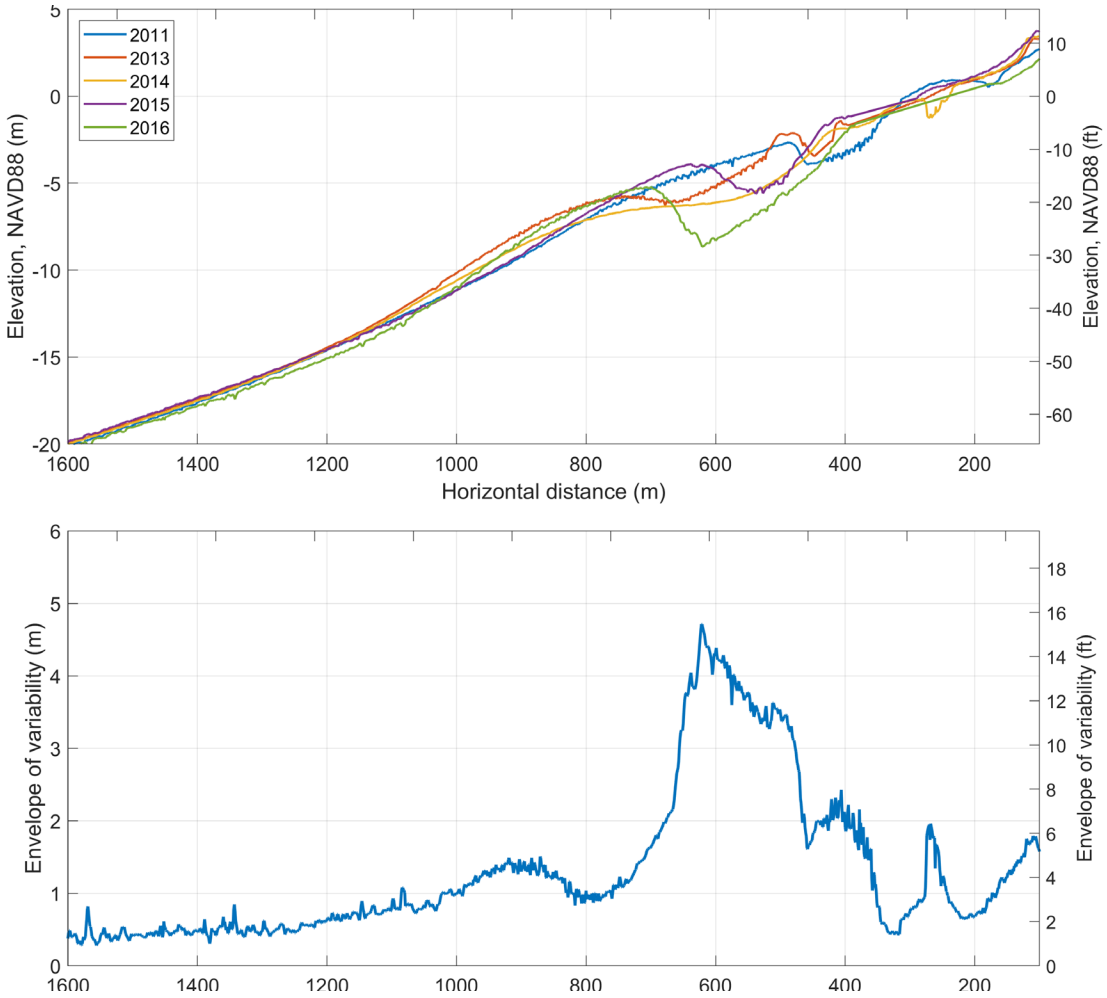

4.4 Coastal Change Rates and Patterns

4.4.1 Previous studies

Numerous studies have attempted to define the patterns and rates of erosion for different rock lithologies for coastal bluffs along the Oregon Coast (**Table 4-2**), including Lincoln County (Seal Rock to Roads End (Priest and others, 1994); Cascade Head to Seal Rock (Priest and Allan, 2004), Seal Rock to Cape Perpetua (Witter and others, 2007), Sisters Rock to North Gold Beach, Curry County (Priest and others, 2004), and southern Clatsop County (Witter and others, 2009). Erosion rates were defined using discrete measurements of identified features in serial imagery, typically a house to top of bluff measurement. Although the results from these studies are useful, they lack sufficient spatial coverage and have potentially large uncertainties in the calculated rates of change as the temporal period of observation is

limited to the period of study. For example, efforts by Priest and Allan (2004) used early 1939 aerial images where coverage was good, while other studies have used 1967 aerial images to estimate change. Unfortunately, there is no sustained effort to document the long-term rates and patterns of bluff erosion, which remains a limitation for projecting future erosion responses.

Table 4-2. Bluff erosion rates defined for different lithologic compositions with measurement errors from aerial photos (Error) and variation at multiple sites (σ). Negative rates indicate erosion; positive rates show accretion.

Location	Lithology	Erosion Rate m/yr (ft/yr)	Error m/yr (ft/yr)	σ m/yr (ft/yr)
[1]***Clatsop County***	Miocene Grande Ronde Basalt	-0.03	0.09	0.02
		(-0.01)	(0.3)	(0.07)
	Resistant sedimentary rock	-0.03	0.03	0.02
		(-0.1)	(0.1)	(0.07)
	Interbedded mudstone	-0.06	0.09	0.04
		(-0.2)	(0.3)	(0.13)
	Quaternary deposits	-0.08	0.08	0.11
		(-0.3)	(0.3)	(0.36)
[2]***Tillamook County***	Basalt and hard sandstone	-0.02	0.05	0.036
		(-0.07)	(0.16)	(0.12)
	Interbedded sandstone, siltstone, claystone	-0.06	0.08	0.039
		(-0.2)	(0.26)	(0.128)
	Soft Quaternary sediments	-0.08	0.07	0.081
		(-0.26)	(0.23)	(0.27)
[3]***Lincoln County***				
Beverly Beach	Sedimentary rock (Astoria)	-0.25 (-0.82)	0.12 (0.4)	0.024 (0.08)
Holiday Beach to Lost Creek	Sedimentary rock (Nye Mudstone)	-0.09 (-0.3)	0.04 (0.13)	0.006 ()
Lincoln City/Gleneden Beach	Marine terrace sand	-0.09 (-0.3)	0.06 (0.2)	0.003 (0.01)
[4]***Curry County***				
Headlands/Bluffs	Hard Mesozoic metamorphic rocks	-0.02 (-0.07)	0.09 (0.3)	0.028 (0.09)
Nesika Beach to Gold Beach	Cretaceous and Jurassic sedimentary and metamorphic rocks	-0.02 (-0.07)	0.09 (0.3)	0.028 (0.09)
Euchre Creek to Nesika Beach	Marine terrace deposits over Jurassic sedimentary and metamorphic rocks	-0.40 (-0.13)	0.09 (0.3)	0.003 (0.01)
South Nesika Beach		-0.59 (-1.9)	0.09 (0.3)	0.012 (0.04)
Nesika Beach to Otter Point		0.26 (0.85)	0.09 (0.3)	0.098 (0.32)
		0.16 (0.52)	0.09 (0.3)	0.064 (0.21)
Otter Point to North Jetty		-0.02 (-0.07)	0.09 (0.3)	

(Data sources: [1]Witter and others, 2009; [2]Allan and Priest, 2001; [3]Priest and Allan, 2004; [4]Priest and others, 2004).

Change rates for sandy beaches have typically been measured by evaluating shoreline positions determined from historical National Ocean Service (NOS) topographic "T" sheets that define a mean high water (MHW) line on maps, extracting wet/dry shorelines from aerial imagery, and, more recently, by analyzing tidal datum-based shorelines (e.g., MHW or mean higher high water (MHHW)) from airborne lidar data (e.g., Allan and others, 2003; Ruggiero and others, 2013; Light, 2021). Each dataset has limitations. For example, NOS surveys of MHW shorelines of the Oregon Coast in the late 1920s mapped

at 1:20,000 scale, have large (~±20 m (~± 66 ft)) positional uncertainties (Moore, 2000). Although the earliest coastwide aerial imagery of the Oregon Coast was collected in 1939, georeferencing these images is extremely challenging, time consuming, and often not possible due to the absence of suitable ground control points. High-quality imagery did not begin to be collected until 1967, which ultimately formed the baseline on which many recent studies of coastal change have been based. The 1967 aerial photographs were flown by the Oregon Department of Transportation for the purposes of helping to delineate a shore zone boundary (Jung and others, 2022), and were eventually used to establish the "statutory vegetation line" for determining the permitting of coastal engineering structures. The images were flown at low altitude (1:6,000 scale, ~900 m (~2,950 ft) elevation) during summer months (June to October) and provide an excellent snapshot of the coastal strip at the time. These data were eventually orthorectified in 2008 using Leica Photography Suite, from which a wet/dry shoreline was digitized. Since the 1990s, high-resolution orthorectified aerial imagery specifically for the coast has been collected on a more regular basis, the most recent of which was in 2020. Beginning in 1997, high-resolution airborne lidar data have been collected along the Oregon Coast that complement the use of aerial imagery for evaluating coastal change.

Ruggiero and others (2013) analyzed a combination of aerial imagery and lidar tidal datum-based shorelines to derive both long (1920s-2002) and short-term (1967-2002) change rates for the coast of Oregon and Washington. Light (2021) provided updated rates to those of Ruggiero and others (2013), having incorporated more recent lidar collected in 2016. The challenge with these data is each of the shorelines reflect discrete "snapshots" of the position of the beach in time. Analyses of this imagery and the identified coastal changes undertaken by Allan and others (2003) reveal very large variability in the position of the shoreline snapshot due to their sensitivity to seasonal and interannual (e.g., El Niños) variations in ocean water levels and storms. This makes determining reliable erosion rates from MHW shorelines challenging, due to the large envelope of variability, and hence greater uncertainty.

To address some of the aerial imagery and lidar challenges, the Oregon Department of Geology and Mineral Industries (DOGAMI) coastal field office implemented a coastal monitoring program in the Rockaway Beach area in October 2004 to begin documenting seasonal to interannual coastal changes. This monitoring is undertaken at discrete beach profile sites, but also involves the collection of tidal datum-based shorelines (e.g, **Figure 4-8)**. Coastal change monitoring is accomplished using real-time kinematic differential GPS (RTK-DGPS) surveying and is carried out at multiple sites along the Oregon Coast, including the Rockaway and Clatsop littoral cells (Allan and others, 2008), Neskowin (Allan and Hart, 2007), Gold Beach-Nesika Beach-Netarts (Allan and Stimely, 2013), the Cannon Beach cell (Allan and others, 2018) and many other sites (http://nvs.nanoos.org/BeachMapping). Although a rich dataset of coastal change is now established for many north coast beach sites, with identified trends (e.g., **Figure 4-9**), regular, repeat surveys of many other sites (especially those on the south coast) do not have the same temporal sampling resolution. Nevertheless, **Figure 4-9** highlights certain important characteristics that are typical of Pacific Northwest (PNW) beach responses that provide guidance on the role of coastal processes in driving change. First, observations at the 3 m (10 ft) contour (nearest to the intertidal zone and hence the MHW shoreline) demonstrate considerable horizontal variability in the beach responses due to the strong seasonality of ocean waves and tides that characterize PNW beaches. These excursions can be very large (**Figure 4-9**), spanning ~±10 to 20 m (~±30 to 60 ft) between summer and winter. This is further demonstrated in **Figure 4-8**, which is derived from RTK-DGPS surveys of the MHHW shoreline (light blue lines); the calculated change rate at the 3 m (10 ft) elevation at the Neskowin site is -1.21 ±0.71 m/year (-3.94 ±2.33 ft/year). These data highlight one of the challenges when using discrete "snapshots"

of shorelines derived from aerial imagery, where the time intervals between measurements may be long, such that the results may be strongly affected by those few discrete measurements.

Figure 4-8. MHHW shorelines (blue lines) derived from repeat surveys of the beach for Transect 3 (red line) at Neskowin.

Figure 4-9. Seasonal surveys of beach responses in the Neskowin littoral cell at station Neskowin 3 (Figure 4-8; http://nvs.nanoos.org/BeachMapping). Plot shows the seasonal to interannual variability at different contour elevations across the beach. Negative positions in the contours indicate erosion; positive values denote accretion.

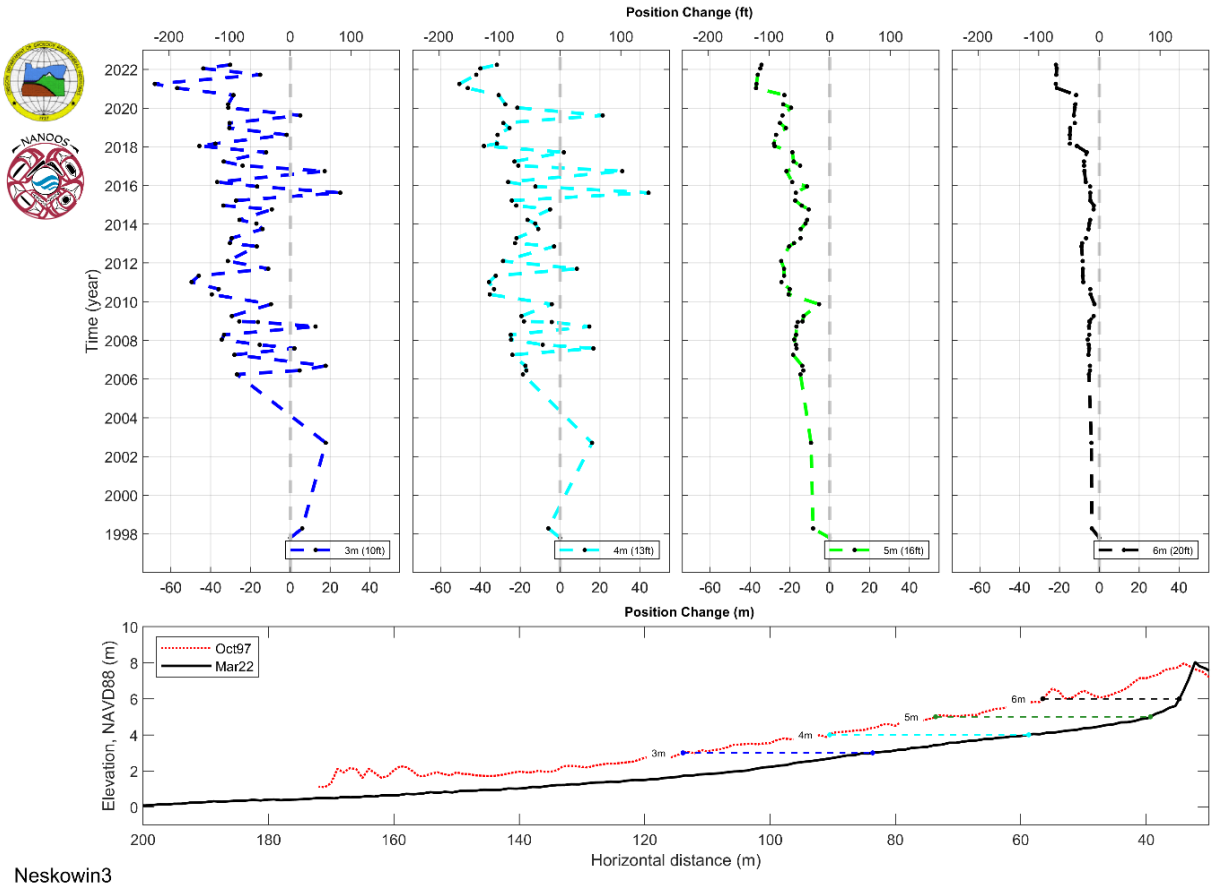

At higher elevations on the beach, such as the 6 m (20 ft) elevation located close to the dune or bluff toe, there is much less variability (**Figure 4-9**) with a calculated erosion rate of -0.45 ±0.14 m/year (-1.5 ±0.0.46 ft/year). At these higher elevations, the erosion of the backshore is driven entirely by the effects of extreme total water levels, which results in periodic abrupt landward movements in the position of the contour over time (e.g., the 6 m (20 ft) contour in **Figure 4-9**), while highlighting a smoother long-term trend. Although monitoring efforts such as this are extremely valuable for dune-backed beaches where errors in the approach are low relative to the magnitude of changes being observed, the same cannot be said for performing RTK-DGPS measurements of sea cliff profiles given that the approach of surveying down a bluff face using GPS is prone to large errors and uncertainty due to the generally slower rates of change. Resolution of this limitation can only be achieved by establishing a monitoring program that is founded on repeat measurements of the bluff face using terrestrial lidar.

In summary, many studies have identified estimates of short to long-term coastal change rates for different areas of the Oregon Coast (**Table 4-2**), which have been derived from a variety of datasets, each with their own pros and cons. While it is not unreasonable to use these datasets to make projections of potential future change for the coast, we chose to undertake some additional analyses of long-term change rates for the Oregon Coast.

4.4.2 Bluff/Dune toe change rates, 1997 – 2016

Given the high variability of MHW shorelines compared with smoother trends for contours derived for the back of the beach near the dune or bluff toe, we chose to produce new change rates for the Oregon Coast by evaluating responses occurring at the back of the beach. **Figure 4-10** consists of a series of histograms of previously identified dune/bluff toe elevations undertaken for different lidar years on the northern Oregon coast (data originally from Allan and Harris, 2012). The figure indicates the wide range of dune/bluff toe elevations present on the coast, and further how these elevations can vary from year to year. For this updated change analysis, we chose to use the 6 m (18 ft) contour elevation (blue dash line in **Figure 4-10**) since it is more likely to yield a less noisy result. the 6 m (18 ft) contour elevation. For this analysis, we used lidar data that cover the period from 1997 to 2016 (**Table 4-3**). The lidar data were downloaded from the National Oceanic and Atmospheric Administration's Coastal Service Center and gridded using ArcGIS Pro. The pre 2016 lidar was gridded using a 1 m (3 ft) cell size, and 0.5 m (1.6 ft) grid cell for 2016 lidar. Although the 1 m (3 ft) grid resolution used in the pre-2008 lidar likely pushes the point density limits of those earlier flights, they are probably not unreasonable for the generally low-sloping beaches of the Oregon Coast.

Figure 4-10. Histogram showing beach dune/bluff toe elevations determined from lidar data and for different years (data originally from Allan and Harris, 2012).

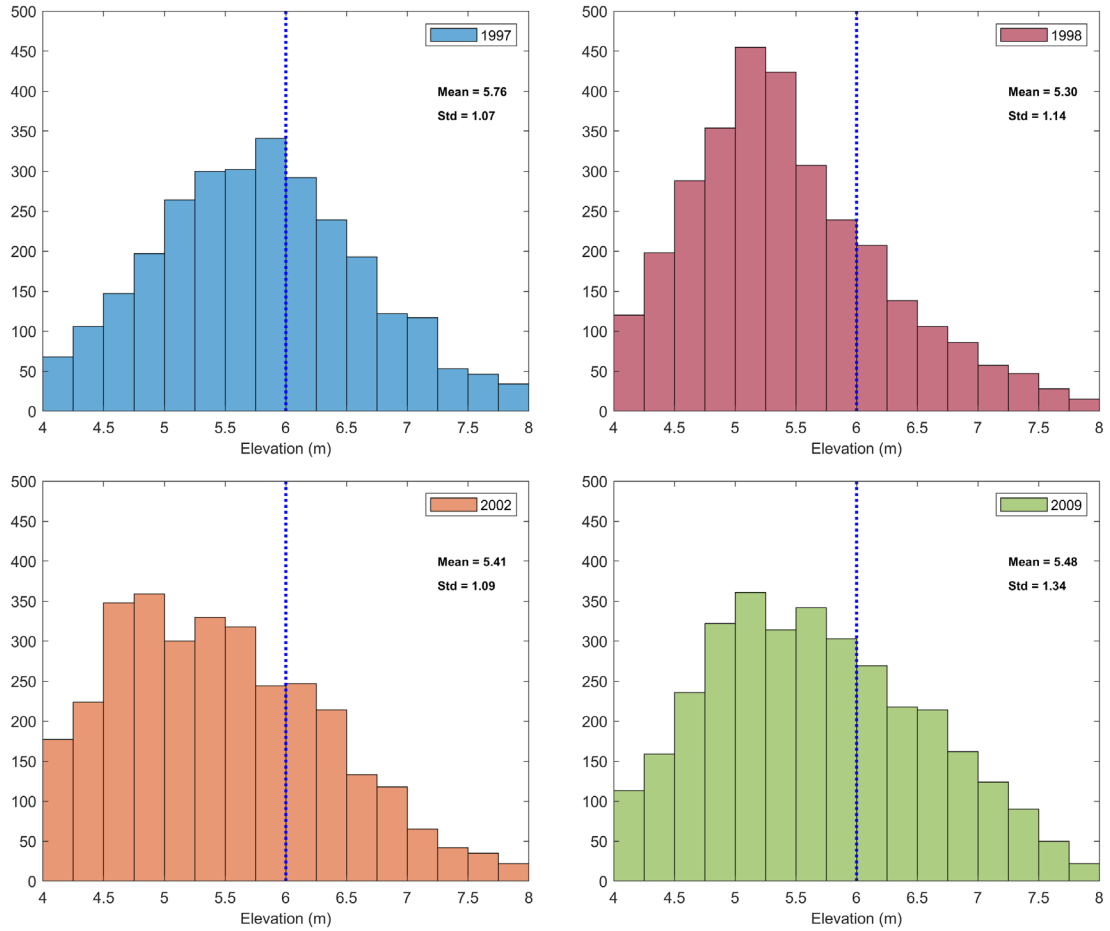

Table 4-3. Airborne lidar summary metadata.

Collection Date	Agency source	Accuracy Hor. (m) [ft]	Accuracy Vert. (m) [ft]	Typical Point density (point/m²)	Metadata link
10/12/1997 – 10/26/1997	NASA/USGS[1]	0.8 (2.6)	0.15 (0.5)	3	https://www.fisheries.noaa.gov/inport/item/48150
4/8/1998 – 4/28/1998	NASA/USGS[1]	0.8 (2.6)	0.15 (0.5)	3	https://www.fisheries.noaa.gov/inport/item/48155
09/18/2002 – 10/03/2002	NASA/USGS[1]	0.8 (2.6)	0.15 (0.5)	3	https://www.fisheries.noaa.gov/inport/item/49634
04/27/2008 – 04/05/2009	DOGAMI[2]	N/A	0.15 (0.5)	9	https://www.fisheries.noaa.gov/inport/item/49903
04/05/2009 – 08/09/2009	DOGAMI[2]	N/A	0.15 (0.5)	9	https://www.fisheries.noaa.gov/inport/item/49906
07/30/2014 – 09/13/2014	USACE[2]	1.0 (3.3)	0.1 (0.33)	9	https://www.fisheries.noaa.gov/inport/item/49456
04/28/2016 – 05/28/2016	USGS[2]	0.21 (0.7)	0.06 (0.2)	9	https://www.fisheries.noaa.gov/inport/item/48222

Note: [1]single return; [2]multiple return; projection used = Oregon State Plane Coordinate System (north and south), NAD83 (m); vertical datum = NAVD88.

Having developed consistent coastwide grids, we extracted various contours of interest (e.g., MHW, 6 m (20 ft)). Because the pre-2008 lidar point data exhibited considerable noise, the contours were smoothed using the Polynomial Approximation with Exponential Kernel method in ArcGIS Pro. Once the contours were produced, we performed visual checks of the contours, comparing the results against lidar hillshades to identify additional spurious noise; noise can be attributed to a combination of insufficient points or spikes in the lidar returns. Noise in the contours were removed by either clipping out portions of the lines or deleting select vertices.

The derived contours were then processed to identify temporal change using the Digital Shoreline Analysis System (DSAS) tool developed by the U.S. Geological Survey (Himmelstoss and others, 2018). The DSAS tool is an add-in to Esri ArcGIS Desktop version 10.4–10.7 that enables a user to calculate rate-of-change statistics from a time series of vector shoreline positions. DSAS includes an automated method to establish measurement locations and perform rate calculations and evaluates the statistical data necessary to assess the reliability of the change rate calculations (Himmelstoss and others, 2018). To operate the tool, a user first defines a series of baselines along a coastline of interest. For the purposes of this study, we developed baselines that spanned individual counties. Transects are then automatically cast by DSAS seaward and perpendicular to each baseline of interest. Although DSAS provides several functional controls that help account for areas subject to large shoreline curvature, we typically created shorter baselines, and manipulated the DSAS controls to ensure the transects were aligned shore-normal (perpendicular to the coast) and addressed moderate scale coastline curvature at alongshore scales of 200 m (~650 ft). For the purposes of this study, we chose to cast transects spaced 10 m (33 ft) apart for the entire coast. The tool then requires input of the shoreline "contour" features for change detection along with various metadata, which includes specification of any errors associated with each line feature. For this study, we determined a contour uncertainty of 3 m (10 ft) for pre-2008 lidar data, and 1 m (3 ft) for post-2008 data. Once the necessary data are input into the tool, DSAS is then run to define the rate-of-

change statistics for the period of interest. This is accomplished by querying the position of each shoreline feature (with assigned dates) and its intersection with every transect line. Several statistics are then output from the tool, including net shoreline movement, endpoint rate calculations, linear regression rates, and weighted linear regression rates (e.g., see Table 10 in Himmelstoss and others, 2021).

Having processed the individual transect change rates, discrete shore reaches were identified in ArcGIS and compiled in an Excel worksheet. Additional processing was performed in Mathworks Matlab (vR2022b) in order to smooth the 10 m (33 ft) spaced transect data; we used a 50 m (164 ft) smoothing function to reduce the noise in the change data. Each reach was defined based on a combination of the dominant coastal geomorphology (e.g., dune- and bluff-backed beaches, cobble shorelines, rock coast, etc.) and the identified change rates. An example of the compiled results is presented in **Table 4-4** for Clatsop County, which includes the net shoreline movement for the study period, endpoint rate calculation and standard deviation, percent of transects eroding or accreting, calculated 1% (100-year) storm-induced erosion (dune-backed beaches only), and projected future erosion due to sea-level rise by 2050 and 2100. For the latter, we used a simple 2D geometric response that accounts for the slope of the beach at ~MHW (defined for each shore reach based on 2016 lidar) and the projected sea-level rise (Bruun, 1988; Dean and Houston, 2016) defined in **Table 4-1**. Storm-induced dune erosion defined in **Table 4-1** (and for subsequent counties) is based on analyses of the calculated erosion associated with a 1% storm and is fully described in Allan and others (2012), Allan and others, (2015a), Allan and others (2015b), Allan and others (2015c), Allan and others (2015d), Allan and others (2017).

Table 4-4. Example DSAS change information for select reaches in Clatsop County.

Site Name	Transect Id	Net Shoreline Movement 1997-2016 (m) [ft]	Endpoint Rate (m/year) [ft/year]	Sigma (m) [ft]	Transects Eroding %	Transects Accreting %	[1]Storm Induced Erosion 1% event (m) [ft]	Sea-Level Rise Erosion 2050 (m) [ft]	Sea-Level Rise Erosion 2100 (m) [ft]
South jetty dynamic revetment	1 – 34	3.69 (12.1)	0.20 (0.7)	0.18 (0.59)	12	88	-17.9 (-58.7)	-11.9 (-39.0)	-51.9 (-170.3)
East jetty	35 – 108	-3.62 (-11.9)	-0.20 (-0.7)	0.23 (0.75)	89	11	-17.9 (-58.7)	-6.3 (-20.7)	-27.2 (-89.3)
Clatsop Spit	109 – 163	1.68 (5.5)	0.09 (0.3)	0.05 (0.16)	0	100	-17.9 (-58.7)	-5.4 (-17.7)	-23.5 (-77.1)
Iredale	226 – 1039	9.24 (30.3)	0.50 (1.6)	0.33 (1.08)	3	97	-9.5 (-31.2)	-5.7 (-18.7)	-25.0 (-82.0)
Rilea	1040 – 1507	35.78 (117.4)	1.93 (6.3)	0.44 (1.44)	0	100	-10.8 (-35.4)	-6.4 (-21.0)	-27.7 (-9.09)
Delray	1508 – 2076	40.06 (131.4)	2.16 (7.08)	0.45 (1.48)	0	100	-10.9 (-35.8)	-6.0 (-19.7)	-26.2 (-86.0)
Gearhart	2077 – 2430	27.29 (89.5)	1.47 (4.82)	0.40 (1.31)	1	99	-13.7 (-44.9)	-5.9 (-19.4)	-25.8 (-84.6)
Necanicum estuary	2431 – 2448	-44.90 (-147.3)	-5.91 (-19.4)	3.87 (12.7)	94	6	-19.8 (-65.0)	-12.5 (-41.0)	-54.5 (-178.8)
Seaside	2465 – 2810	42.40 (139.1)	2.28 (7.48)	1.93 (6.33)	5	95	-9.8 (-32.2)	-7.5 (-24.6)	-32.6 (-106.9)

([1]100-year storm erosion data is derived from Allan and others, 2017; Allan and others, 2015a; Allan and others, 2015b; Allan and others, 2015c; Allan and others, 2015d; Allan and others, 2012)

Figure 4-11 to **Figure 4-16** present the smoothed change results for all seven coastal counties. Overall, the figures demonstrate significant variability along the Oregon Coast, from extreme erosion to areas undergoing considerable accretion. Overall, we note the following general observations by county:

Clatsop

- The coast north of Tillamook Head is experiencing relatively high rates of accretion (**Figure 4-11**). For example, our change analyses indicate that Seaside is experiencing rates of accretion of ~2 to 3 m/year (~6 to 10 ft/year), and ~0.5 to 2.5 m/year (1.6 to 8 ft/year) along the Clatsop Plains.
- Significant accretion also dominates the area north of Ecola Creek in Cannon Beach.
- South of Cannon Beach, the coastline is experiencing gradual erosion.

Tillamook

- Change analysis along the Tillamook County coast exhibits significant alongshore variability that ranges from high rates of erosion to high rates of accretion (**Figure 4-12**). Overall, the identified rates and patterns are entirely consistent with GPS measurements of discrete beach profile sites monitored by DOGAMI staff (https://nvs.nanoos.org/BeachMapping).

- Accretion dominates much of Nehalem (~0.5 to >2 m/year (~1.6 to >6 ft/year)) and Bayocean Spits (~0.5 to >3 m/year (~1.6 to >10 ft/year)), north of the Sand Lake estuary (~0.5 to 1 m/year (~1.6 to 3 ft/year)) and along Sitka Sedge Spit (>1.5 m/year (>5 ft/year)).
- Significant erosion dominates areas such as Neskowin to Nestucca estuary (~-1 m/year (~-3 ft/year)), Netarts Spit (~-1 to -2 m/year (~-3 to -6 ft/year)), and Twin Rocks and Rockaway Beach shore (~-1 to -3 m/year (~-3 to -10 ft/year)).

Lincoln

- Gradual rates of erosion are dominant along the length of the Lincoln County coastline (**Figure 4-13**), where average rates of change are in the range of -0.1 to –0.2 m/year (-0.3 to -0.6 ft/year). These rates are consistent with long-term measurements derived from aerial imagery and provided in **Table 4-2**.
- Exceptions to the above include significant accretion taking place at the mouths of Alsea Bay, Yaquina Bay, and at the tip of Siletz Spit.

Lane and Douglas

- Accretion dominates much of the Lane and Douglas County shoreline (**Figure 4-14**). In particular, we note relatively high rates of accretion in the vicinity of Heceta Beach and the mouth of the Siuslaw estuary (~1 to >2 m/year (~3 to >6 ft/year)).
- Low rates of erosion dominate the coastline north of Heceta Head.

Coos

- Relatively low to moderate rates of erosion (~-0.1 to -1 m/year (~-0.3 to –3 ft/year)) dominate much of the Coos North Spit (**Figure 4-15**).
- The shoreline south of the Coquille estuary exhibits significant variability that ranges from relatively low rates of erosion (~-0.1 to -1 m/year (~-0.3 to –3 ft/year)), to significant accretion in places such as at Johnson Creek and along the New River Spit (~1 to >2 m/year (~3 to >6 ft/year)).
- Variability along the New River Spit is likely being affected by periodic river mouth breaching.

Curry

- Much of the Curry County coastline is characterized by relatively low to moderate rates of erosion (~-0.1 to -1 m/year (~-0.3 to –3 ft/year)). The main exception is Gold Beach, where relatively high rates of erosion (~-2 m/year (~-6 ft/year)) are dominating the current coastal response (**Figure 4-16**).
- Accretion is largely occurring in a few isolated areas such as at Garrison Lake, south of Hunter Creek, and along the Pistol River.
- Accretionary responses occurring along the Garrison Lake coastline should be viewed with caution as Allan and others (2003) documented the effects of extreme erosion along that shore following the 1997-98 El Niño.

Figure 4-11. Coastal change rates (m/year) and patterns for the period 1997 to 2016 for Clatsop County. Cyan line reflects a 50 m (164 ft) smoothing of the individual transects, while the solid circles with uncertainty depicts the mean change for the identified study reach. Negative values indicate erosion, while positive values denote accretion.

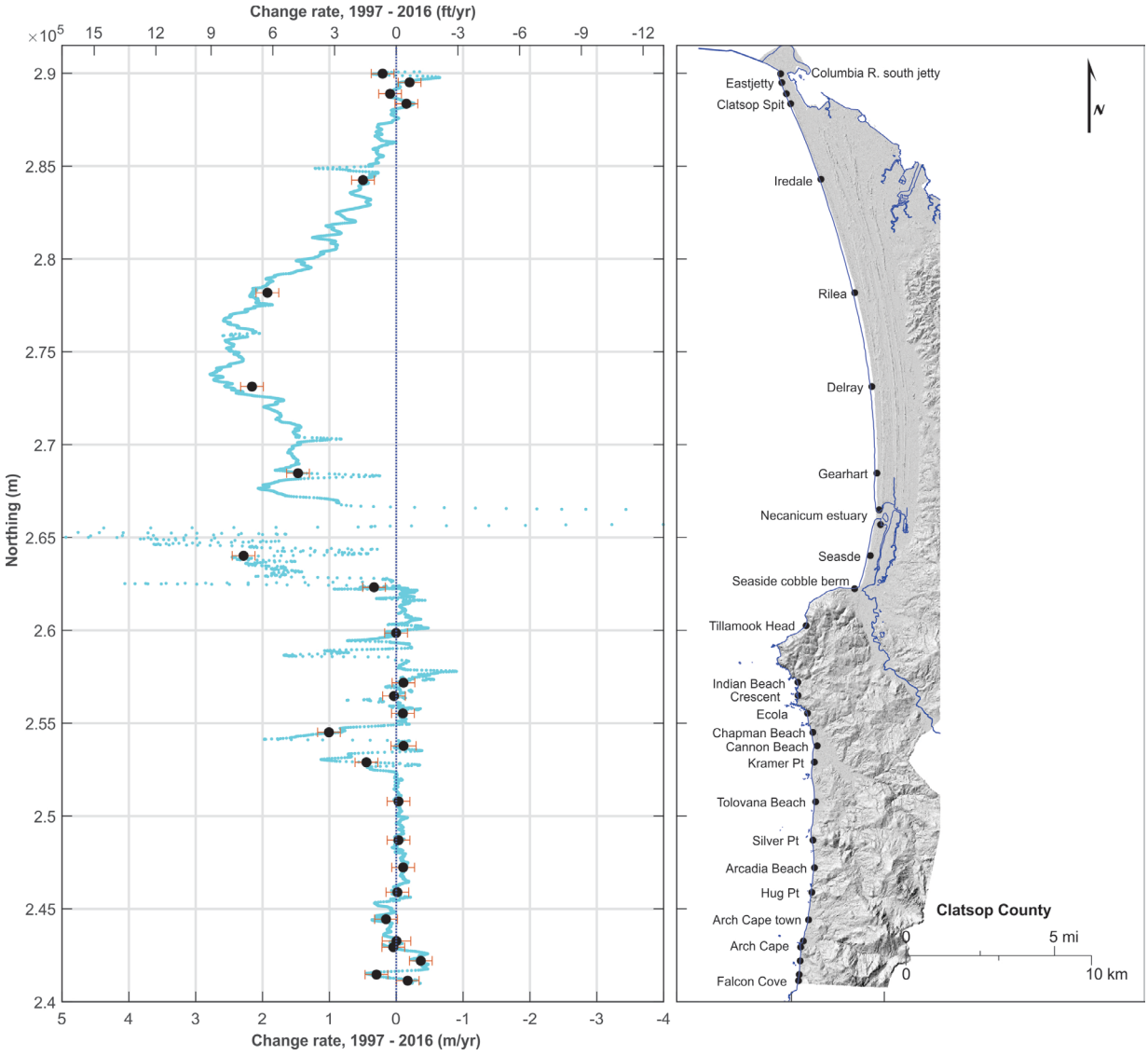

Figure 4-12. Coastal change rates (m/year) and patterns for the period 1997 to 2016 for Tillamook County. Cyan line reflects a 50 m (164 ft) smoothing of the individual transects, while the solid circles with uncertainty depicts the mean change for the identified study reach. Negative values indicate erosion, while positive values denote accretion.

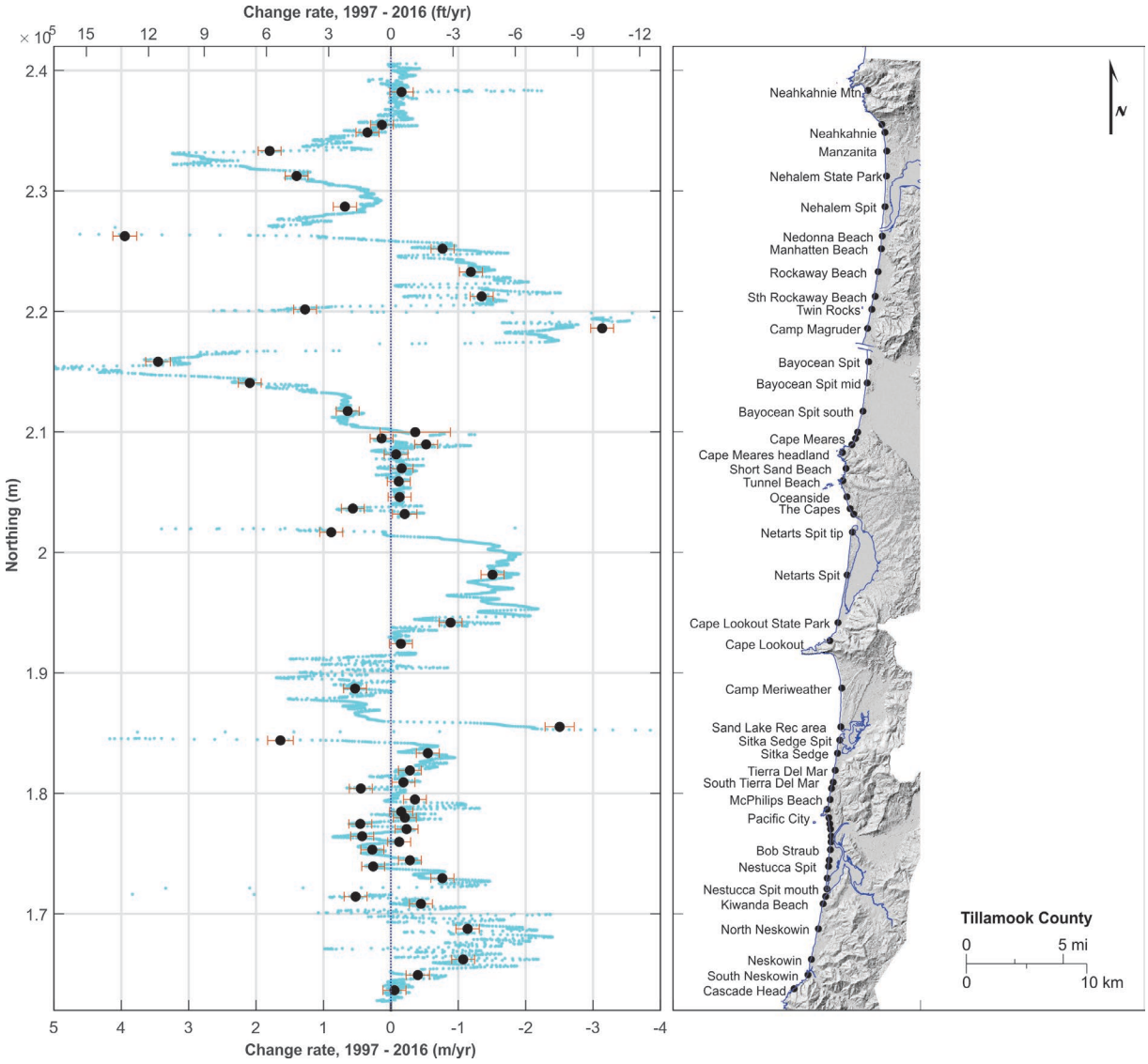

Figure 4-13. Coastal change rates (m/year) and patterns for the period 1997 to 2016 for Lincoln County. Cyan line reflects a 50 m (164 ft) smoothing of the individual transects, while the solid circles with uncertainty depicts the mean change for the identified study reach. Negative values indicate erosion, while positive values denote accretion.

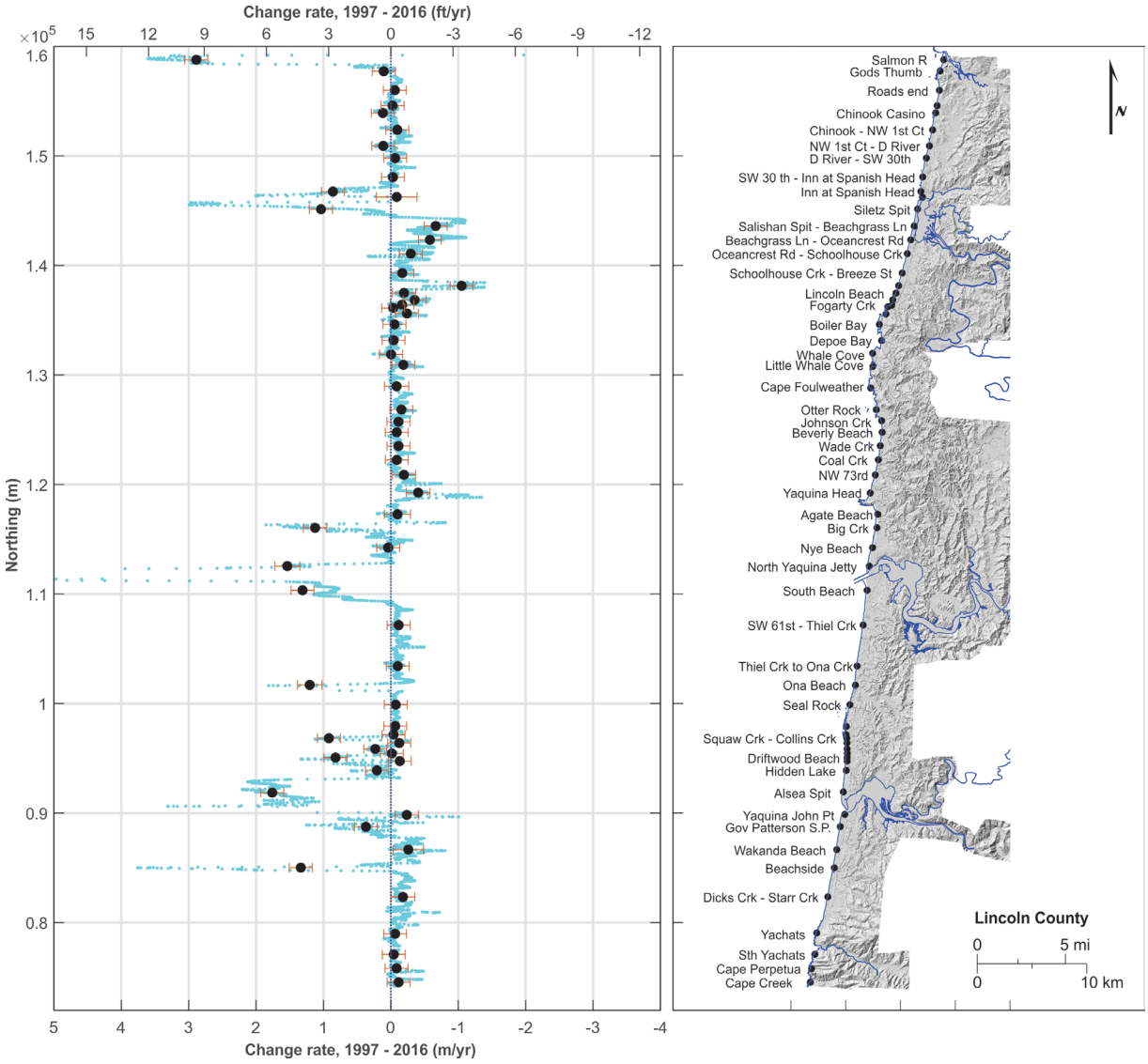

Figure 4-14. Coastal change rates (m/year) and patterns for the period 1997 to 2016 for Lane and Douglas Counties. Cyan line reflects a 50 m (164 ft) smoothing of the individual transects, while the solid circles with uncertainty depicts the mean change for the identified study reach. Negative values indicate erosion, while positive values denote accretion.

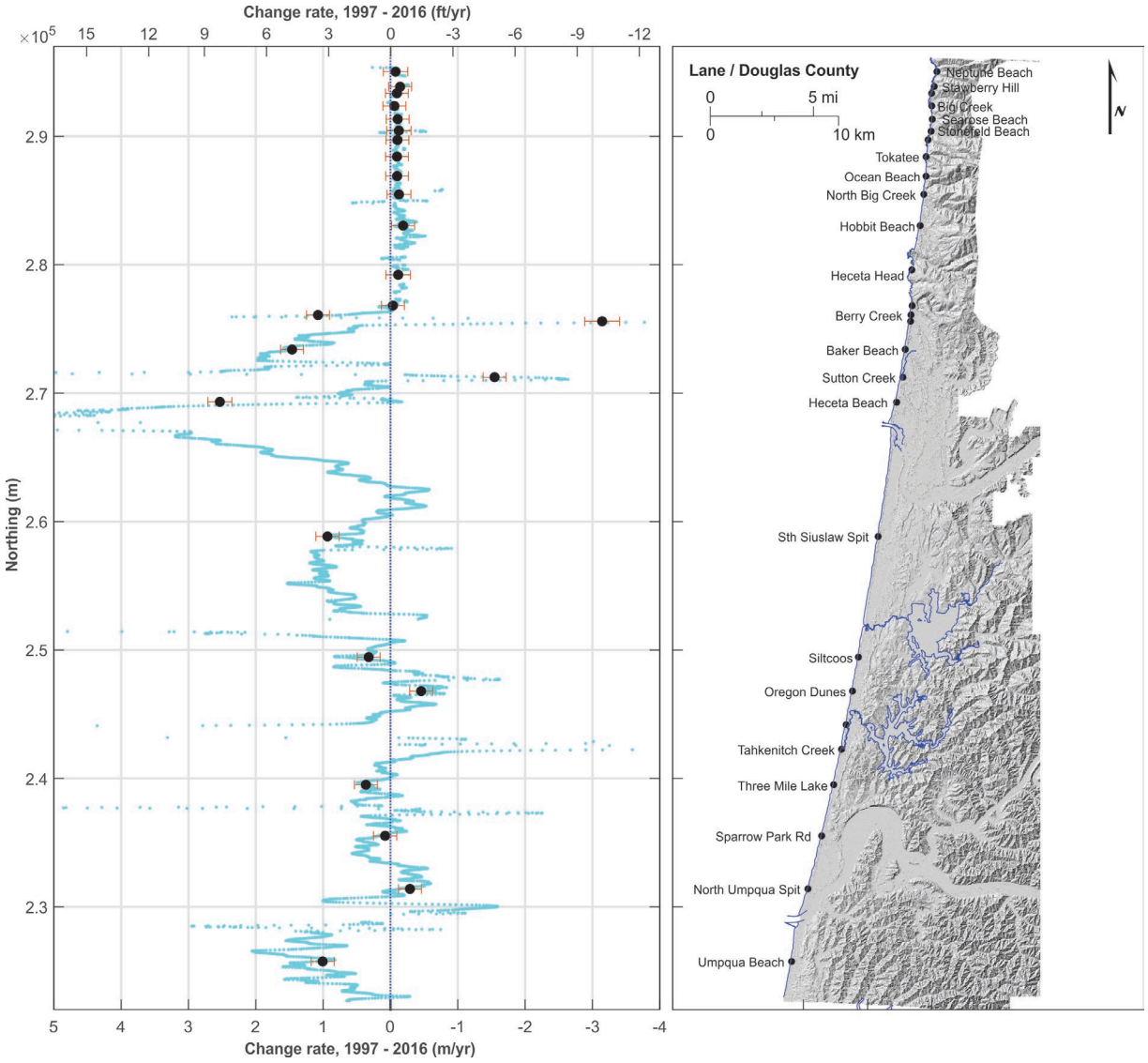

Figure 4-15. Coastal change rates (m/year) and patterns for the period 1997 to 2016 for Lane and Coos Counties. Cyan line reflects a 50 m (164 ft) smoothing of the individual transects, while the solid circles with uncertainty depicts the mean change for the identified study reach. Negative values indicate erosion, while positive values denote accretion.

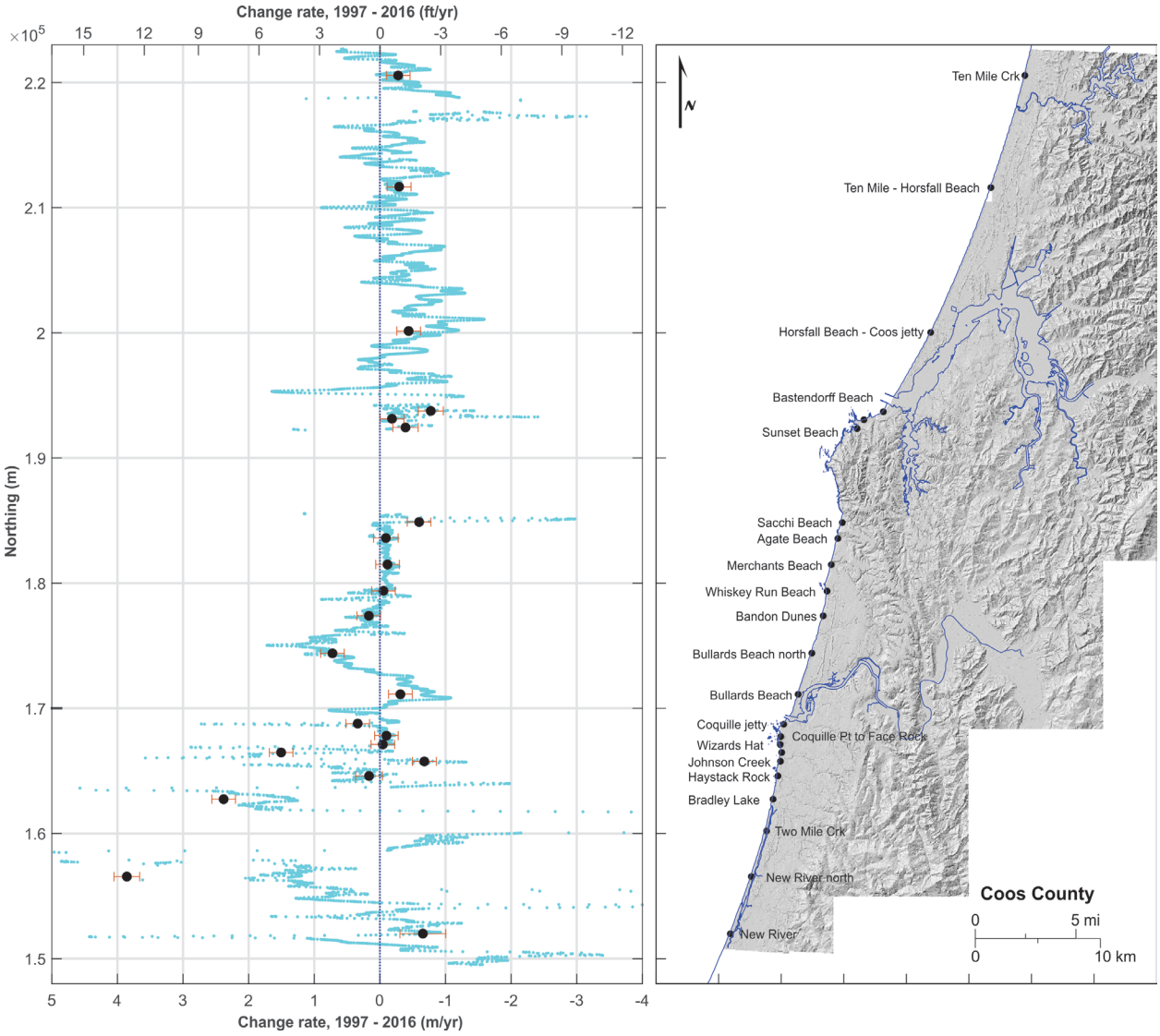

Figure 4-16. Coastal change rates (m/year) and patterns for the period 1998 to 2016 for Curry County. Cyan line reflects a 50 m (164 ft) smoothing of the individual transects, while the solid circles with uncertainty depicts the mean change for the identified study reach. Negative values indicate erosion, while positive values denote accretion.

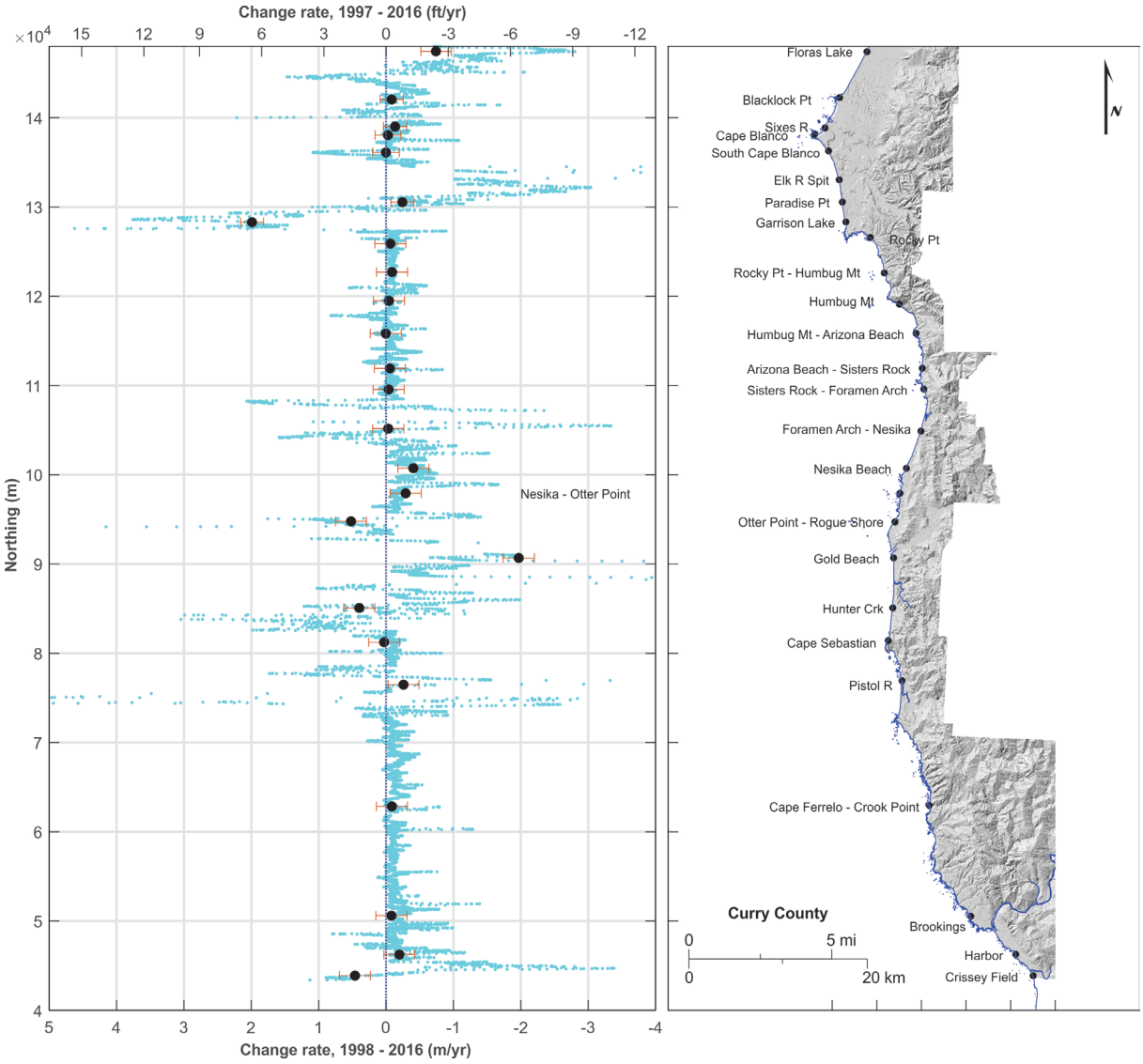

4.5 Final Projected Shoreline Change Index

For every study reach, we defined a mean change rate and projected future erosion associated with SLR in a table (e.g., Clatsop County example, (**Table 4-4**). The mean change rate is only used to project coastal retreat along coastal bluffs where shoreline migration rate is controlled by resistance of rock to erosion (**Table 4-2**). In contrast, along dune-backed beaches, particularly those beaches presently experiencing accretion, historical patterns and rates of shoreline change are unlikely to reflect future patterns under a rising sea level. Thus, for the dune-backed beaches it is simpler to account for the storm-induced erosion, as this is less likely to change significantly in the future, and then separately account for the long-term erosion trend using a simple Bruun type expression (final two columns in the example **Table 4-4**).

To produce projections of future erosion along the entire Oregon Coast, we divided the 6 m (18 ft), 2016 lidar elevation contour into segments of 10 m (33 ft) length. Shoreline change projections were transferred to the shoreline segments using GIS based on the geomorphic setting and projections for the nearest observational transect. We made projections of future shoreline migration for each shoreline segment based on estimated storm-induced erosion and sea level at two time horizons: 2050 CE and 2100 CE. For each future time, our script estimated future shoreline change using either SLR-derived projections for dune areas or extrapolated change rates for bluffs.

Finally, we generated an index of erosion susceptibility relevant to coastal infrastructure such as cable landings. For each shore segment, the three projected erosion calculations were combined using the following weights: storm erosion = 1; 2050 CE sea-level rise erosion = 0.5; 2100 CE sea-level rise erosion = 0.1. The decision to use reduced weights over time accounts for the fact that existing cable landings have a limited lifespan (~25 years), such that future effects of SLR (beyond ~2050) are less important when compared with erosion events taking place today or in the next two decades. The three weighted projected erosion distances were then summed to give a final score. The units of these scores are not meaningful as they are weighted and summed over multiple time periods. From these scores, we then defined a final erosion category based on the following criteria: a zero score = no projected erosion; 0 < Score ≤ 5: Low; 5 < Score ≤ 15: Medium; 15 < Score ≤ 25: High; and 25 < Score: Extreme. These scores provide a coastwide, consistent assessment of future erosion potential and we used the information to assess suitability of the coastline for cable landing sites (Section **6.0**).

5.0 UPDATED COASTAL GEOLOGIC DATASETS

In this section we describe data relevant to cable landings that were produced or updated through this project. We combined the best available landslide susceptibility information to generate a comprehensive layer for the coastal zone in an internally consistent framework. Rocky reefs identified through high-resolution nearshore bathymetric surveys provided new information on the geomorphology and substrate of the seafloor. We generated estimates of bluff heights along the entire Oregon Coast from high-resolution lidar topographic data to assess the nearest extensive low-relief land surfaces that exist above the shoreline.

5.1 Oregon Coastal Landslide Hazard

Exposure to landslide hazards is relevant to resilient coastal infrastructure, and we compiled datasets that integrate best available data for coastwide landslide hazards. The Statewide Landslide Information Database for Oregon (SLIDO) assesses hazard from landslides across the state (Franczyk and others, 2021). The susceptibility layer is a grid that was produced at 10 m (33 ft) resolution based on gridded topography and the statewide geologic map (Burns and others, 2016). The areas most susceptible to future landslide activity are those with geomorphic evidence of observed historic and prehistoric landslides (e.g., Sears and others, 2019). We use more detailed landslide inventories based on 1 m (3 ft) resolution topographic data (Burns and Madin, 2009; Burns and Mickelson, 2016) to improve the statewide susceptibility grid. These inventories were completed for the entire Oregon Coastal zone, with the exception of the Coos County section of the coast and are included in the SLIDO v4.4. compilation (Franczyk and others, 2021). Additionally, a detailed susceptibility analysis was completed for western Tillamook County based on high-resolution lidar data (Calhoun and others, 2020).

5.1.1 Deep-seated landslide hazard

We developed a susceptibility layer for the nominal 3 NM (5.6 km/3.5 mi) inland coastal project area that combines the best available landslide hazard in a seamless mosaic with internally consistent hazard classes. Our approach follows other recent work that integrated the detailed information from the landslide inventory with the full spatial coverage of the statewide layer (Williams and Burns, 2022). Additionally, we integrated information from the detailed landslide susceptibility analysis where it has been completed within portions of Tillamook County (Calhoun and others, 2020).

The strategy for combining the landslide inventory data into the statewide susceptibility layer involved reclassification of the existing layer. Susceptibility is rated in four classes: low, moderate, high, and very high (Burns and others, 2016; Franczyk and others, 2021). Following Williams and Burns (2022), we use the observed landslide occurrences (Franczyk and others, 2021) as better estimates of the "very high" hazard classification. The existing "very high" class was converted to "high," and the areas corresponding to mapped landslide occurrences became the new highest susceptibility class. By definition, the inventoried landslides are the areas assigned the highest hazard classification (Burns and others, 2016); this process sharpened the resolution of where slopes are most likely to fail.

Integration of the detailed landslide susceptibility mapping for the Tillamook County area required additional processing to produce consistency. The new assessment addresses the susceptibility of deep and shallow landslides in separate layers (Calhoun and others, 2020). The statewide susceptibility map of SLIDO v4.4 is most relevant to the hazard of deep-seated landsliding (Burns and others, 2016; Franczyk and others, 2021). Thus, we used the polygon-based deep landslide component of the new data to integrate into the previous layer. Whereas the statewide layer has four susceptibility classes, the detailed layer divides potential into three classes of low to high. The detailed "high" category generally corresponds to the extent of inventoried deep-seated landslides (like the "very high" category of the statewide grid) with additional area added to encompass hazard associated with future downhill movement and uphill growth in landslide extent (Burns and Mickelson, 2016). The detailed-assessment medium-hazard polygons are most similar to the "high" category of the SLIDO layer. Where our coastal polygon intersected the new detailed mapping, we retained the statewide SLIDO categories "low" and "moderate" in areas of lowest hazard in the detailed compilation. The new areas of "high" and "very high" are defined by the two highest hazard classes in the detailed polygon layer. Full resolution examples of the landslide susceptibility layer are provided for the Gold Beach and Rockaway Beach areas (Plates 1 and 2)

5.1.2 Slope, shallow landslide hazard, and constructability

Detailed shallow landslide susceptibility has not yet been assessed for the majority of the coastal counties of Oregon. However, high-resolution topographic data exist for the entirety of the coastal focus area quantifying surface slope, which is one of the strongest predictor variables for assessing shallow landslide occurrence. Steep slopes also pose challenges for general construction, and we view flatter areas as being more suitable for building cable landing infrastructure.

We assessed four general classes for slope stability based on observed shallow landslide occurrence in Oregon and geotechnical construction standards. There are 6,725 shallow landslides in the SLIDO v4.4 compilation (Franczyk and others, 2021). Of the observed landslides, only 2% occurred on slopes less than 10°, and we use this category as the lowest susceptibility. Approximately 11% of shallow landslides occurred on slopes of less than 15°, and this slope value also corresponds to a threshold commonly used in Oregon for land-use planning (Sears and others, 2019). Nearly 40% of the shallow landslides occurred on slopes between 15° and 26°. Slopes of 26° have slope ratios of 2 horizontal units to 1 vertical unit, and

represent a commonly used threshold in geotechnical engineering for most types of soil and geologic materials (Burns and others, 2011; Sears and others, 2019). Roughly half of the shallow slope failures occurred on slopes greater than 26° (Burns and others, 2011; Franczyk and others, 2021), and we use this range to represent areas most susceptible to shallow landsliding and most challenging for safe construction.

We use the 1 m (3 ft) resolution bare-earth lidar topography collected from 2008 to 2020 to produce a slope map for the coastal polygon (OLC, 2023). Slope values are calculated in degrees and rounded to the nearest integer. The slope map does not correspond to shallow landslide hazard directly, as it does not include information about surficial geologic materials or other factors that influence slope stability (e.g., Calhoun and others, 2020). We use the slope map and the classes described above to assess relative suitability of potential cable landing sites in terms of general constructability and slope stability.

5.1.3 Observed historic landslide locations

The third source of landslide data that we use is the record of historically observed landsliding included in SLIDO v4.4 (Franczyk and others, 2021). The occurrence of landslides in the very recent geologic past indicates that an area has characteristics that may promote future slope instability in the same location or adjacent areas. Plates 1 and 2 show examples of the detailed landslide point inventory.

5.2 Nearshore Reef Geomorphology

Areas of rocky seafloor are generally avoided for cable routes to avoid negative impacts on marine life and damage to cables. Additionally, the presence of rocky reefs in nearshore environments is indicative of variations in the erosional resistance of rocks and may indicate the presence of lithologic variations that would be challenging for HDD construction. We supplemented previous mapping of the seafloor (e.g., Goldfinger and others, 2014) with information from high-resolution bathymetric surveys covering roughly 60% of the Oregon coast (**Figure 5-1**).

Figure 5-1. Map showing extent of jet ski bathymetric surveys.

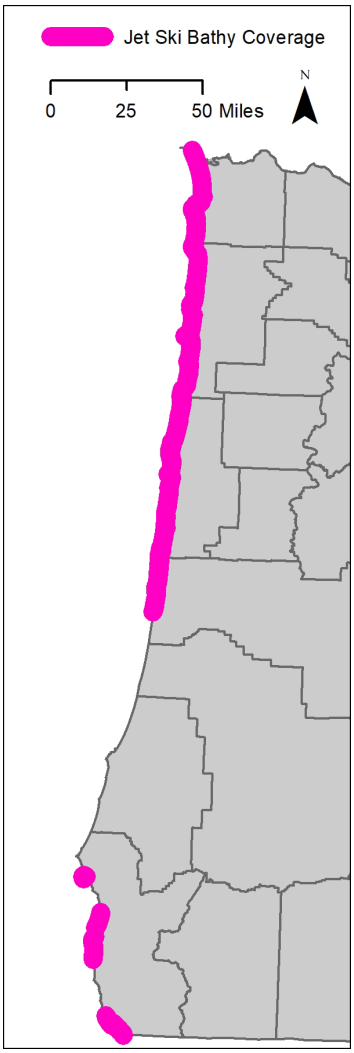

The high-resolution bathymetric data were collected through a set of surveys conducted from a jet ski platform, spaced at roughly 0.5 km (0.3 mi) intervals along the coast. The transects extend through the surf zone to an offshore distance of 2 to 3 km (1.2 to 1.9 mi). Bathymetric elevation data were interpolated in GIS to derive an elevation raster spanning the extent of the transect lines (**Figure 5-2**). We used the presence of spatially extensive, high gradient portions of the seafloor to define likely extents of rocky reefs in the nearshore zone. Candidate reefs were identified from a slope raster calculated from the elevation data using a 10° threshold for defining rocky seafloor. Reefs identified in this project have areas of slope greater than 10° that cover 200 m^2 (2153 ft^2) or more. Laterally extensive features that meet these criteria were extracted as polygon features. In many cases, the reefs correspond to areas of mapped rock substrate (PMEP, 2022) in areas where the two datasets overlap. However, in other locations, reefs are identified in areas previously thought to be unconsolidated sediment (Plates 1 and 2). These complementary data strengthen our understanding of high relief rocky habitat in the nearshore environment.

Figure 5-2. left) Jet ski transects and bathymetric slope map for a sample location. Right) bathymetric elevation with rocky reefs identified using criteria described in text.

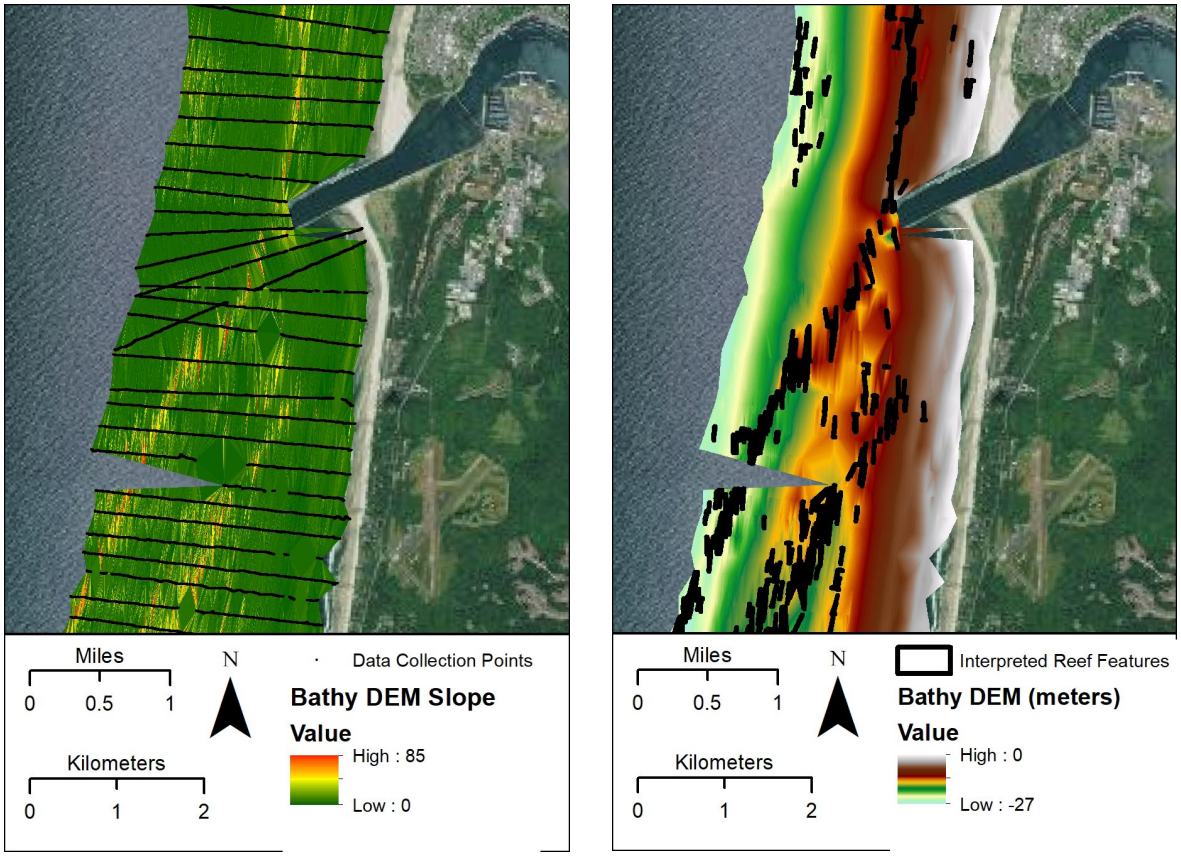

5.3 Coastal Bluff Height

Bluffs capping sea cliffs and steeper hillslopes form prominent features of the Oregon Coast landscape. The heights of bluffs vary widely, reflecting spatial variation in surface geology, erosional processes, and Quaternary uplift rates. Low-relief bluff tops comprise a common setting for building towns, roads, and other infrastructure. Coastal bluffs host some cable landing infrastructure currently, and represent locations elevated above some coastal hazards. However, higher bluffs create challenges for HDD construction across the shoreline. We produced systematic measurements of bluff heights using gridded airborne lidar data along portions of the coast classified as bluff-backed or rocky shore in the coastal geomorphology layer.

Bluff heights were determined semi-automatically using transects spaced at 100 m (328 ft) intervals along relevant portions of the Oregon shoreline. Transect lines were oriented perpendicular to the shoreline extending 400 m (1312 ft) landward (**Figure 5-3**). Elevation values from lidar digital elevation models (OLC, 2023) were extracted at points spaced along the lines at a 1 m (3.3 ft) interval. Profiles based on paired elevation and landward distance values are the basis of the bluff identification process.

Figure 5-3. Example of measuring bluff height from topographic profile data.

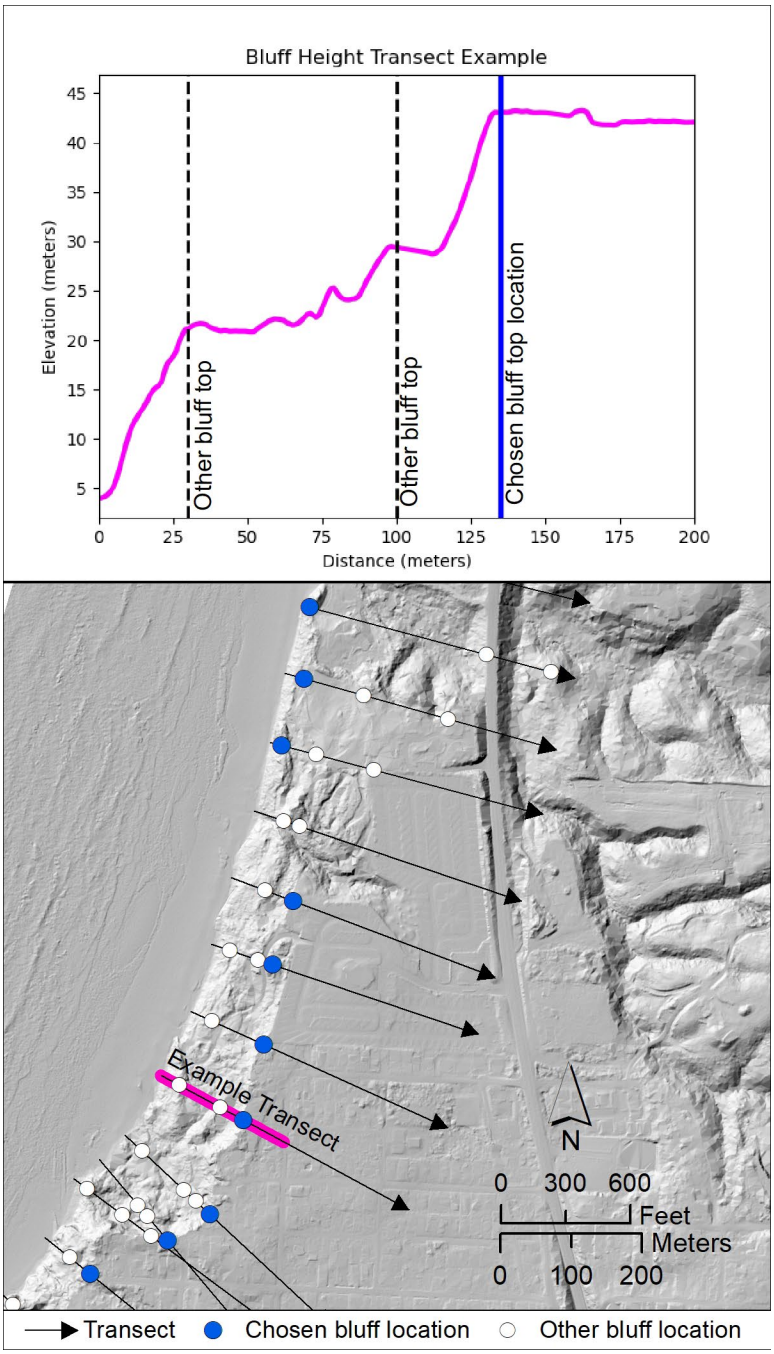

We defined bluff tops as low relief areas with cumulative elevation change of 3 m (10 ft) or less over a horizontal profile distance of 10 m (33 ft). Candidate bluff edges are defined as the seaward point on a 10 m window of low relief topography. Multiple bluff heights were considered using 7 different minimum heights at intervals of 5 m (16 ft) from 10 m (33 ft) to 40 m (131 ft) to identify the most appropriate bluff top location and avoid biases resulting from obliquity of profile lines to the topographic slope. In instances where two or more candidate bluff edge points were identified along a profile, the point that best

represents the topography was chosen manually. In cases where the automatic processing did not yield meaningful bluff locations, bluff top locations were digitized manually.

Our data provide a comprehensive view of cliff and hillslope heights along the Oregon Coast and are available in full detail in the GIS data of this report. Map examples of the locations and heights of bluff tops are illustrated in Plates 1 and 2 for the Gold Beach and Rockaway Beach areas.

5.4 Sediment Thickness above Bedrock

Quaternary surficial sediment mantles much of the coastal margin. One consideration for HDD construction is the depth at which unconsolidated sediment lies in contact with indurated rock below. Geophysical surveys for past subsurface construction projects are limited in scope and often not published. Widespread observations of subsurface geologic materials have been made during construction for water and geotechnical wells. Logs showing depths at which different geologic units were encountered during well drilling are archived and distributed by the Oregon Water Resources Department (OWRD, 2023). We used coastal well completion reports to build a database of well locations with depth intervals of consistent sediment and rock types in built wells. Most of the wells are not precisely located in the well reports, with many locations based on Public Land Survey System section notation that carries ambiguity up to ~1.1 km (~0.7 mi). Along the southern coast wells without precise coordinates were more precisely located based on property addresses and inspection of georeferenced aerial and satellite imagery (McClaughry and others, 2013; Wiley and others, 2014; 2015).

During this study we extended the database of subsurface well information (McClaughry and others, 2013; Wiley and others, 2014; 2015) to include wells north of Coos Bay. We only included wells with locations defined by GPS surveys that have location accuracy ~10 m (~33 ft) or better. This resulted in coastwide coverage of subsurface well information, although the well density is lower in northern Oregon counties than along the southern coast. For this study we focus on the thickness of sediment above bedrock. Of the 2039 wells in our dataset, bedrock was not encountered at the bottom of 269 wells, and these points provide only a minimum estimate of the total sediment thickness in those locations. Plates 1 and 2 show examples of the well sediment thickness measurements in areas of the southern and northern Oregon Coast, and the accompanying GIS data provide the full dataset. Given the variable spatial density of wells along the coast and short-scale spatial variation in the depth to bedrock, we did not use these data to assess suitability for cable landings. The well data provide a useful guide to understanding the depth to bedrock where the spatial density of located wells is higher that will inform future subsurface construction projects. Additionally, this dataset contributes to understanding the history of erosion and sedimentation during the Quaternary along the Oregon Coast.

6.0 SUITABILITY ANALYSIS FOR CABLE LANDINGS ALONG THE OREGON COAST

We analyzed the suitability of cable landings along the full Oregon Coast to systematically integrate the factors that the Territorial Sea Plan, Part 4 Working Group and ourselves have identified as relevant for constructing resilient cable infrastructure that crosses the Oregon Territorial Sea with minimal impact on the environment and coastal communities. Our analysis emphasized geologic and geomorphic factors and did not consider many biological, cultural, or logistical factors that may be relevant to holistic consideration of potential cable landing sites. To this end, we have sought to integrate the best available data that spans the entirety of the state coastal zone. We focused specifically on assessing suitability at

points where prospective cables would cross the shoreline at a beach manhole (**Figure 1-2**), as those locations are viewed as most pivotal by the cable industry (Wopschall, 2023). Cable landing stations and electrical substations likely have greater flexibility in positioning within some radius of a cable landing site (**Figure 1-2**), although many of the terrestrial layers that we have compiled within a three nautical mile distance of the shoreline are relevant background for future detailed siting studies. We note that our analysis is necessarily broad and is not a substitute for detailed, site-specific studies that will confirm or deny the most important details of prospective sites. Additionally, our analysis does not identify good sites that may exist in small pockets of the coastline or that may be accessed through more complex cable routing through areas of otherwise less desirable seafloor. Based on the diversity of settings in existing Oregon cable landings, different settings may be used successfully if engineering and construction practices are aligned with the particular characteristics of the specific sites.

6.1 Suitability Analysis Methodology

We developed a flexible framework for scoring the suitability of small sectors of the coastline based on the available spatial layers relevant to the question of constructing new cable landings. All of the layers used in our analysis are available along the full coast to minimize spatial biases in data availability. We integrated diverse types of geospatial data ranging from raster (gridded) data to vector features including data represented with polygons, lines, and points. Scores were calculated based on the various layer feature characteristics or raster values, and with different strategies based on spatial coincidence, line lengths, or proximity to candidate sites, depending upon the relationship of a factor to the siting and construction of a cable landing. Additionally, we applied a weighting strategy to emphasize the factors that are most important for siting cable landings. The scoring strategy is necessarily subjective, and all of the layers are available publicly, enabling others with different priorities to make independent assessments.

6.1.1 Spatial framework

The core of our analysis is a linear representation of the shoreline along the Oregon Coast. We found no existing shoreline dataset that described the boundary between more active areas of the beach and upland areas that are rarely impacted by even the largest storms in a detailed way consistent with high-resolution lidar topographic data. High-resolution shorelines based on tidal datums such as MHHW exist for the Oregon Coast, but in areas of more gently sloping beaches without large dunes or bluffs, the shoreline may regularly be crossed by distances of tens of meters (tens to hundreds of feet) by storm waves. Consequently, the horizontal setbacks from MHHW necessary for best practices of beach manhole siting vary widely depending upon the geomorphic setting of candidate sites along the coast. We developed a shoreline for this project based on a combination of different tidal and lidar elevation datums and interpretation of modern aerial orthophotography imagery. The line has gaps across stream mouths and bays, and has a total length of 583 km (362 mi). We seeded the shoreline with a series of 5,817 points placed every 100 m (328 ft) of line distance. These points represent potential locations where cables could cross the shoreline in the vicinity of hypothetical beach manholes.

Sampling of the geospatial data that represent the different factors is accomplished using multiple linear transects that extend seaward and landward of each shoreline point. Most of the input suitability factors are sampled by rectangular polygons that are centered on each transect line. Each rectangle extends 50 m (164 ft) to either side of its associated transect line, ensuring roughly complete spatial sampling of the relevant coastal zone. We consider three seaward distances from each point

corresponding to different aspects of siting and construction (**Figure 6-1**). The shortest distance increment is from the shoreline point to the local 10-meter (33-foot) water depth bathymetric contour as derived from a bathymetric grid for DOGAMI tsunami studies. This zone is relevant to HDD construction between the shoreline and the nominal seafloor punchout depth of ~10 m (~33 ft) (Wopschall, 2023), and its outer edge approximates the observed sediment closure depth along the Oregon Coast (Section **4.3.1**). The second distance increment corresponds to the distance between the 10 m (33 ft) water depth and the outer edge of the Oregon Territorial Sea at a nominal 3 nautical mile distance from a spatially smooth shoreline (OPAC, 1994). The third distance extends from the edge of the Territorial Sea to a distance of 15 km (9.3 mi) from the shoreline point to provide additional information on the characteristics of the seafloor that must be traversed by cables across the continental shelf seaward of Oregon territorial waters.

The marine transects associated with each shoreline point sample a limited area of seafloor on a defined azimuth. At a broad scale, the Oregon shoreline is oriented north-south, although in detail it is much more irregular. To account for the broad similarity in the orientation of depth contours on the offshore shelf, and to avoid biases from projecting lines from the local shoreline geometry, we choose a primary due-west orientation for sample transects from the shoreline points (**Figure 6-1**). However, we note that many existing cables approach the shoreline obliquely, so for each point we consider two alternative sample rectangles that are oriented 30° north and south of west (**Figure 6-2**), roughly guided by the obliquity of some existing cables (**Figure 1-1**). The oblique rectangles are of greater length to reach equivalent offshore distances measured straight west of each point as the corresponding west-oriented sample rectangles.

Figure 6-1. Map showing examples of west-oriented marine transect lines colored by the three offshore zones and the land sample interval. The marine sample windows are particularly variable in southern Oregon as depicted here based on bathymetry and width of the Territorial Sea. Individual lines are spaced 100 m (330 ft) apart and are absent where the shoreline crosses mouths of major streams.

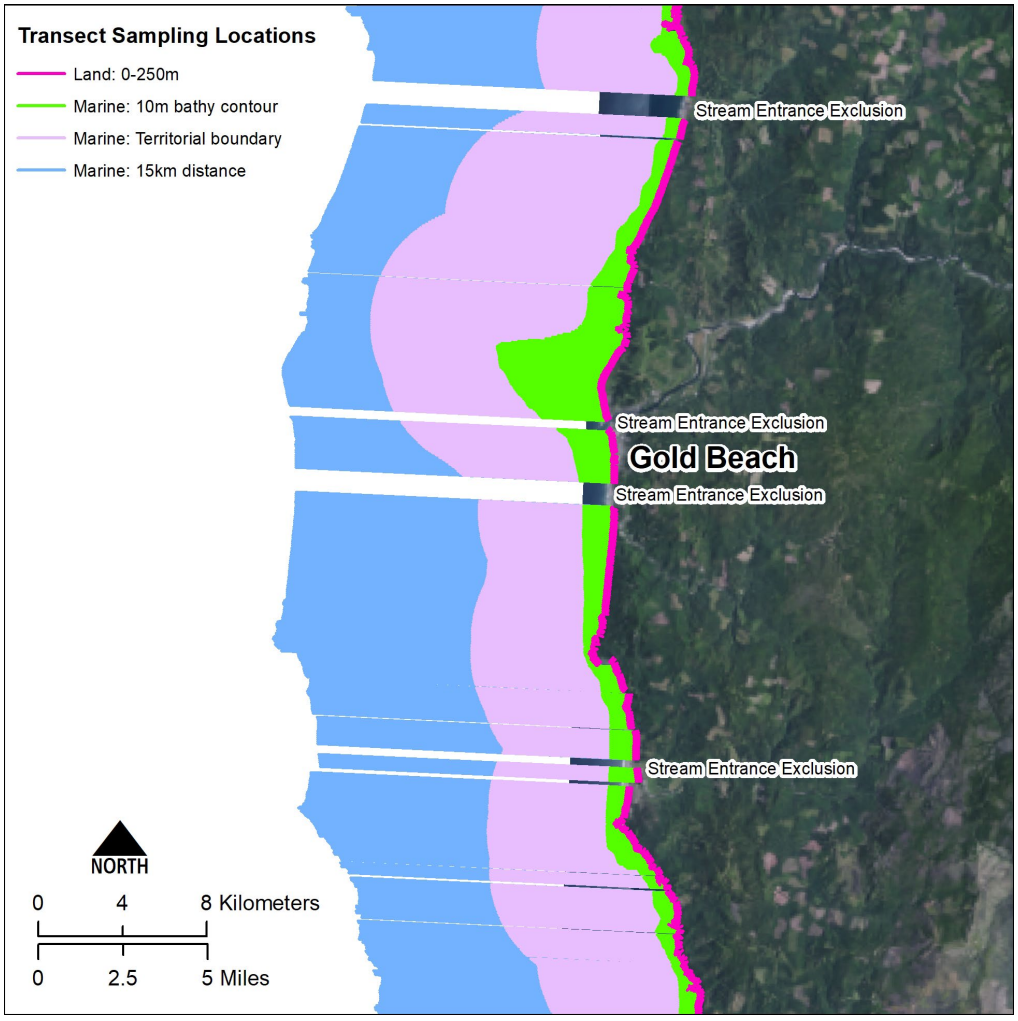

Figure 6-2. Map showing examples of alternative northwest-oriented marine transect lines colored by the three offshore zones and the land sample interval for the same area as Figure 6-1. We also sampled the marine data with a set of analogous oblique lines that trend southwest from each shoreline point (not depicted).

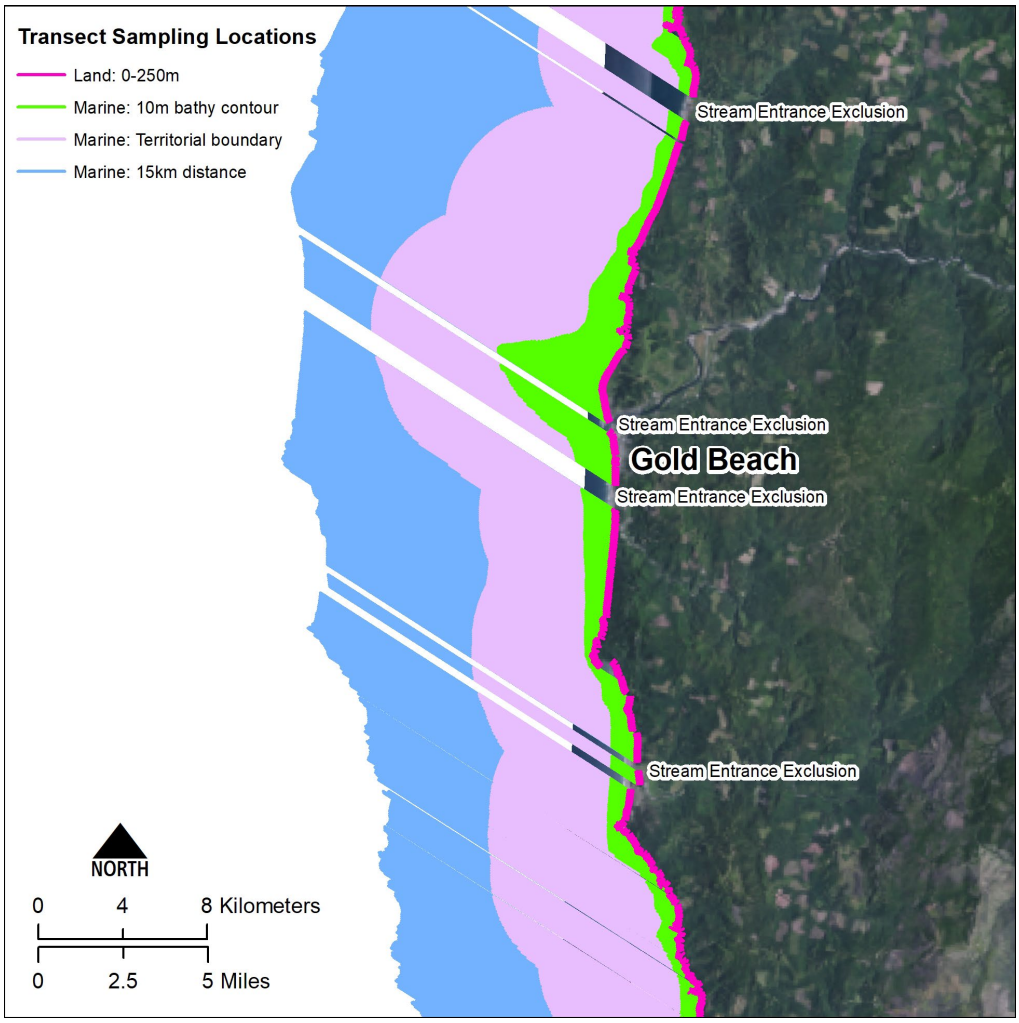

The landward factors of potential sites are sampled by rectangles of the same 100 m (330 ft) widths centered on each sample point (**Figure 6-2**). The land transects extend inland 250 m (820 ft) from the shoreline points to encompass the distance range where most of the existing cable beach manholes are located along the Oregon Coast (**Figure 1-1**; Wopschall, 2023). Given the shorter distance of the landward sample rectangles and local topography that better corresponds to the adjacent shoreline orientation, we oriented these polygons normal to the local shoreline.

6.1.2 Spatial data sampling and factor scoring

On both the land and ocean side of each shoreline point, relevant geospatial layers are sampled using one of three general strategies: area sampling, distance sampling, or proximity sampling; scores are calculated in a consistent framework. Each factor is scored on a relative scale where negative values are worst and higher positive values are more suitable. More neutral characteristics are typically assigned a zero value. This convention allows effective weighting and does not produce a favorable bias if any site is missing

factor data. The most definitive negative factors (marine protected areas, rocky headlands, and actively moving landslides) are used to set relevant shoreline points to have zero final total scores. Marine suitability factors are sampled over the relevant distance range(s) along each of the three transect orientations from each point. Shoreline points where complex shoreline geometry did not allow a straight-line path to the open ocean were assigned zero score. The sample line orientation with the highest total score for all of the combined marine factors is retained for scoring each shoreline point. The following section describes the methods used to score varying types of criteria.

6.1.2.1 Area sampling

Factor datasets that are represented with spatially continuous raster or polygon data are sampled using an area strategy (**Figure 6-3**). Examples of such layers include seafloor substrate types offshore, geologic rock types onshore, and the gridded landslide susceptibility data on land. The input data are subset to each candidate sampling rectangle, scores are applied to each factor, and the factor score is calculated as the area-weighted score for the full sample rectangle.

Figure 6-3. Example of area sampling of offshore geology data using rectangular polygons along the southwest-oriented marine sample transect and onshore geology from an example candidate shoreline point. Different colors show the underlying geologic unit polygons transformed to scores on the relevant scoring system for each layer. Scores for each spatial sample interval (e.g., Marine 0-10 m (0-30 ft) bathymetry) are the area-weighted average of all of the scored input polygons that intersect this sample rectangle.

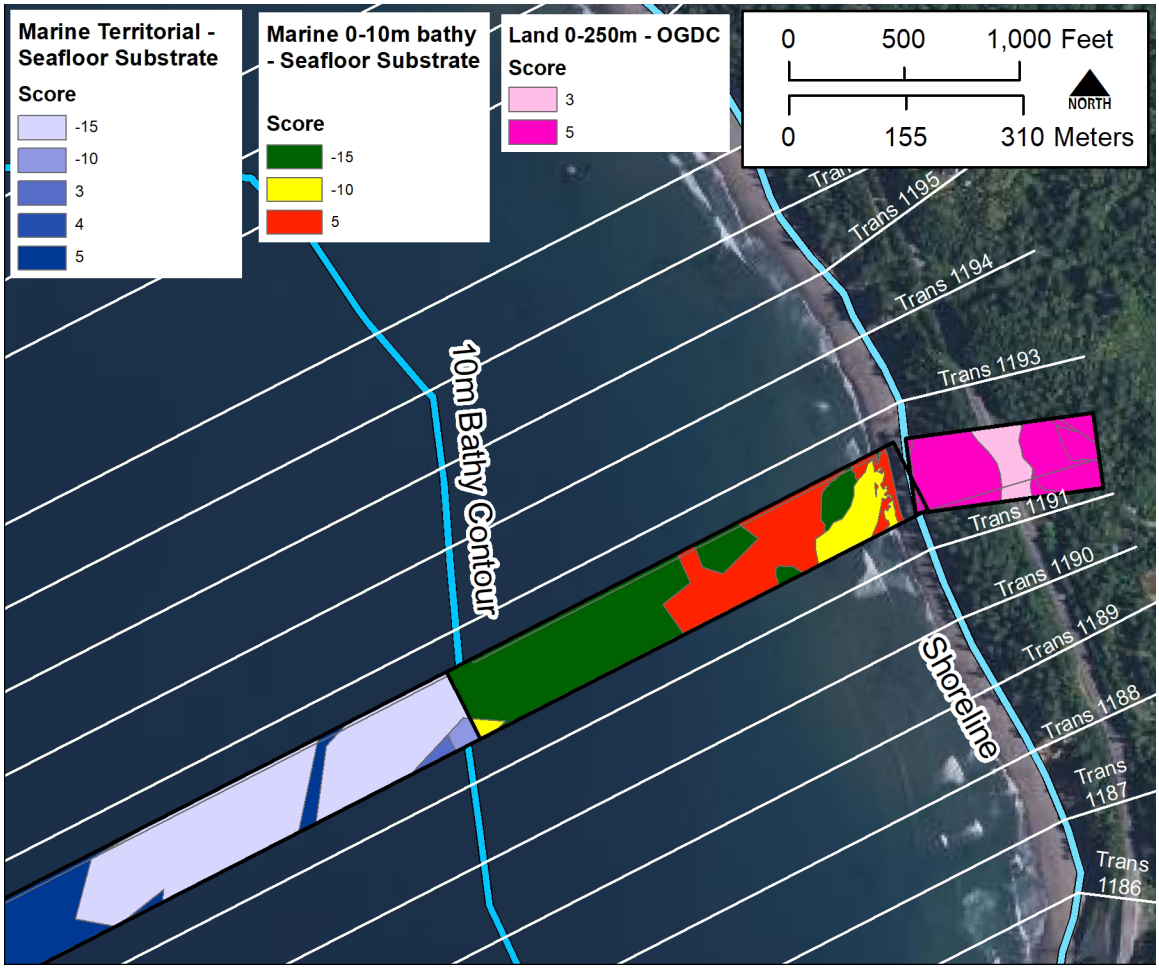

6.1.2.2 Line distance sampling

Other datasets are lines such as faults that have impact on construction considerations and/or longer-term hazards. We calculate the spatial density of such mapped features and corresponding inferred impacts on a potential cable route as the cumulative line length contained within each sampling polygon. Scores are assigned in proportion to the frequency of each line type within each sampling region.

6.1.2.3 Proximity sampling

Other datasets are sampled according to the distance between the sampling rectangle or shoreline point to factors of interest. For example, HDD construction is generally capable of making boreholes that span about 1.5 km (0.9 mi) from an entry point to the punchout location on the seafloor (Wopschall, 2023). The punchout depth is commonly about 10 m (33 ft) deep to protect the cables in the subsurface where the seafloor is shallow enough to be affected by wave energy and currents (Wopschall, 2023). We calculate horizontal distance from each shoreline point to the 10 m (33 ft) depth contour and score sites to favor

shorter drilling distances. Other datasets are scored as being present or absent within the sample rectangle, such as shallow, linear reef structures or marine reserves. Finally, on-land features are scored as either favorable (roads) or unfavorable (wetlands or observed landslides) based on their nearest proximity to the boundaries of the sampling rectangles.

6.1.3 Score weighting

The final score is calculated by summing the individual factor scores, scaled by the weights assigned to each factor. The summed weighted scores are transformed to the range of zero (worst) to 100 (best) by normalizing all of the scores to the numerical score of the most favorable site in the analysis and reporting percentages. The impact of each factor on total score is determined by both the weight for the factor and the possible range of scores that vary between factors as described in the following section. Sites with negative total numerical scores are assigned a zero score in the final dataset.

6.2 Suitability Analysis Inputs and Scoring Details

In this section we provide details on the specific layers used, what sampling strategies were used for each layer, and how the different factors are scored and weighted. **Table 6-1** shows all of the layers grouped by spatial zones from land through the shore to the marine zones. This table also provides references to subsequent tables that give details of how scores are assigned to the data in our analysis. The final column of **Table 6-1** lists the weights applied to the overall score for each dataset. **Table 6-2** provides details on the GIS layer names that correspond to each dataset, the dataset availabilities, and data origins. We distribute all of the new datasets generated for this project, as well as versions of most of the preexisting datasets. Further information on the datasets can be found in the metadata included with the geodatabase produced for this project.

We used 13 different layers for the land area that are relevant to HDD construction and hazards and infrastructure longevity (**Table 6-1**). Four layers describe the shoreline characteristics and potential for shoreline change. Seven layers are sampled in the three marine zones. Two of the layers are sampled in only one zone each, and the remaining layers are sampled in all three of the marine zones. Sampling in the three marine zones allowed us to emphasize the importance of factors nearer to shore in the Oregon Territorial Sea as well as using different weights for the same layers for the different spatial zones (**Table 6-1**).

Table 6-1. List of datasets used in suitability scoring analysis with relevant value tables and weights.

Transect Sampling Area	Sample Method	Dataset	Value Table	Weight
Land 0-250 m (0-820 ft)	Proximity	Coastal Roads	Proximity Roads	3
		Historic Landslides	Proximity Miscellaneous	0.5
		Groundwater Sources	Proximity Miscellaneous	1
		Surface Water Sources	Proximity Miscellaneous	1
		Wetlands	Proximity Miscellaneous	3
	Line Length	Contacts and Faults	Land Faults	2
		Quaternary Faults	Land Faults	1
	Area	Liquefaction Susceptibility	Liquefaction Susceptibility	1
		Landslide Susceptibility	Landslide Susceptibility	2.5
		Topographic Slope	Topographic Slope	2
		Tsunami Inundation	Tsunami Zones	2
		Geologic Units	Geologic Units	4
		Beaches and Dunes	Beaches & Dunes	2
Shoreline	Shoreline Attributes	Coastal Geomorphology	Coastal Geomorphology	3
		Headlands Spits Landslides	Headlands, Spits, & Landslides	2*
		Bluff Heights	Bluff Heights	2
		Coastal Erosion	Coastal Erosion	3
10m (30 ft) bathymetric depth	Proximity	Reefs	Reefs	1
		Marine Reserves and MPAs	Marine Reserves	1†
		10m bathy distance	10m bathy contour	2
	Line Length	Offshore Faults	Offshore Structures	2
		Offshore Folds	Offshore Structures	0.75
	Area	Seafloor Substrate	Seafloor Substrate	1
Territorial Sea	Proximity	Reefs	Reefs	2
		Marine Reserves and MPAs	Marine Reserves	1†
	Line Length	Offshore Faults	Offshore Structures	1
		Offshore Folds	Offshore Structures	0.5
	Area	Seafloor Substrate	Seafloor Substrate	3
15km (9.3 mi) Distance	Proximity	Marine Reserves and MPAs	Marine Reserves	1†
	Line Length	Offshore Faults	Offshore Structures	0.5
		Offshore Folds	Offshore Structures	0.25
	Area	Seafloor Substrate	Seafloor Substrate	2
		DOD Offshore Assessment	DOD Assessment	1

*Headlands and landslides: if a headland or active landslide is present in this layer, the final score is set to zero

†Marine Reserves: If any marine sampling zone intersects a reserve or marine protected area, the final score is set to zero

Table 6-2. Layers used with specific filenames, sources, and relevant value fields.

GIS Layer Name (SP54_Coastal_Cable_Data_Inventory.gdb)	Data Type	Source	Value Field (with subset)
Land Sampling			
Beaches_and_Dunes	Polygon	DOGAMI	Suitability
Coastal_Roads	Line	DOGAMI	
Groundwater_Sources	Polygon	DEQ	
Surface_Water_Sources	Polygon	DEQ	
Tsunami_Inundation	Polygon	DOGAMI	Tsunami_Region
Wetlands	Polygon	NWI	WETLAND_TY
Contacts_and_Faults	Line	DOGAMI	LTYPE
Quaternary_Faults	Line	USGS	
Historic_Landslides	Point	DOGAMI	MOVE_CLASS
Geologic_Units	Polygon	DOGAMI	ThematicRockType
Lidar_Slope	Raster	DOGAMI	
Liquefaction_Susceptibility_Map	Raster	DOGAMI	
Landslide_Susceptibility	Raster	DOGAMI	
Shoreline Sampling			
Bluff_Heights	Point	DOGAMI	Bluff_Elev_m
Coastal_Erosion	Line	DOGAMI	Coastal_Erosion
Coastal_Geomorphology	Line	DOGAMI	Coastal_Geomorph
Headlands_Spits_Landslides	Line	DOGAMI	Category
Marine sampling			
Reefs	Polygon	OSU/ DOGAMI	
Bathy_10m_Contour	Line	DOGAMI	
Marine_Reserves_and_MPAs	Polygon	DLCD	
Offshore_Faults	Line	Goldfinger and others (2023)	struc_type
Seafloor_Substrate	Polygon	PMEP/ DLCD/ OSU	CMECS_SC_Name
DOD Offshore Assessment*	Polygon	DOD/BOEM	Color
Other layers not sampled			
Shoreline	Line	DOGAMI	
Well_Sediment_Thickness	Point	OWRD/ DOGAMI	

* The Department of Defense/Bureau of Ocean Energy Management Combined Wind Assessment for the Oregon Offshore, was not available for redistribution. GIS data exist online at https://offshorewind.westcoastoceans.org/.

6.2.1 Scoring systems

We used three scoring systems to assign relative score values to the information sampled from each dataset. The score system strategy was dependent upon the dataset structure as well as our sampling methodologies. The first class of scoring system applies to layers that are assessed based on numerical values (**Table 6-3**). We applied this scoring to layers that were assessed based on proximity, cumulative line distance, and layers with numerical values like bluff height and slope (**Table 6-3**).

Table 6-3. Scoring systems for layers with quantified numerical results. See Table 6-1 for which layers these score systems are applied.

Score	Min	Max	Units	Min	Max	Units
Proximity Roads						
5	0	0	km	0	0	mi
4	0	0.15	km	0	0.09	mi
3	0.15	0.25	km	0.09	0.16	mi
2	0.25	0.5	km	0.16	0.31	mi
0	0.5	1	km	0.31	0.62	mi
-5	1	+	km	0.62	+	mi
Proximity Miscellaneous						
5	1	+	km	0.62	+	mi
4	0.5	1	km	0.31	0.62	mi
3	0.25	0.5	km	0.16	0.31	mi
2	0.1	0.25	km	0.06	0.16	mi
-2	0	0.1	km	0	0.06	mi
-5	0	0	km	0	0	mi
Land Faults						
5	0	0	m	0	0	ft
4	0	50	m	0	164	ft
2	50	100	m	164	328	ft
0	100	150	m	328	492	ft
-2	150	200	m	492	656	ft
-5	200	+	m	656	+	ft
Bluff heights						
5	0	15	m	0	49	ft
3	15	25	m	49	82	ft
2	25	35	m	82	115	ft
1	35	45	m	115	148	ft
0	45	+	m	148	+	ft
Topographic slope						
5	0	10	degrees			
3	10	15	degrees			
0	15	26	degrees			
-5	26	90	degrees			
10 m bathy contour						
5	0	0.5	km	0	0.31	mi
3	0.5	1	km	0.31	0.62	mi
0	1	1.5	km	0.62	0.93	mi
-5	1.5	+	km	0.93	+	mi
Offshore Structures						
5	0	0	meters	m	0	0
4	0	75	meters	m	0	246
3	75	150	meters	m	246	492
2	150	250	meters	m	492	820
1	250	500	meters	m	820	1640
0	500	+	meters	m	1640	+

The other two types of scoring systems are for layers that have information represented by a limited number of categorical values. We divide the categorical scores into **Table 6-4** for non-numerical data such as geology or seafloor substrate, and **Table 6-5** for factors scored based on limited number of possible numerical values or presence or absence of features. In the case of the Beaches and Dunes layer, many categorical values were grouped into numerical classes that represent our assessment of relative suitability for this project. More descriptive information is retained in a field in the geodatabase layer.

Table 6-4. Scoring systems for layers with non-numerical categorical information.

Score	Value List
Tsunami Zones	
5	Outside Hazard Area
3	Local Tsunami Evacuation Zone, OPTIONAL – Outside Hazard Area
0	Distant Tsunami Evacuation Zone
Geologic Units	
5	sediments, mud, muddy sand, sand
3	gravel, terrestrial sedimentary rocks, marine sedimentary rocks
-5	melange rocks
-15	intrusive volcanic rocks, volcanic rocks, marine volcanic rocks, invasive extrusive rock
Coastal Geomorphology	
5	Dune-backed beach, Gravel beach
4	Cobble beach, Low bluff-backed beach
3	Bluff-backed beach
1	Bluff-backed cobble beach
-5	Rocky shore (Bluffs & Cliffs), Jetties, Estuary
Headlands, Spits, & Landslides	
0	Normal
-50	Spit
*	Headland, Landslide
Coastal Erosion	
5	None
4	Low
2	Medium
-3	High
-5	Extreme
Seafloor Substrate	
5	Coarse Sand, Sand, Fine Sand, Fine Unconsolidated Substrate, Medium Sand
4	Muddy Sand, Sandy Mud
3	Mud, Shell Hash, Slightly Gravelly Sand
0	Very Coarse Woody Debris, Sandy Gravel, Slightly Gravelly Mud, Unconsolidated Mineral Substrate
-10	Cobble, Coarse Unconsolidated Substrate, Gravel, Gravel Mixes
-15	Anthropogenic Rock Rubble, Bedrock, Boulder, Unclassified, Rock Substrate
DOD Assessment	
0	Green
-5	Red

*Headlands and landslides: if a headland or active landslide is present in this layer, the final score is set to zero

Table 6-5. Scoring systems for layers with numerical categories or presence/absence.

Score	Value
Liquefaction Susceptibility	
5	0
4	1
2	2
0	3
-2	4
-5	5
Landslide Susceptibility	
5	1
3	2
0	3
-5	4
Beaches & Dunes	
5	Absent
5	3
2	2
-5	1
Reefs	
0	Absent
-5	Present
Marine Reserves	
0	Absent
*	Present

*Marine Reserves: If any marine sampling zone intersects a reserve or marine protected area, the final score is set to zero

6.3 Suitability Analysis Results

6.3.1 Summary of full results

Application of the strategy described in the previous section provides relative suitability scores for cable landing construction at 5,817 shoreline points along the Oregon Coast. Summary histograms of all the scores show the distribution of the favorability at the scale of the entire state coastline and the impacts of implementing the weighting strategy (**Figure 6-4**). Approximately 36% of the total candidate points have a zero score (completely unfavorable) due to complex shoreline geometry, headlands, active landslides, or being landward of marine protected areas or reserves. Overall, use of weights provides greater resolution of differences between the most suitable sites and less favorable locations, but the effect is relatively modest (**Figure 6-4**). Excluding the points with zero scores, the histogram is bimodal, with peaks at ~ 67% and ~18%. The lower peak generally corresponds to areas of spits and areas where multiple factors with negative scores coincide. The median nonzero score is 67% and the top 40% of points have scores greater than ~70%, corresponding to shades of orange to red in the color scheme used here (**Figure 6-4**). We consider the upper 40% of scores to represent relatively favorable characteristics. The top 10% of nonzero scores are ~83% or higher.

Figure 6-4. Histograms of the statewide cable landing suitability scores using unweighted and weighted strategies. The weighted histogram is colored using the same scheme as the suitability map figures.

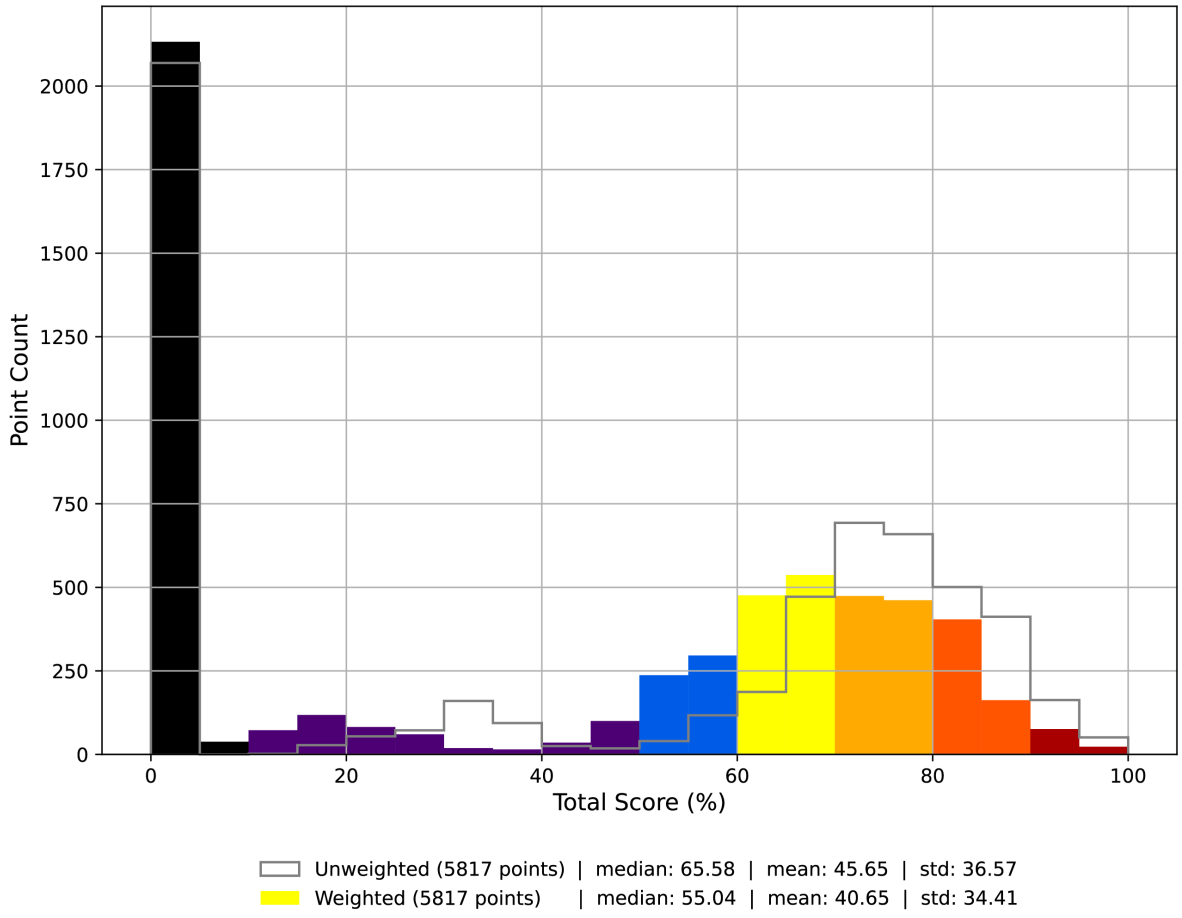

Figure 6-5 shows the influence of each of the factors on the total score through the Pearson correlation coefficient. Aside from the "Special Line" (Headlands, Spits, Landslides) factor that includes the heavily penalized spit category, the correlation values are weak (~ ±0.3 or less). The influences of individual factors on the total score reflect a combination of the factor scores and weights as well as spatial correlations between characteristics that are scored either positively or negatively. The subsequent section presents the spatial pattern of cable landing suitability we calculated in six sectors of the coast.

Figure 6-5. Pearson correlation between individual factors and the overall total score for all points with nonzero scores for both weighted and unweighted cases.

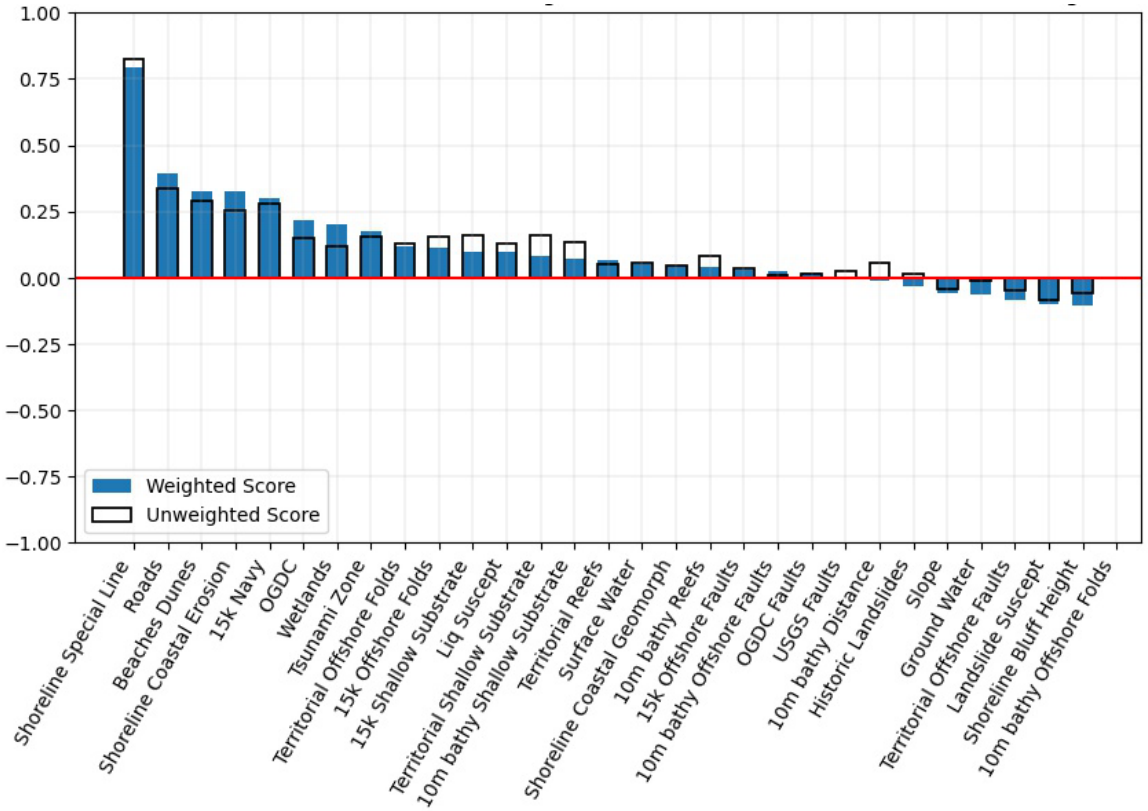

6.3.2 Suitability results by Oregon coastal counties

One cable currently lands in Clatsop County (**Figure 6-6**). The northernmost cable landing site at Warrenton is located in a highly favorable location based on our analysis. Adjacent sandy coastal areas appear generally favorable as well. The Cannon Beach area also has suitable physical characteristics.

Figure 6-6. Suitability analysis results for Clatsop and northern Tillamook counties.

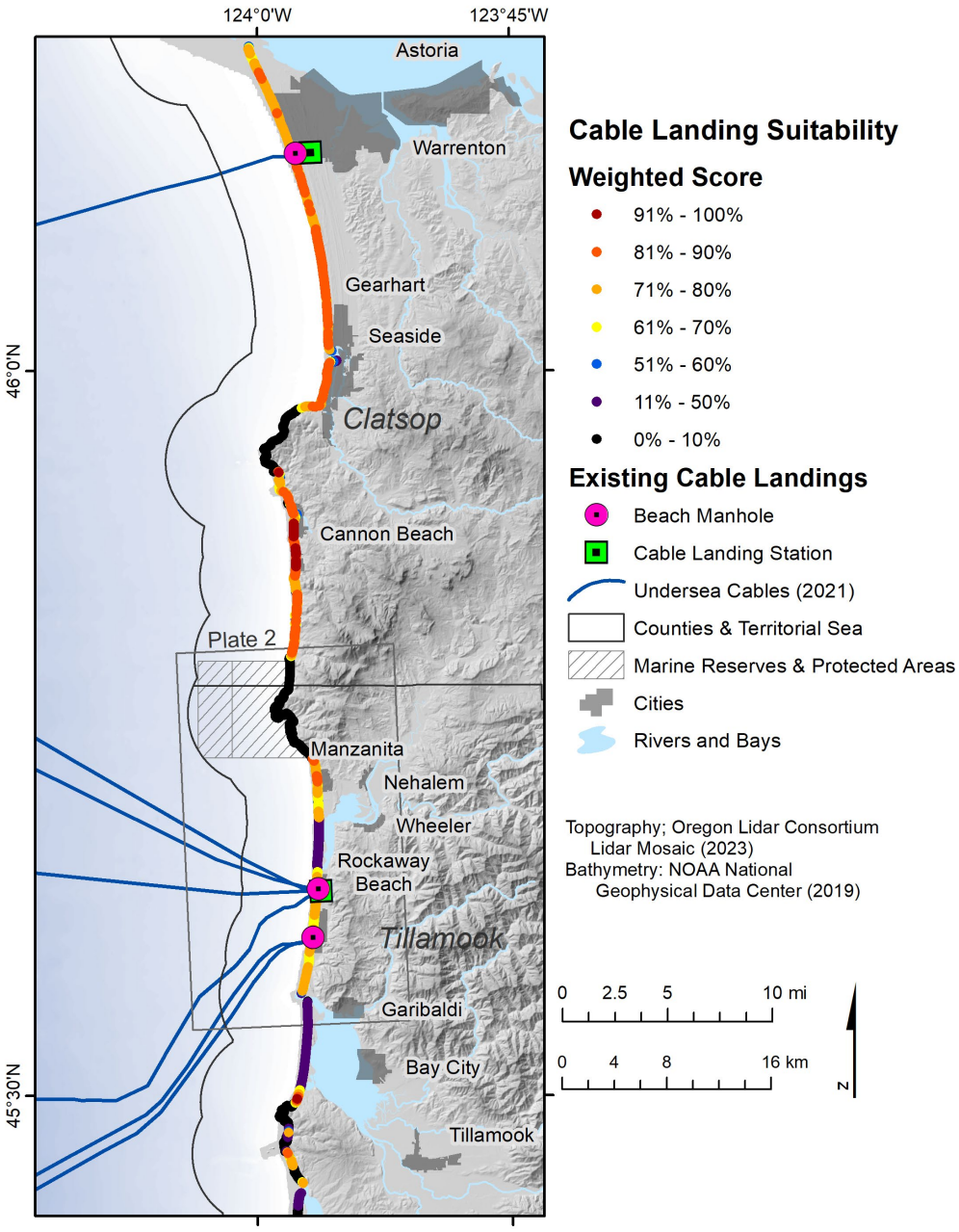

Tillamook County hosts the most current cable landings, and the sectors of the coastline around Pacific City and Rockaway Beach where current cables land are rated as favorable in the suitability analysis (**Figure 6-7**). Some of the cables in the 2021 compilation shown here have been decommissioned (S. McMullen, personal commun. 2022), and the newly built Jupiter cable lands at the beach manhole in Tierra del Mar, north of Pacific City (**Figure 6-7**). Plate 2 shows details of individual factors and scoring around Rockaway Beach. Extensive sandy spits with greater mobility are identified as unfavorable. The suitability analysis does not take into account potential crowding issues with a limited number of potential routes through rocky areas west of the Oregon Territorial Sea (e.g., **Figure 1-1**).

Figure 6-7. Suitability analysis results for Tillamook County.

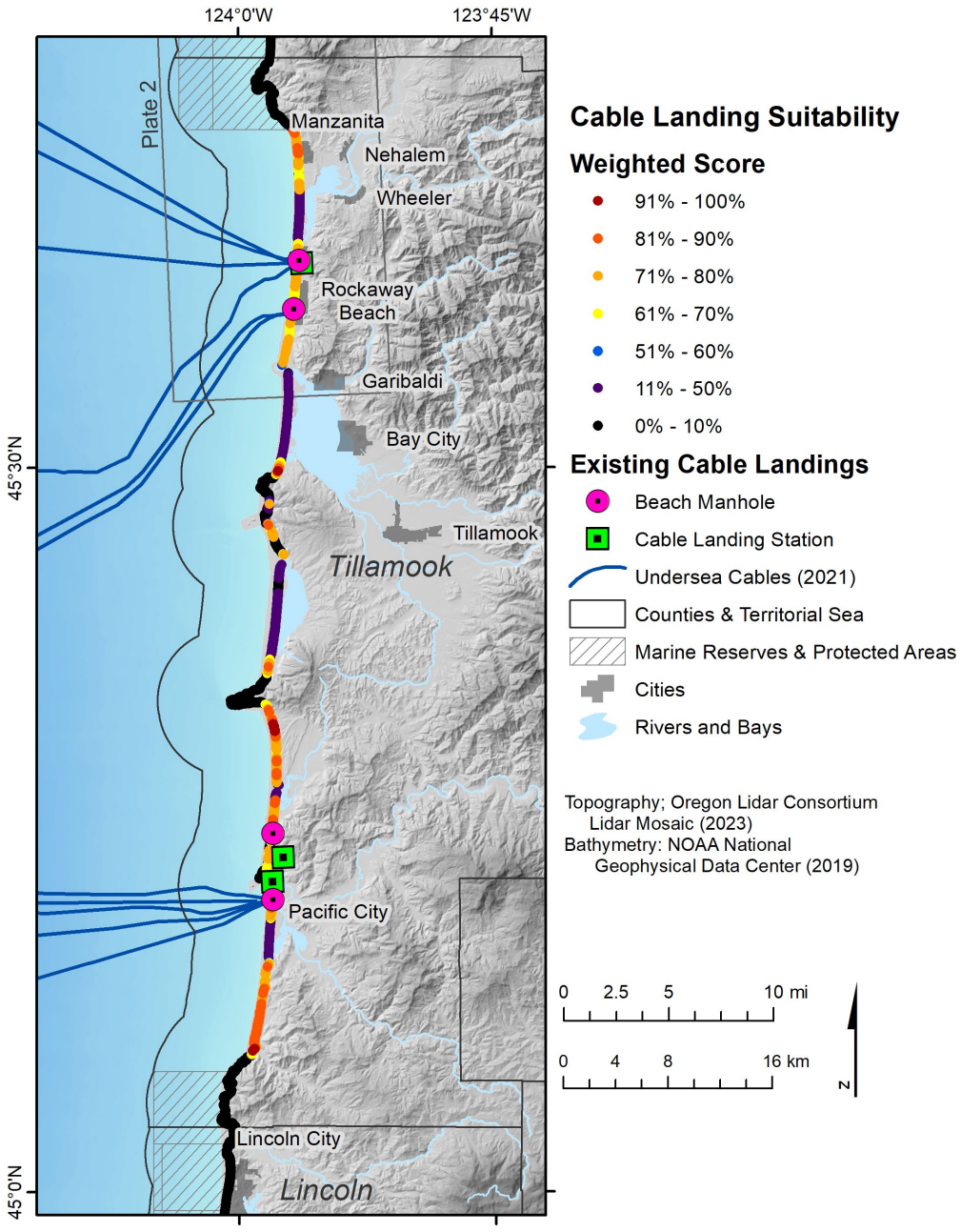

The Lincoln County sector of the coast has numerous rocky headlands and coastal areas composed of hard, basaltic rock that are identified as unfavorable for cable landing construction in our analysis (**Figure 6-8**). We identify three favorable areas: two near Waldport and the other between Depoe Bay and Lincoln City. The recently constructed cable landing site for the PacWave Energy offshore wave energy facility is located in a highly suitable portion of the coastline between Newport and Waldport (**Figure 6-8**).

Figure 6-8. Suitability analysis results for Lincoln County.

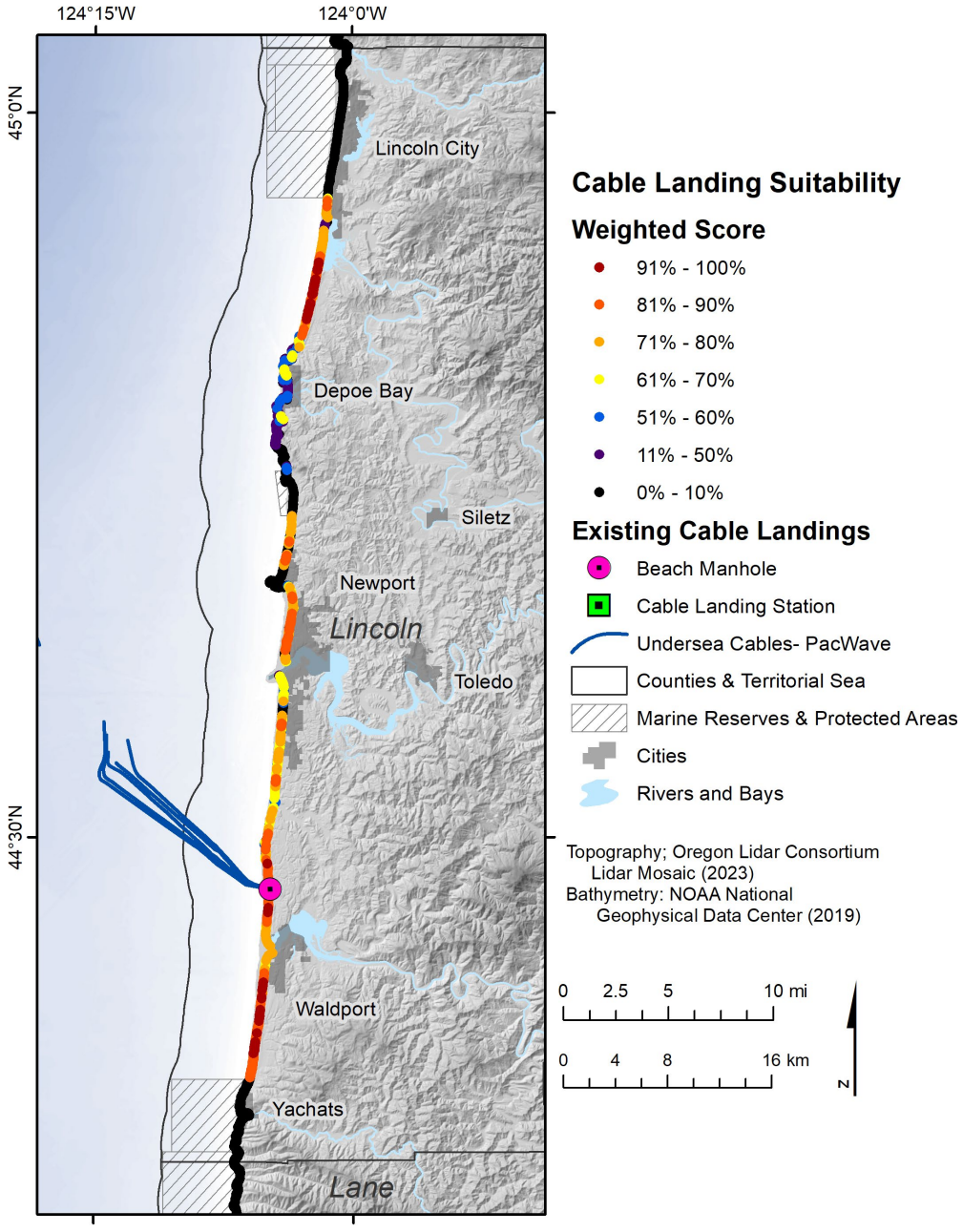

Although the shelf offshore of the Douglas and Lane County sector of the shoreline is relatively amenable to offshore cable burial (**Figure 1-1**), most of this part of the coastline is rated as relatively unfavorable due to the shoreline erosion index in the highest categories, extensive dunes, sand spits, nearshore wetlands, lack of roads at the coast, and the DOD exclusion zone offshore (**Figure 6-9**). The Florence cable landing is in the most suitable part of this coastal sector. This area north of Florence appears favorable for additional cables, and to our knowledge, only one telecommunication cable uses the Florence cable landing station (**Figure 6-9**).

Figure 6-9. Suitability analysis results for Lane and Douglas Counties.

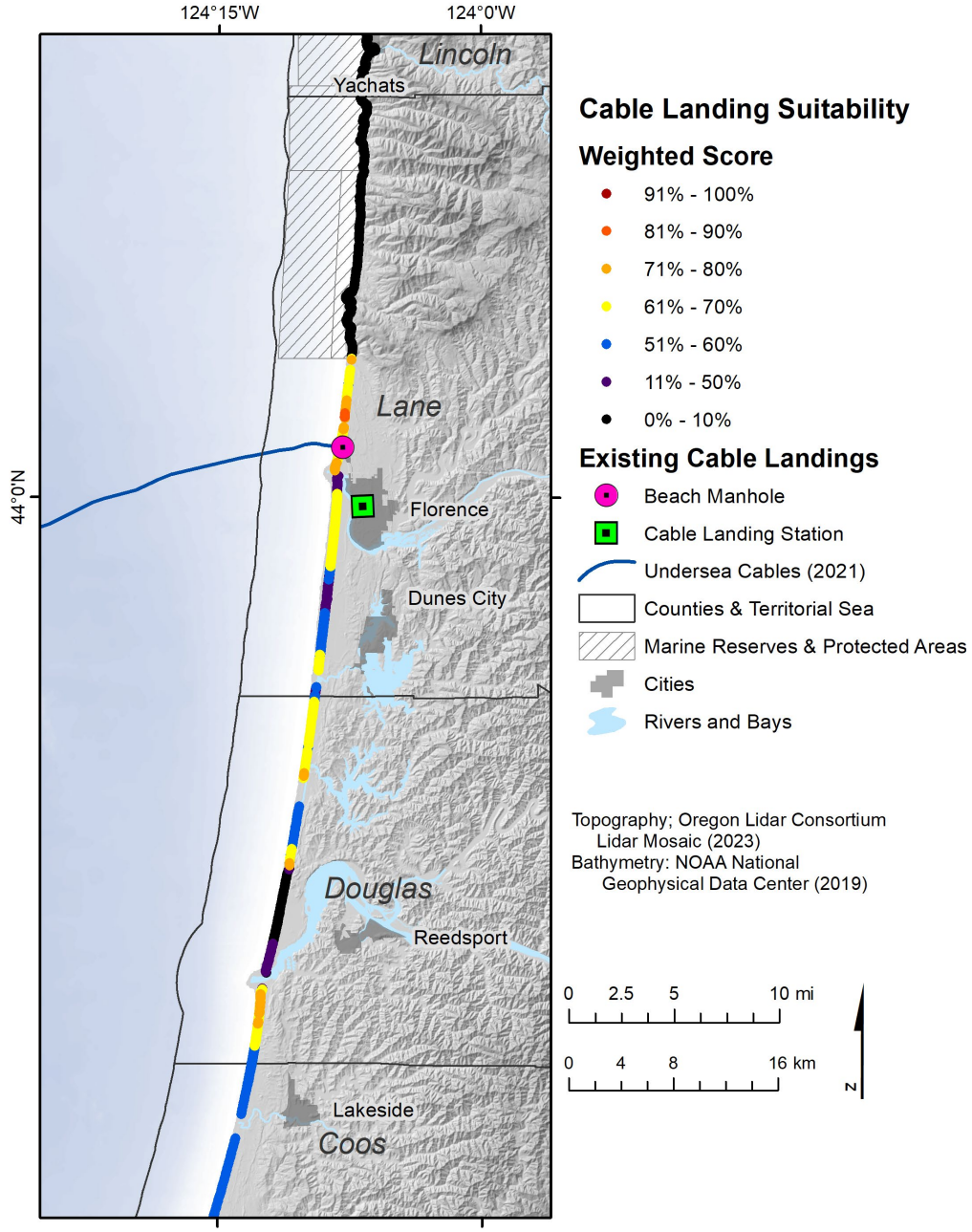

Coos County hosted some of the first transoceanic telecommunications cables to land in Oregon. The vicinity of the two nearby Bandon cable landing sites is rated as relatively unfavorable in our suitability analysis, although nearby areas north of Bandon appear favorable (**Figure 6-10**). The low scores for the Bandon landing site are a product of the rocky seafloor offshore as well as the relatively high, steep, and rocky coastal topography. The scoring likely reflects both changing attitudes toward routing cables over rocks as well as the ability to successfully design cable routes that avoid rock along complex paths. The coastline south of Bandon has favorable characteristics in our analysis (**Figure 6-10**).

Figure 6-10. Suitability analysis results for Coos and northern Curry Counties.

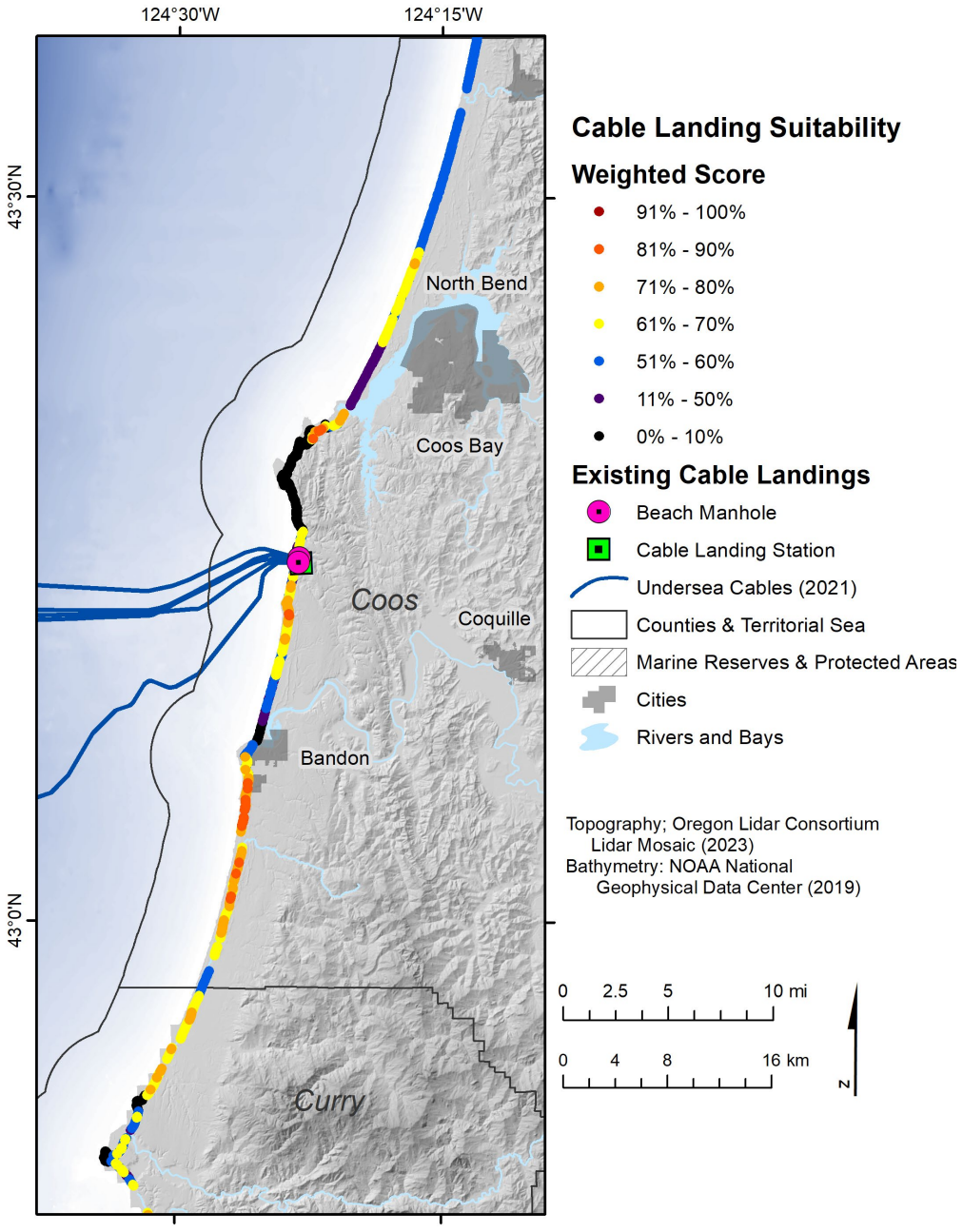

The southern sector of the Oregon coastline has relatively rugged inland topography, and the coastline has mixed suitability scores that show relative variation over kilometer/mile length scales (**Figure 6-11**). More detail for the area around Gold Beach is shown on Plate 1, as an example of the geospatial data that contribute to our analysis and the full resolution of the 100 m spacing of suitability points. Our analysis indicates that favorable areas exist in the vicinity of Brookings, Gold Beach, and Port Orford. Other pockets of more favorable coastline are distributed along the shoreline (**Figure 6-11**) and likely indicate that more detailed planning would allow cable landing siting assuming that the logistical needs related to interconnecting power and/or telecommunications networks could be met.

Figure 6-11. Suitability analysis results for Curry County.

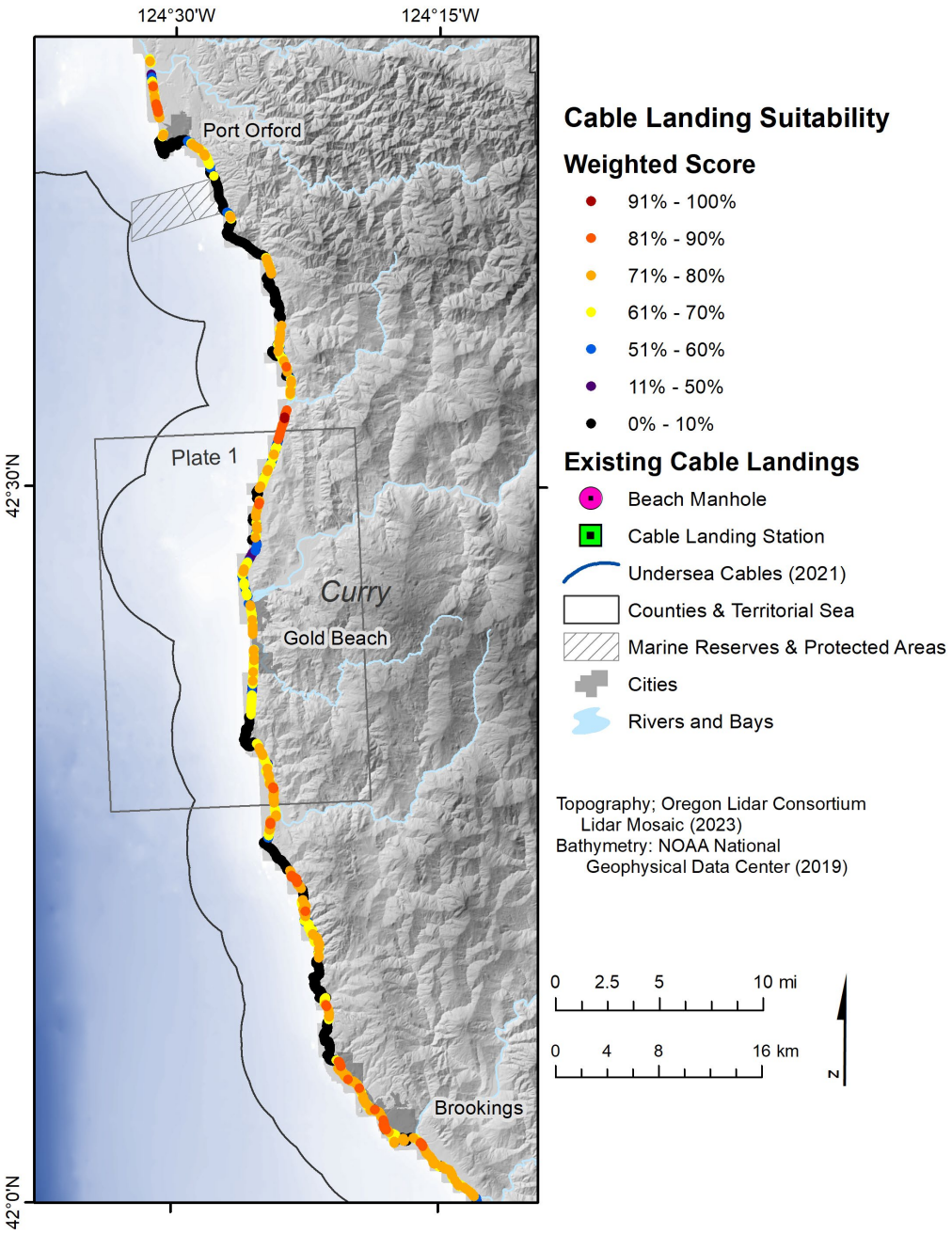

7.0 CONCLUSION

This study provides a regional-scale view of factors that influence locating submarine cables in the Oregon Territorial Sea, and points out where cables cross onto the land to transmit communication data or power to the state. The unique geologic history of the Oregon Coast has produced spatially varying characteristics that have affected how cables may be placed, and how cable landings should be constructed with a minimum of impact on the coastal environment and communities. The new analysis of coastal change over recent decades gives new observations that can help guide placement of cable infrastructure as well as other coastal development in a resilient manner.

Our suitability analysis highlights areas along the coast from the Clatsop Plains in the north to the Gold Beach area in southern Oregon that have characteristics that are generally amenable to construction of new cable landings. Existing cable landings generally occupy relatively favorable settings in our analysis, and suggest that our regional-scale study is compatible with priorities that have guided past placement of specific landing sites. We note that the coarse approach to analysis applied here may miss critical details that would favor or preclude a site being developed for cable landings.

From our review of cable landing site construction and issues experienced on the Oregon Coast in recent years, it appears that cable landings may be developed in a safe way when engineering and design practices are well aligned with the details of local geology. Completion of detailed, site-specific subsurface surveys using geotechnical and geophysical methods prior to construction of HDD boreholes will mitigate many potential problems. We note that HDD construction over the ~1-km-length (0.6 mi) scales required for cable landings brings technical challenges and short spatial-scale heterogeneity in rock or sediment properties may lead to unanticipated damaging effects. These issues motivate locating new cable landings in areas where an engineering issue will not cause unresolvable impacts to the local natural or built environment. Another note is that the publicly available geotechnical reports from the recent PacWave and Jupiter cable projects are helpful for understanding the relevant conditions along the coast. Wider dissemination of geotechnical knowledge from past projects would help in avoiding challenges that might otherwise not be recognized in advance. Design and construction by contractors with state-of-the-art regional expertise is another factor that should improve outcomes for minimally disruptive emplacement of cable landings.

8.0 ACKNOWLEDGMENTS

We thank the Oregon Department of Land Conservation and Development for supporting this project through Interagency Agreement DLCD IAA #21068/DOGAMI #22-0607. We particularly thank Marcus Chatfield and Andy Lanier for helpful guidance and review of an earlier version of the report. Tanya Haddad generously provided data. We thank Delia Kelly, Becky Anthony, and Scott Marion of the Oregon Department of Fish and Wildlife for helpful discussions and review comments. We appreciate the feedback and guidance provided by all of the members of the Territorial Sea Plan, Part 4 Working Group. Ryan Wopschall provided valuable insights on the cable industry. We thank Bill Burns at DOGAMI for help using the best available landslide data. We thank Dr. Michael Darin from DOGAMI for an insightful review of the report and plates. We are especially grateful to Dr. Alan Niem (Emeritus Professor, Oregon State University) for his constructive comments and careful review of the geology section, and Wendy Niem for reviewing the entire report. Finally, we would also like to acknowledge the comments provided by Dr. Peter Ruggiero, Oregon State University.

9.0 REFERENCES

Aalto, K. and Dott Jr, R., 1970, Late Mesozoic conglomeratic flysch in southwestern Oregon, and the problem of transport of coarse gravel in deep water. Flysch sedimentology in North America: Geol. Assoc. Canada Spec. Paper, 7: 53-65.

Aalto, K., 1989, Sandstone petrology and tectonostratigraphic terranes of the northwest California and southwest Oregon Coast Ranges. Journal of Sedimentary Research, 59(4): 561-571.

Aalto, K.R., 1968, Sedimentology of the Late Jurassic (Portlandian) Otter Point Formation of Southwest Oregon. University of Wisconsin--Madison.

Addicott, W.O., 1983. *Biostratigraphy of the marine Neogene sequence at Cape Blanco, southwestern Oregon*. United States Geological Survey Professional Paper 774-G. p. G1-G20.

Alcorn, R., E. Amon, S. Armstrong, B. Batten, D. Bull, B. Cahill, E. Cotilla-Sanchez, G. Dalton, D. Hellin, S. Henkel, A. Husky, J. Klure, B. Langley, B. Polagye, J. Rea, M. Sanders, A. Stewart, G. Sutton and J. Weber 2017, The Pacific Marine Energy Center South Energy Test Site (PMEC-SETS) Final Report: Final Site Selection, Preliminary Facility Design, and Cost & Schedule Estimates. Pacific Marine Energy Center (PMEC): p. 604.

Allan, J.C. and Harris, E.L., 2012, An "Expanded" Geospatial Database of Beach and Bluff Morphology Determined from LIDAR Data collected on the Northern Oregon Coast; Tillamook to Clatsop County. Open file report O-12-08, Oregon Department of Geology and Mineral Industries, Portland, 23 pp.

Allan, J.C. and Hart, R., 2007, Assessing the temporal and spatial variability of coastal change in the Neskowin littoral cell: Developing a comprehensive monitoring program for Oregon beaches Open-file-report O-07-01, Oregon Department of Geology and Mineral Industries, Portland, Oregon, 27 p.

Allan, J.C. and Hart, R., 2008, Oregon beach and shoreline mapping and analysis program: 2007-2008 beach monitoring report. Open-File Report O-08-15, Oregon Department of Geology and Mineral Industries, Portland, 60 p.

Allan, J.C., Hart, R. and Geitgey, R., 2005, Dynamic revetments for coastal erosion stabilization: A feasibility analysis for application on the Oregon Coast. Special Paper 37, Oregon Department of Geology and Mineral Industries, Portland, Oregon, 71 p.

Allan, J.C. and Komar, P.D., 2002, Extreme storms on the Pacific Northwest Coast during the 1997-98 El Niño and 1998-99 La Niña. Journal of Coastal Research, 18(1): 175-193.

Allan, J.C. and Komar, P.D., 2006, Climate controls on U.S. West Coast erosion processes. Journal of Coastal Research, 22(3): 511-529.

Allan, J.C. and Stimely, L., 2013, Oregon Beach Shoreline Mapping and Analysis Program: Quantifying Short to Long-term Beach and Shoreline Changes in the Gold Beach, Nesika, and Netarts Littoral Cells. O-13-07, Oregon Department of Geology and Mineral Industries, Portland, Oregon, 46 p.

Allan, J.C., Gabel, L. and O'Brien, F., 2018, Beach and shoreline dynamics in the Cannon Beach littoral cell: Implications for dune management. Special Paper 49, Oregon Department of Geology and Mineral Industries, Portland, Oregon, 123 p.

Allan, J.C., Komar, P.D. and Priest, G.R., 2003, Shoreline variability on the high-energy Oregon Coast and its usefulness in erosion-hazard assessments. In: M.R. Byrnes, M. Crowell and C. Fowler (Editors), Shoreline mapping and change analysis: Technical considerations and management implications. Journal of Coastal Research, p. 83-105.

Allan, J.C. and Priest, G.R., 2001, Coastal erosion hazard zones along the Clatsop Plains, Oregon: Gearhart to Fort Stevens. Open file report O-01-04, Oregon Department of Geology and Mineral Industries, Portland, Oregon, 56 p.

Allan, J.C., Priest, G.R., Zhang, J. and Gabel, L., 2018, Maritime Tsunami Evacuation Guidelines for the Pacific Northwest Coast of Oregon. Natural hazards, 94(1): 21-52.

Allan, J.C., Ruggiero, P. and Roberts, J.T., 2012, Coastal Flood Insurance Study, Coos County, Oregon. Special Paper 44, Oregon Department of Geology and Mineral Industries, Portland, Oregon, 132 p.

Allan, J.C., Ruggiero, P., Cohn, N., Garcia, G., O'Brien, F., Serafin, K.A., Stimely, L. and Roberts, J.T., 2015a, Coastal Flood Hazard Study, Lincoln County, Oregon. Open File Report O-15-06, Oregon Department of Geology and Mineral Industries, Portland, Oregon, 361 p.

Allan, J.C., Ruggiero, P., Cohn, N., O'Brien, F., Serafin, K.A., Roberts, J.T. and Gabel, L., 2017, Coastal Flood Hazard Study, Lane and Douglas County, Oregon. Open File Report O-17-05, Oregon Department of Geology and Mineral Industries, Portland, Oregon, 190 p.

Allan, J.C., Ruggiero, P., Cohn, N., O'Brien, F., Serafin, K.A., Roberts, J.T. and Stimely, L., 2015b, Coastal Flood Hazard Study, Curry County, Oregon. Open File Report O-15-07, Oregon Department of Geology and Mineral Industries, Portland, Oregon, 246 p.

Allan, J.C., Ruggiero, P., Garcia, G., Harris, E.L., Roberts, J.T. and Stimely, L., 2015c, Coastal Flood Hazard Study, Clatsop County, Oregon. Open File Report O-15-05, Oregon Department of Geology and Mineral Industries, Portland, Oregon, 210 p.

Allan, J.C., Ruggiero, P., Garcia, G., O'Brien, F., Stimely, L. and Roberts, J.T., 2015d, Coastal Flood Hazard Study, Tillamook County, Oregon. Special Paper 47, Oregon Department of Geology and Mineral Industries, Portland, Oregon, 283 p.

Allan, J.C., Witter, R.C., Ruggiero, P. and Hawkes, A.D., 2009 Coastal geomorphology, hazards, and management issues along the Pacific Northwest coast of Oregon and Washington. In: J.E. O'Connor, R.J. Dorsey and I.P. Madin (Editors), Volcanoes to vineyards: Geologic field trips through the dynamic landscape of the Pacific Northwest: Geological Society of America Field Guide 15. The Geological Society of America, p. 495-519.

Allen, J.E. and Baldwin, E.M., 1944, Geology and coal resources of Coos Bay quadrangle. B-027.

Anderson, R.S. and Burbank, D.W., 2012. Tectonic Geomorphology (Second Edition). John Wiley & Sons.

Anderson, D., Ruggiero, P., Antolinez, J.A., Mendez, F.J. and Allen, J., 2018. A climate index optimized for longshore sediment transport reveals interannual and multi-decadal littoral cell rotations. Journal of Geophysical Research: Earth Surface.

AVISO, 2023. Mean Sea Level rise. https://www.aviso.altimetry.fr/en/data/products/ocean-indicators-products/mean-sea-level.html.

Baldwin, E.M., 1945. Some revisions of the late Cenozoic stratigraphy of the southern Oregon coast. *The Journal of Geology*, *53*(1), pp.35-46.

Baldwin, E.M., 1974, Eocene stratigraphy of SW Oregon. Bulletin B-083., Oregon Department of Geology and Mineral Industries, 40 p.

Balco, G., Finnegan, N., Gendaszek, A., Stone, J.O. and Thompson, N., 2013, Erosional response to northward-propagating crustal thickening in the coastal ranges of the US Pacific Northwest. American Journal of Science, 313(8), p.790-806.

Bandon Cable, 2023, History, https://bandoncable.org/history.asp.

Bandy, O. L., 1941, Invertebrate paleontology of Cape Blanco: Corvallis, Oregon., Oregon State University M.S. thesis, 138 p.

Bennett, D. and Ariaratnam, S.T., 2017, NASTT's Horizontal Directional Drilling (HDD): Good Practices Guidelines, 4th Edition. North American Society for Trenchless Technology, 275 p.

Birkemeier, W.A., 1985, Field data on seaward limit of profile change. Journal of Waterway, Port, Coastal and Ocean Engineering 111(3): 598–602.

Blake, M.C., Jayko, A.S., and McLaughlin, R.J., 1985, Tectonostratigraphic terranes of the northern Coast Ranges. In: D.G. Howell (Editor), Tectonostratigraphic Terranes of the Circum-Pacific Region, Circum-Pacific Council for Energy and Mineral Resources, Earth Science Series, 1, Houston, TX: p. 159–86.

BOEM, Bureau of Ocean Energy Management, 2022, Call for Information and Nominations—Commercial Leasing for Wind Energy Development on the Outer Continental Shelf (OCS) Offshore Oregon, Federal Register, Vol. 87, No. 83, Docket No. BOEM–2022–0009, p. 25529-25539.

Bourgeois, J. and Dott Jr, R., 1985, Stratigraphy and sedimentology of Upper Cretaceous rocks in coastal southwest Oregon: evidence for wrench-fault tectonics in a postulated accretionary terrane. Geological Society of America Bulletin, 96(8): 1007-1019.

Brutsché, K.E., Rosati, J., Pollock, C.E. and McFall, B.C., 2016, Calculating Depth of Closure Using WIS Hindcast Data. CHETN-VI-45, Engineer Research Development Center/Coastal Hydraulics Laboratory, 9 p.

Bruun, P., 1988, The Bruun rule of erosion by sea-level rise: A discussion on large-scale two- and three-dimensional uses. Journal of Coastal Research, 4(4): 627-648.

Burbank, D.W. and Anderson, R.S., 2012, Tectonic Geomorphology, second edition, Wiley-Blackwell, 472 p.

Burgette, R.J., Weldon, R.J. and Schmidt, D.A., 2009, Interseismic uplift rates for western Oregon and along-strike variation in locking on the Cascadia subduction zone. Journal of Geophysical Research: Solid Earth, 114(B1).

Burns, W.J., Coe, J.A., Kaya, B.S. and Ma, L., 2010. Analysis of elevation changes detected from multi-temporal LiDAR surveys in forested landslide terrain in western Oregon. Environmental & Engineering Geoscience, 16(4), pp.315-341.

Burns, W. J., Mickelson, K. A., and Madin, I. P., 2016, Landslide susceptibility overview map of Oregon: Oregon Department of Geology and Mineral Industries Open-File Report O-16-02, 48 p. https://www.oregongeology.org/pubs/ofr/p-O-16-02.htm.

Burns, W.J., Hughes, K. B., Olson, K. V., McClaughry, J. D., Mickelson, K. A., Coe, D. E., English, J.T., Roberts, J. T., Lyles Smith, R. R., Madin, I.P., 2011, Multi-Hazard and Risk Study for the Mount Hood Region, Multnomah, Clackamas, and Hood River Counties, Oregon, Oregon Department of Geology and Mineral Industries, Open-File Report O-11-16. http://www.oregongeology.org/pubs/ofr/p-O-11-16.htm

Burns, W.J., and Madin, I.P., 2009, Protocol for Inventory Mapping of Landslide Deposits from Light Detection and Ranging (lidar) Imagery, Oregon Department of Geology and Mineral Industries, Special Paper 42https://www.oregongeology.org/pubs/sp/p-SP-42.htm.

Burns, W.J., Mickelson, K.A., 2016, Protocol for deep landslide susceptibility mapping: Oregon Department of Geology and Mineral Industries, Special Paper 48. http://www.oregongeology.org/pubs/sp/p-SP-48.htm.

Cady, W.M., 1975. Tectonic setting of the Tertiary volcanic rocks of the Olympic Peninsula, Washington. Journal of Research of the US Geological Survey, 3(5), p.573-582.

Calhoun, N. C., Burns, W. J., and Franczyk, J. J., 2020, Landslide hazard and risk study of Tillamook County, Oregon: Oregon Department of Geology and Mineral Industries, Open-File Report O-20-13, scale 1:8,000.

Carter, L., R. Gavey, P.J. Talling, and J.T. Liu. 2014, Insights into submarine geohazards from breaks in subsea telecommunication cables. Oceanography 27(2):58–67, http://dx.doi.org/10.5670/oceanog.2014.40

Church, J.A. and White, N.J., 2006, A 20th century acceleration in global sea-level rise. Geophysical Research Letters, 33: L01602.

Clarke, S.H., Jr., Field, M.E. and Hirozawa, C.A., 1985, Reconnaissance Geology and Geologic Hazards of the Offshore Coos Bay Basin, Oregon. U.S.G.S Survey Bulletin 1645 p. 52.

Cohn, N., Ruggiero, P., Garcia-Medina, G., Anderson, D., Serafin, K. and Biel, R., 2019. Environmental and Morphologic Controls on Wave Induced Dune Response. Geomorphology, 329: 108-128.

Coleman, R.G., 1972. The Colebrooke Schist of southwestern Oregon and its relation to the tectonic evolution of the region (Vol. 1339). US Government Printing Office.

Darin, M.H., Armentrout, J.M., and Dorsey, R.J., 2022, Oligocene onset of uplift and inversion of the Cascadia forearc basin, southern Oregon Coast Range, USA. Geology, 50(5), p. 603-609.

Dean, R.G. and Houston, J.R., 2016, Determining shoreline response to sea level rise. Coastal Engineering, 114: 1-8.

Diller, J.S, 1903, Port Orford Folio, Geologic Atlas of the United States, Issue 89, U.S. Geological Survey.

Dott Jr, R., 1965, Mesozoic-Cenozoic tectonic history of the southwestern Oregon Coast in relation to cordilleran orogenesis. Journal of Geophysical Research, 70(18): 4687-4707.

Dott Jr, R., 1966, Eocene deltaic sedimentation at Coos Bay, Oregon. The Journal of Geology, 74(4): 373-420.

Dott, R.H., 1971, Geology of the southwestern Oregon Coast west of the 124th meridian. Department of Geology and Mineral Industries.

Edge Cable Holdings USA LLC, 2020, Drill Break Avoidance Plan, 3 p. https://www.oregon.gov/oprd/PRP/Documents/Edge_Drill%20Break%20Avoidance%20and%20response%20Plan_Dec2020_RevJan2021.pdf.

Edge Cable Holdings USA LLC, 2021a, Horizontal Directional Drill Construction Plan, January 2021, 13 p., https://www.oregon.gov/oprd/PRP/Documents/Edge%20HDD%20Construction%20Plan_Dec2020_RevJan2021.pdf.

Edge Cable Holdings USA LLC, 2021b, Jupiter Cable Project, Beach Void Monitoring and Response Plan, 8p, https://www.oregon.gov/oprd/PRP/Documents/Edge_OPRD%20Beach%20Void%20Monitoring%20and%20Response%20Plan_ERM%20Tech%20Memo%204888-2091-0340%20v.1.pdf

Emerson, L. F., 2007, Miocene coastal vegetation preserved by volcanic eruption at Cape Blanco, Oregon: Geological Society of America Abstracts with Programs, v. 39, no. 6, p. 401.

ERM, 2020, Independent Hazard Analysis, Jupiter Drill Break, Tierra del Mar Subsea Cable Landing Site, Tillamook County, Oregon, Peer-reviewed report, https://www.oregon.gov/oprd/PRP/Documents/Jupiter%20Independent%20Hazard%20Analysis_08-28-20.pdf.

Fleishman, E., editor. 2023. Sixth Oregon climate assessment. Oregon Climate Change Research Institute, Oregon State University, Corvallis, Oregon. DOI: 10.5399/osu/1161.

Franczyk, J.J., Burns, W.J., and Calhoun, N.C., 2021, Statewide Landslide Information Database for Oregon, release 4 (SLIDO-4.4), Oregon Department of Geology and Mineral Industries, Digital Data Series. https://www.oregongeology.org/slido/index.htm.

Freeman, M. C., O'Neil, R., Garavelli, L., Hellin, D., & Klure, J. 2022, Case study on the novel permitting and authorization of PacWave South, a US grid-connected wave energy test facility: Development, challenges, and insights. Energy Policy, 168, 113141.

Fowler, G. A., Orr, W. N., and Kulm, L. D., 1971, An upper Miocene diatomaceous rock unit on the Oregon Continental Shelf: The Journal of Geology, v. 79, no. 5, p. 603–608.

Fuis, G.S., and Wald, L.A., 2003, Rupture in South-Central Alaska—The Denali Fault Earthquake of 2002, USGS Fact Sheet 014-0.

Giaramita, M.J. and Harper, G.D., 2006, Geochemistry of ophiolitic rocks associated with the western part of the Elk outlier of the western Klamath terrane, southwestern Oregon In: A.W. Snoke and C.G. Barnes (Editors) Geological studies in the Klamath Mountains province, California and Oregon; a volume in honor of William P. Irwin, Geological Society of America Special Paper 410, p. 153-176.

Goldfinger, C. and Beeson, J., 2023, Neotectonic map of the Cascadia margin, Oregon Department of Geology and Mineral Industries, Open-File Report, O-23-05, *in press*.

Goldfinger, C., Kulm, L.D., Yeats, R.S., Appelgate, B., MacKay, M.E. and Moore, G.F., 1992. Transverse structural trends along the Oregon convergent margin: Implications for Cascadia earthquake potential and crustal rotations. Geology, 20: 141-144.

Goldfinger, C., Henkel, S.K., Romsos, C.Havron, A., Black, B., 2014, Benthic Habitat Characterization Offshore the Pacific Northwest Volume 1: Evaluation of Continental Shelf Geology, Report OCS BOEM 2014-662, Bureau of Ocean Energy Management, U.S. Department of the Interior, 161 p.

Goldfinger, C., Nelson, C.H., Morey, A.E., Johnson, J.E., Patton, J.R., Karabanov, E.B., Gutierrez-Pastor, J., Eriksson, A.T., Gracia, E., Dunhill, G. and Enkin, R.J., 2012, Turbidite event history—Methods and implications for Holocene paleoseismicity of the Cascadia subduction zone (No. 1661-F). US Geological Survey.

Goldfinger, C., Galer, S., Beeson, J., Hamilton, T., Black, B., Romsos, C., Patton, J., Nelson, C. H., Hausmann, R., and Morey, A., 2017, The importance of site selection, sediment supply, and hydrodynamics: A case study of submarine paleoseismology on the Northern Cascadia margin, Washington USA: Marine Geology, v. 384, p. 4-46.

González, F., Geist, E.L., Jaffe, B., Kânoğlu, U., Mofjeld, H., Synolakis, C., Titov, V.V., Arcas, D., Bellomo, D. and Carlton, D., 2009, Probabilistic tsunami hazard assessment at Seaside, Oregon, for near-and far-field seismic sources. Journal of Geophysical Research: Oceans, 114(C11).

Goodwin, C.J., 1972, Stratigraphy and sedimentation of the Yaquina Formation, Lincoln County, Oregon, M.S. thesis, Oregon State University.

Hallermeier, R.J., 1981, Seaward limit of significant sand transport by waves: An annual zonation for seasonal profiles. 81-2, U.S. Army, Corps of Engineers, Coastal Engineering Research Center, Fort Belvoir, Va, 23 p.

Hapke, C.J. Adams, P.N., Allan, J., Ashton, A., Griggs, G.B., Hampton, M.A., Kelly, J. and Young, A.P., 2014, The rock coast of the USA. In: D.M. Kennedy, W.J. Stephenson and L. Naylor (Editors), Rock Coast Geomorphology: A Global Synthesis. The Geological Society of London, Memoirs, 40, London, p. 137-154.

Harvey, T.C., Hamlington, B.D., Frederikse, T., Nerem, R.S., Piecuch, C.G., Hammond, W.C., Blewitt, G., Thompson, P.R., Bekaert, D.P.S., Landerer, F.W. and Reager, J.T., 2021, Ocean mass, sterodynamic effects, and vertical land motion largely explain US coast relative sea level rise. Communications Earth & Environment, 2(1), p.233.

He, X., Montillet, J.P., Fernandes, R., Melbourne, T.I., Jiang, W. and Huang, Z., 2022, Sea Level Rise Estimation on the Pacific Coast from Southern California to Vancouver Island. Remote Sensing, 14(17), p.4339.

Heller, P.L. and Ryberg, P.T., 1983, Sedimentary record of subduction to forearc transition in the rotated Eocene basin of western Oregon. Geology, 11(7): 380-383.

Heller, P.L., Peterman, Z.E., O'NEIL, J.R. and Shafiqullah, M., 1985, Isotopic provenance of sandstones from the Eocene Tyee Formation, Oregon Coast Range. Geological Society of America Bulletin, 96(6): 770-780.

HGI, 2021, Geophysical Investigation- Tierra del Mar, Oregon, Report,RPT-2021-025, Rev 0, https://www.oregon.gov/oprd/PRP/Documents/2021-025%20-%20ERM%20-%20Geophysical%20Investigation%20-%20Tierra%20Del%20Mar%20-%20FINAL%20(002).pdf. Himmelstoss, E.A., Henderson, R.E., Kratzmann, M.G. and Farris, A.S., 2018, Digital shoreline analysis system (DSAS) version 5.0 user guide. 2331-1258, US Geological Survey.

Howell, D.G., Jones, D.L. and Schermer, E.R., 1985, Tectonostratigraphic terranes of the Circum-Pacific region. In: D.G. Howell (Editor), Tectonostratigraphic Terranes of the Circum-Pacific Region, Circum-Pacific Council for Energy and Mineral Resources, Earth Science Series, 1, Houston, TX: p. 3–30.

Hunter, R.E., Richmond, B.M. and Rho Alpha, Tau, 1983. Storm-controlled oblique dunes of the Oregon Coast. Geological Society of America Bulletin, 94(12), pp.1450-1465

IPCC, 2021, Summary for Policymakers. In: Climate Change 2021: The Physical Science Basis. Contribution of Working Group I to the Sixth Assessment Report of the Intergovernmental Panel on Climate Change [Masson-Delmotte, V., P. Zhai, A. Pirani, S.L. Connors, C. Péan, S. Berger, N. Caud, Y. Chen, L. Goldfarb, M.I. Gomis, M. Huang, K. Leitzell, E. Lonnoy, J.B.R. Matthews, T.K. Maycock, T. Waterfield, O. Yelekçi, R. Yu, and B. Zhou (eds.)]. Cambridge University Press, Cambridge, United Kingdom and New York, NY, USA, p. 3−32, doi:10.1017/9781009157896.001.

Jones, D.L., Howell, D.G., Coney, P.J. and Monger, H.W.H., 1983. Recognition, character and analysis of tectonostratigraphic terranes in western North America. Journal of Geological Education, 31(4), pp.295-303.

Jung, J., Parrish, C.E., Callahan, B. and Dennis, M.L., 2022, Recovery and Readjustment of Historical Ocean Coast Control Stations in Oregon. Journal of Surveying Engineering, 148(2): 05021007.

Kelsey, H. M. and J. G. Bockheim, 1994. Coastal landscape evolution as a function of eustasy and surface uplift rate, Cascadia margin, southern Oregon. Geological Society of American Bulletin 106: 15.

Kelsey, H.M., Engebretson, D.C., Mitchell, C.E. and Ticknor, R.L., 1994. Topographic form of the Coast Ranges of the Cascadia margin in relation to coastal uplift rates and plate subduction. Journal of Geophysical Research: Solid Earth, 99(B6), p.12245-12255.

Kelsey, H.M., Ticknor, R.L., Bockheim, J.G. and Mitchell, E., 1996. Quaternary upper plate deformation in coastal Oregon. Geological Society of America Bulletin, 108(7), p.843-860.

Kezdi, M., 2022, 2022 Trenchless Technology Project of the Year New Installation Honorable Mention-Pacwave South, Trenchless Technology, https://trenchlesstechnology.com/2022-trenchless-technology-project-of-the-year-new-installation-honorable-mention-pacwave-south/.

Kobor, J.S. and Roering, J.J., 2004. Systematic variation of bedrock channel gradients in the central Oregon Coast Range: implications for rock uplift and shallow landsliding. Geomorphology, 62(3-4), pp.239-256.

Koch, J.G., 1966, Late Mesozoic stratigraphy and tectonic history, Port Orford-Gold Beach area, southwestern Oregon Coast. AAPG Bulletin, 50(1): 25-71.

Komar, P.D., 1986, The 1982-83 El Nino and erosion on the coast of Oregon. Shore and Beach, 54(2): 3-12.

Komar, P.D., 1997, The Pacific Northwest Coast: Living with the Shores of Oregon and Washington. Duke University Press, Durham and London, 195 p.

Komar, P.D., 1998, The 1997-98 El Niño and erosion on the Oregon Coast. Shore & Beach, 66(3): 33-41.

Komar, P.D., Allan, J.C. and Ruggiero, P., 2011, Sea Level Variations along the U.S. Pacific Northwest Coast: Tectonic and Climate Controls Journal of Coastal Research, 27(5): 808-823.

Kramer, B., 2022, Surfing the PacWave: The HDD Company Adapts Pipeline Know-How for Wave Energy Project, North American Energy Pipelines. https://www.napipelines.com/surfing-the-pacwave-hdd-company-pipeline-wave-energy/

Kulm, L.D. and Scheidegger, K.F., 1979, Quaternary sedimentation on the tectonically active Oregon continental slope. SEPM Special Publication No. 27 p. 247-263.

LaHusen, S.R., Duvall, A.R., Booth, A.M., Grant, A., Mishkin, B.A., Montgomery, D.R., Struble, W., Roering, J.J. and Wartman, J., 2020, Rainfall triggers more deep-seated landslides than Cascadia earthquakes in the Oregon Coast Range, USA. Science Advances, 6(38), p.eaba6790.

LaMaskin, T.A., Rivas, J.A., Barbeau, D.L., Schwartz, J.J., Russell, J.A. and Chapman, A.D., 2022, A crucial geologic test of Late Jurassic exotic collision versus endemic re-accretion in the Klamath Mountains Province, western United States, with implications for the assembly of western North America. GSA Bulletin, 134(3-4), p.965-988.

Light, J., 2021, Morphodynamic Evolution of Coastal Oregon: Using New Lidar-derived Beach and Sand Dune Morphometrics to Explore Multi-decadal Change. M.Sc Thesis, Oregon State University, 106 p.

Lund, E.H., 1972, Coastal landforms between Yachats and Newport, Oregon. Ore Bin, 34(5): 73-92.

Macauley Trenchless and Jacobs, 2020, Technical Memorandum 7: Trenchless Engineering, Supporting Design Report, PacWave South Underground Construction, 14 p., https://oregonstate.app.box.com/s/w6ak5y176s2mcgjd85u77nju26shnqfv/file/755184812351.

MacDonald, J. H., et al. (2006). Petrology, geochemistry, and provenance of the Galice Formation, Klamath Mountains, Oregon and California. Geological Studies in the Klamath Mountains Province, California and Oregon: A volume in honor of William P. Irwin. GSA Special Paper 410.

Madin, I.P., Franczyk, J.J., Bauer, J.M., and Azzopardi, C.J.M., 2021. Oregon Seismic Hazard Database, release 1.0, Oregon Department of Geology and Mineral Industries, Digital Data Series OSHD-1. https://www.oregongeology.org/pubs/dds/p-OSHD-1.htm

McCaffrey, R., et al. (2007). "Fault locking, block rotation and crustal deformation in the Pacific Northwest." Geophysical Journal International 169(3): 1315-1340.

McClaughry, J.D., Wiley, T.J., Ferns, M., Madin, I. and McConnell, V.S., 2010, Digital Geologic Map of the Southern Willamette Valley, Benton, Lane, Linn, Marion, and Polk Counties, Oregon. Oregon Department of Geology and Mineral Industries.

McClaughry, J.D., Ma, L., Jones, C.B., Mickelson, K.A., and Wiley, T.J., 2013, Geologic map of the southwestern Oregon Coast between Crook Point and Port Orford, Curry County, Oregon: Oregon Department of Geology and Mineral Industries Open-File Report O-13-21, 55 p., 4 plates, scale 1:24,000, geodatabase. https://www.oregongeology.org/pubs/ofr/p-O-13-21.htm.

McCrory, P.A. and Wilson, D.S., 2013, A kinematic model for the formation of the Siletz-Crescent forearc terrane by capture of coherent fragments of the Farallon and Resurrection plates. Tectonics, 32(3): 718-736.

McInelly, G.W. and Kelsey, H.M., 1990, Late Quaternary tectonic deformation in the Cape Arago-Bandon region of coastal Oregon as deduced from wave-cut platforms. Journal of Geophysical Research: Solid Earth, 95(B5), p. 6699-6713.

McKeel, D.R., 1984, Biostratigraphy of Exploratory Wells in Western Coos, Douglas, and Lane Counties, Oregon. State of Oregon, Department of Geology and Mineral Industries.

McKenzie, K.A., Kelsey, H.M., Kirby, E., Rittenour, T.M. and Furlong, K.P., 2022. Differential coastal uplift quantified by luminescence dating of marine terraces, central Cascadia forearc, Oregon. Quaternary Science Reviews, 298, p. 107853.

McMullen, S., 1999, Report on the NorthStar Cable Installation, Oregon Fishermen's Cable Committee, http://www.ofcc.com/northstar_installation_report.pdf.

McNeill L.C., Goldfinger C., Kulm L.D., and Yeats R.S.,2000, Tectonics of the Neogene Cascadia forearc basin: Investigations of a deformed late Miocene unconformity: Geological Society of America Bulletin 112: 1209-1224.

Melgar, D., 2021, Was the January 26th, 1700 Cascadia earthquake part of a rupture sequence?. Journal of Geophysical Research: Solid Earth, 126(10), p.e2021JB021822.

Molenaar, C., 1985, Depositional Relations of Umpqua and Tyee Formations (Eocene), Southwestern Oregon1. AAPG Bulletin, 69(8): 1217-1229.

Moore, L.J., 2000, Shoreline mapping techniques. Journal of coastal research, 16(1): 111-124.

Nachman, D., Sousa, R., Meng, X., Sarkar, D., Velinsky, D., and Axe, L., 2021, Horizontal Directional Drilling Final Report, New Jersey Department of Environmental Protection Science Advisory Board, Water Quality and Quantity Standing Committee, 22 p.

NACSN, 2005, North American Stratigraphic Code. AAPG Bulletin, 89(11): 1547-1591.

Nelson, A.R., Aspuith, A.C. and Grant, W.C., 2004, Great earthquakes and tsunamis of the past 2000 years at the Salmon River estuary, central Oregon Coast, USA. Bulletin of the Seismological Society of America, 94: 1276-1292.

Nelson, A.R., DuRoss, C.B., Witter, R.C., Kelsey, H.M., Engelhart, S.E., Mahan, S.A., Gray, H.J., Hawkes, A.D., Horton, B.P. and Padgett, J.S., 2021, A maximum rupture model for the central and southern Cascadia subduction zone—reassessing ages for coastal evidence of megathrust earthquakes and tsunamis. Quaternary Science Reviews, 261: 106922.

Newton, V.C., Jr, 1980, Prospects for Oil and Gas in the Coos Basin, Western Coos, Douglas, and Lane Counties, Oregon. In: Oregon Department of Geology and Mineral Industries, Oil and Gas Investigation 6, 81 p.

Niem, A.R., 1975, Geology of Hug Point State Park, Northern Oregon Coast. The Ore Bin, 37(2), p. 17-36.

Niem, A.R. and Niem, W.A., 1985, Geologic map of the Astoria Basin, Clatsop and northernmost Tillamook Counties, northwest Oregon. Oregon Department of Geology and Mineral Industries, Portland, Oregon.

Niem, A.R., Niem, W.A. and Baldwin, E.M., 1989, Geology and oil, gas, and coal resources, southern Tyee Basin, southern Coast Range. O-89-03, Oregon Dept. of Geology and Mineral Industries.

Niem, W.A. and Niem, A.R., 1992. Ages of rocks in southwestern Washington and northwestern Oregon as indicated by paleontological and isotopic dates. Open-File Report 92-344 US Department of the Interior, US Geological Survey, 115 p.

Nokleberg, W.J., Parfenov, L.M., Monger, J.W., Baranov, B.B., Byalobzhesky, S.G., Bundtzen, T.K., Feeney, T.D., Fujita, K., Gordey, S.P., Grantz, A. and Khanchuk, A.I., 1994. Circum-North Pacific tectonostratigraphic terrane map (No. 94-714). US Department of the Interior, US Geological Survey.

OLC, Oregon Lidar Consortium, 2023, Oregon Digital Terrain Model Mosaic, Oregon Department of Geology and Mineral Industries, 3 ft resolution, https://gis.dogami.oregon.gov/arcgis/rest/services/lidar/DIGITAL_TERRAIN_MODEL_MOSAIC/ImageServer.

Onsarigo, L., Adamtey, S., & Atalah, A., 2014, Analysis of Horizontal Directional Drilling Construction Risks Using the Probability-Impact Model: A Contractor's Perspective. In Shah Rahman and David McPherson, Ph.D., P.E., eds., Pipelines 2014: From Underground to the Forefront of Innovation and Sustainability , American Society of Civil Engineers, Reston, Virginia, p. 1772-1783.

OPAC, Oregon Ocean Policy Advisory Council, 1994, Oregon Territorial Sea Plan, https://www.oregon.gov/lcd/OCMP/Pages/Territorial-Sea-Plan.aspx.

OPRD, Oregon Parks and Recreation Department, 2022, Edge Cable Ocean Shore Permit, https://www.oregon.gov/oprd/PRP/Pages/edgecableoceanshorepermit.aspx.

Orr, W. N., Ehlen, J., and Zaitzeff, J. B., 1971, A late Tertiary diatom flora from Oregon: Proceedings of the California Academy of Sciences, Fourth Series, v. 37, no. 16, p. 489–500.

Orr, W. N., and Zaitzeff, J. B., 1970, Miocene silicoflagellates from southeast Oregon: Northwest Science, v. 44, no. 1, p. 12–15.

OWRD, Oregon Water Resources Department, Well Reports, https://apps.wrd.state.or.us/apps/gw/well_log/.

PMEP, Pacific Marine and Estuarine Fish Habitat Partnership, 2022, West Coast USA Nearshore Substrate Habitat, v 1.0, https://www.pacificfishhabitat.org/data/nearshore-cmecs-substrate-habitat/.

PacWave and 3U Technologies, 2020, PacWave subsea cable system overview, v2.0, 7 p, https://pacwaveenergy.org/wp-content/uploads/2020/07/Subsea_Cable_System_Overview_v2.pdf.

PacWave Energy, 2022, PacWave Construction Updates,
https://pacwaveenergy.org/constructionupdates/, accessed 9/23/2022.

Parker, D.F. Hodges, F.N., Perry, A., Mitchener, M.E., Barnes, M.A. and Ren, M., 2010, Geochemistry and petrology of late Eocene Cascade Head and Yachats Basalt and alkalic intrusions of the central Oregon Coast Range, USA., Journal of Volcanology and Geothermal Research, 198(3-4): 311-324.

Parker, M. J., 1990. The Oligocene and Miocene geology of the Tillamook embayment Tillamook County, northwest Oregon. M.S. Thesis. Oregon State University. A. Niem (advisor)

Personius, S.F., 1995. Late Quaternary stream incision and uplift in the forearc of the Cascadia subduction zone, western Oregon. *Journal of Geophysical Research: Solid Earth*, *100*(B10), pp.20193-20210.

Peterson, C.D., Jackson, P.L., O'Neil, D.J., Rosenfeld, C.L. and Kimerling, A.J., 1990, Littoral cell response to interannual climatic forcing 1983-1987 on the central Oregon Coast, USA., Journal of Coastal Research, 6(1): 87-110.

Peterson, C.D., Stock, E., Price, D.M., Hart, R., Reckendorf, F., Erlandson, J.M. and Hostetler, S.W., 2007. Ages, distributions, and origins of upland coastal dune sheets in Oregon, USA. Geomorphology, 91(1-2), pp.80-102.

Pope, E.L., Talling, P.J. and Carter, L., 2017, Which earthquakes trigger damaging submarine mass movements: Insights from a global record of submarine cable breaks?, Marine Geology, 384, p.131-146.

Priest, G.R. and Allan, J.C., 2004, Evaluation of coastal erosion hazard zones along dune and bluff backed shorelines in Lincoln County, Oregon: Cascade Head to Seal Rock. Technical report to Lincoln County. Open-File Report O-04-09, Oregon Department of Geology and Mineral Industries, Portland, Oregon.

Priest, G.R., Allan, J.C. and Sonnevil, R., 2004, Evaluation of coastal erosion hazard zones from Sisters Rocks to North Gold Beach, Curry County, Oregon: Technical report to Curry County. Open-File Report O-04-20, Oregon Department of Geology and Mineral Industries, Portland, Oregon.

Priest, G.R., Goldfinger, C., Wang, K., Witter, R.C., Zhang, Y. and Baptista, A.M., 2010, Confidence levels for tsunami-inundation limits in northern Oregon inferred from a 10,000-year history of great earthquakes at the Cascadia subduction zone. Natural Hazards, 54(1): 27-73.

Priest, G.R., Saul, I. and Diebenow, J., 1994, Chronic geologic hazard maps of coastal Lincoln County, Oregon, Set of all 19 maps and explanation (O-94-11). O-94-12 through O-94-30, Oregon Department of Geology and Mineral Industries.

Raymond, K. R., Prothero, D., Emerson, L., and Retallack, G., 2008, Magnetogstratigraphy of the lower Miocene sandstone of Floras Lake and the Cape Blanco flora, Oregon: Geological Society of America Abstracts with Programs, v. 40, no. 6, p. 477.

Reidel, S.P., Camp, V.E., Tolan, T.L. and Martin, B.S., 2013, The Columbia River flood basalt province: Stratigraphy, areal extent, volume, and physical volcanology, In: Reidel S.P. et al. (Editors), The Columbia River Flood Basalt Province. Geological Society of America Special Paper 497, p. 1-44.

Revell, D., Komar, P.D. and Sallenger, A.H., 2002, An application of LIDAR to analyses of El Niño erosion in the Netarts littoral cell, Oregon., Journal of Coastal Research, 18(4): 792-801.

Roure, F., Carayon, V. and Rangin, C., 1986, Evolution comparee des bassins franciscains de Californie, de l'Oregon et de Basse Californie (Etats-Unis et Mexique). Bulletin de la Société Géologique de France, 2(6): 931-944.

Ruggiero, P., Kaminsky, G.M., Gelfenbaum, G. and Cohn, N., 2016. Morphodynamics of prograding beaches: A synthesis of seasonal-to century-scale observations of the Columbia River littoral cell. *Marine Geology*, *376*, pp.51-68.

Ruggiero, P., Komar, P.D. and Allan, J.C., 2010, Increasing wave heights and extreme value projections: The wave climate of the U.S. Pacific Northwest. Coastal Engineering, 57(5): 539-552.

Ruggiero, P., Kratzmann, M.G., Himmelstoss, E.A., Reid, D., Allan, J.C. and Kaminsky, G.M., 2013, National Assessment of Shoreline Change: Historical Shoreline Change along the Pacific Northwest coast (Oregon and Washington), Open-File Report 2012-1007. U.S. Geological Survey, Reston, Virginia.

Ryan, W.B.F., Carbotte, S.M., Coplan, J.O., O'Hara, S., Melkonian, A., Arko, R., Weissel, R.A., Ferrini, V., Goodwillie, A., Nitsche, F. and Bonczkowski, J., 2009, Global Multi-Resolution Topography synthesis, Geochemistry, Geophysics, Geosystems., 10(3), Q03014, doi: 10.1029/2008GC002332.

Ryan, W.B., Carbotte, S.M., Coplan, J.O., O'Hara, S., Melkonian, A., Arko, R., Weissel, R.A., Ferrini, V., Goodwillie, A., Nitsche, F. and Bonczkowski, J., 2009. Global multi-resolution topography synthesis. Geochemistry, Geophysics, Geosystems, 10(3).

Ryu, I.-C. and Niem, A.R., 1999, Sandstone diagenesis, reservoir potential, and sequence stratigraphy of the Eocene Tyee Basin, Oregon. Journal of Sedimentary Research, 69(2): 384-393.

Ryu, I.-C., Niem, A.R. and Niem, W.A., 1996, The oil and gas potential of the southern Tyee basin, southern Oregon Coast Range. OGI-019, Oregon Department of Geology and Mineral Industries.

Schlicker, H.G., Deacon, R.J., Beaulieu, J.D., and Olcott, G.W., 1972, Environmental Geology of the coastal region of Tillamook and Clatsop Counties, Oregon: Oregon Department of Geology and Mineral Industries, Bulletin 74, 164 p.

Schlicker, H.G., Deacon, R.J., Olcott, G.W., and Beaulieu, J.D., 1973, Environmental Geology of Lincoln County, Oregon: Oregon Department of Geology and Mineral Industries, Bulletin 81, 171 pages.

Schulz, W.H., Galloway, S.L. and Higgins, J.D., 2012, Evidence for earthquake triggering of large landslides in coastal Oregon, USA. Geomorphology, 141, p. 88-98.

Sears, T.R., Lahav, M., Burns, W.J., and McCarley, J., 2019, Preparing for Landslide Hazards, A Land Use Guide for Oregon Communities, Oregon Department of Land Conservation and Development (DLCD., https://www.oregongeology.org/Landslide/Landslide-Hazards-Land-Use-Guide_FINAL.pdf

Seiders, V. and Blome, C., 1987, Stratigraphy and sedimentology of Upper Cretaceous rocks in coastal southwest Oregon: Evidence for wrench-fault tectonics in a postulated accretionary terrane: Alternative interpretation and reply: Alternative interpretation. Geological Society of America Bulletin, 98(6): 739-742.

Silberling, N.J., Jones, D.L., Blake, M.C. and Howell, D.G., 1987. Lithotectonic terrane map of the western conterminous United States. Miscellaneous Field Studies Map, No. 1874-C. US Geological Survey. Reston, Virginia.

Sliter, W., 1984, Foraminifers from Cretaceous limestone of the Franciscan Complex, northern California, in Franciscan Geology of Northern California; Pacific Section S.E.PM, Vol. 43, p.149-162.

Snavely Jr, P.D., 1987. Tertiary geologic framework, neotectonics, and petroleum potential of the Oregon-Washington continental margin. Geology and Resource Potential of the Western North America and Adjacent Ocean Basins- Beaufort Sea to Baja California, Volume 6. Circum-Pacific Council for Energy and Mineral Resources.

Snavely Jr, P., Wells, R. and Minasian, D., 1993., The Cenozoic geology of the Oregon and Washington Coast Range. US Geological Survey Open -File Report: 93-189.

Snavely Jr, P.D., MacLeod, N., Wagner, H.C. and MacLeod, N.S., 1964. Rhythmic-bedded eugeosynclinal deposits of the Tyee Formation, Oregon Coast Range, Kansas Geological Survey Bulletin, 169, p. 461-480.

Snavely Jr, P.D., MacLeod, N.S. and Wagner, H.C., 1968, Tholeiitic and alkalic basalts of the Eocene Siletz River volcanics, Oregon Coast Range, American Journal of Science, 266(6), p. 454-481.

Snavely Jr, P., MacLeod, N., Wagner, H. and Rau, W., 1976, Geologic map of the Yaquina and Toledo quadrangles, Lincoln County, Oregon.

Snavely Jr, P.D. and MacLeod, N.S., 1974, Yachats Basalt- An Upper Eocene Differentiated Volcanic Sequence in the Oregon Coast Range. Journal of Research of the US Geological Survey, 2(4): 395-403.

Snavely Jr, P.D., Jr., MacLeod, N. S., Wagner, H. C., and Rau, W. W., 1976a, Geologic map of the Waldport and Tidewater quadrangles, Lincoln, Lane, and Benton Counties, Oregon: U.S. Geological Survey Miscellaneous Geologic Investigations Map I-866, scale 1:62 500.

Snavely Jr, P. D., Jr., MacLeod, N. S., Wagner, H. C., and Rau, W. W., 1976b, Geologic map of the Yaquina and Toledo quadrangles, Lincoln County, Oregon: U.S. Geological Survey Miscellaneous Geologic Investigations Map I-867, scale 1:62 500.

Snavely Jr, P. D., Jr., MacLeod, N. S., Wagner, H. C., and Rau, W. W., 1976c, Geologic map of the Cape Foulweather and Euchre Mountain quadrangles, Lincoln County, Oregon: U.S. Geological Survey Miscellaneous Geologic Investigations Map I-868, scale 1:62 500.

Snavely, P.D., 1980. Geologic cross section of the central Oregon continental margin. Geologic Society of America.

Snavely Jr, P.D., Wagner, H.C. and Lander, D.L., 1980. Interpretation of the Cenozoic geologic history, central Oregon continental margin: Cross-section summary. Geological Society of America Bulletin, 91(3), pp.143-146.

SubCom, 2020, Jupiter Cable Geophysical Exploration Survey Report, Tierra del Mar, Oregon, https://www.oregon.gov/oprd/PRP/Documents/Jupiter%20Cable%20HDD%20Geophysical%20Exploration%20Survey_Dec2020.pdf.

Sweet, W.V., Hamlington, B.D., Kopp, R.E., Weaver, C.P., Barnard, P.L., Bekaert, D., Brooks, W., Craghan, M., Dusek, G. and Frederikse, T., 2022, Global and regional sea level rise scenarios for the United States: updated mean projections and extreme water level probabilities along US coastlines. No. CO-OPS 083 National Oceanic and Atmospheric Administration.

Tarduno, J.A., 1987. Cretaceous absolute motion of Pacific oceanic rises: Linking the continental and oceanic records through paleomagnetic analysis. Ph.D. Dissertation. (California) Stanford University.

Terracon, 2020, Technical Services for Terrestrial HDD Route Geotechnical Survey, Seal Rock, Oregon, https://oregonstate.app.box.com/s/w6ak5y176s2mcgjd85u77nju26shnqfv/file/745997321507.

Trehu, A.M., Asudeh, I., Brocher, T.M., Luetgert, J.H., Mooney, W.D., Nabelek, J.L. and Nakamura, Y., 1994, Crustal Architecture of the Cascadia Forearc, Science, 266(5183), pp.237-243.

TSP Part 3, Oregon Territorial Sea Plan, Part Three, Rocky Habitat Management Strategy, Oregon Department of Land Conservation 83 p.

Vokes, H. E., Norbisrath, Hans, and Snavely, P. D., Jr., 1949, Geology of the Newport-Waldport area, Lincoln County, Oregon: U. S. Geological Survey, Oil and Gas Inv. Prelim. Map 88

Walker, G.W., and MacLeod, N.S., 1991, Geologic map of Oregon, 1:500,000, Dept. of the Interior, U.S. Geological Survey, Reston, Va.

Walton, M.A., Staisch, L.M., Dura, T., Pearl, J.K., Sherrod, B., Gomberg, J., Engelhart, S., Tréhu, A., Watt, J., Perkins, J. and Witter, R.C., 2021. Toward an integrative geological and geophysical view of Cascadia subduction zone earthquakes. *Annual Review of Earth and Planetary Sciences*, *49*, pp.367-398.

Wells, R., Bukry, D., Friedman, R., Pyle, D., Duncan, R., Haeussler, P. and Wooden, J., 2014, Geologic history of Siletzia, a large igneous province in the Oregon and Washington Coast Range: Correlation to the geomagnetic polarity time scale and implications for a long-lived Yellowstone hotspot. Geosphere, 10(4): 692-719.

Wells, R.E., Snavely, P.D., Jr., MacLeod, N.S., Kelly, M.M. and Parker, M.J., 1994, Geologic map of the Tillamook Highlands, northwest Oregon Coast Range, US Geological Survey.

Wells, R.E., Jayko, A.S., Niem, A.R., Black, G., Wiley, T., Baldwin, E., Molenaar, K.M., Wheeler, K.L., DuRoss, C.B. and Givler, R.W., 2000. Geologic map and database of the Roseburg 30× 60′ Quadrangle, Douglas and Coos counties, Oregon. US Geological Survey Open-File Report, p.00-0376.

Wells, R.E., Blakely, R.J., Wech, A.G., McCrory, P.A. and Michael, A., 2017. Cascadia subduction tremor muted by crustal faults. Geology, 45(6), p.515-518.

Wiley, T.J., McClaughry, J.D., Niewendorp, C.A., Ma, L., Herinckx, H.H., and Mickelson, K.A., 2015, Geologic map of the southern Oregon coast between Bandon, Coquille and Sunset Bay Coos County, Oregon: Oregon Department of Geology and Mineral Industries Open-File Report O-2015-04, 57 p., 4 plates, scale 1:24,000, geodatabase. https://www.oregongeology.org/pubs/ofr/p-O-15-04.htm.

Wiley, T.J., McClaughry, J.D., Ma, L., Mickelson, K.A., Niewendorp, C.A., Stimely, L.A., Herinckx, H.H., and Rivas, J., 2014, Geologic map of the southern Oregon Coast between Port Orford and Bandon, Curry and Coos Counties, Oregon: Oregon Department of Geology and Mineral Industries Open-File Report O-14-01, 66 p., 3 plates, scale 1:24,000, geodatabase. https://www.oregongeology.org/pubs/ofr/p-O-14-01.htm.

WILEY, Thomas J., Oregon Department of Geology and Mineral Industries, 800 NE Oregon Street #28, Suite 965, Portland, OR 97232, MCCLAUGHRY, Jason D., Oregon Department of Geology and Mineral Industries, Baker City Field Office, 1995 3rd Street, Suite 130, Baker City, OR 97814, RIVAS, Jonathan A., Department of Geography and Geology, University of North Carolina Wilmington, 601 South College Rd., Wilmington, NC 28403 and SCHWARTZ, Joshua J.

Wiley, T.J., McClaughry, J.D., Rivas, J.A., and Schwartz, J.J., 2017, Detrital zircon assemblages in sandstone indicate revised late early to late Cretaceous age for the Dothan Formation in southwestern Oregon, Geological Society of America Abstracts with Programs. Vol. 49, No. 4, doi: 10.1130/abs/2017CD-292968.

Williams, M.C. and Burns, W.J., 2022, Natural Hazard Risk Report for Washington County, Oregon, including the Cities of Banks, Beaverton, Cornelius, Durham, Forest Grove, Gaston, Hillsboro, King City, North Plains, Sherwood, Tigard, and Tualatin: Oregon Department of Geology and Mineral Industries, Open-File Report O-22-04, https://www.oregongeology.org/pubs/ofr/O-22-04/O-22-04_report.pdf.

Wirth, E.A., Grant, A., Marafi, N.A. and Frankel, A.D., 2021, Ensemble shakemaps for magnitude 9 earthquakes on the Cascadia subduction zone. Seismological Research Letters, 92(1), p.199-211.

Witter, R.C., Allan, J.C. and Priest, G.R., 2007, Evaluation of coastal erosion hazard zones along dune and bluff backed shorelines: Southern Lincoln County, Oregon: Seal Rock to Cape Perpetua. Open-file-report O-07-03, Oregon Department of Geology and Mineral Industries, Portland, Oregon.

Witter, R.C., Horning, T. and Allan, J.C., 2009, Coastal erosion hazard zones in southern Clatsop County, Oregon: Seaside to Cape Falcon. Open-file-report O-09-06, Oregon Department of Geology and Mineral Industries, Portland, Oregon.

Witter, R., Zhang, Y., Wang, K., Priest, G.R., Goldfinger, C., Stimely, L.L., English, J.T. and Ferro, P.A., 2013, Simulated tsunami inundation for a range of Cascadia megathrust earthquake scenarios at Bandon, Oregon, USA. Geosphere, 9(6): 1783-1803.

Wopschall, R., 2023, Undersea Cable Placement in the United States and Abroad: Report for Oregon Department of Land Conservation and Development, 65 p.